DIAMOND TURNING OF CONTACT LENS POLYMERS

By

MUHAMMAD MUKHTAR LIMAN

(216651263)

2017

DIAMOND TURNING OF CONTACT LENS POLYMERS

MUHAMMAD MUKHTAR LIMAN

Submitted in fulfilment/partial fulfilment of the requirements for the

Degree of Masters of Engineering: Mechatronics in the Faculty of Engineering, the Built

Environment and Information Technology at the

Nelson Mandela Metropolitan University

April 2017

Promoter/Supervisor: Prof. Khaled Abou-El-Hossein

COPYRIGHT STATEMENT

The copy of this thesis has been provided on condition that anyone who accesses it understands and recognizes that its copyright rests with the Nelson Mandela Metropolitan University and that no information derived from it may be published without the prior consent of the Author unless appropriately reference.

DECLARATION

I**, Liman, Muhammad Mukhtar** do hereby solemnly declare that:

- The work done in this thesis is my own;

- All sources used or referred to have been recognized and duly referenced; and

- This thesis has not been previously submitted in full or partial fulfilment of the requirements for an equivalent or lower qualification at any other educational institution.

_____

Author's signature   **Date: April 2017**

DEDICATION

To my beloved Prophet Muhammad (Peace be upon him).

ACKNOWLEDGEMENTS

times were stressful. I am especially grateful to Dr Sa'idu Ibrahim and Ibrahim Kabir for their advice and input into this research.

ABSTRACT

DIAMOND TURNING OF CONTACT LENS POLYMERS

Liman, M.M

M.Eng., Mechatronics Engineering

Supervisor: Prof Khaled Abou-El-Hossein

Faculty of Engineering, the Built Environment and Information Technology

P.O. Box 77000, Nelson Mandela Metropolitan University,

Port Elizabeth, South Africa

April, 2017

Contact lens production requires high accuracy and good surface integrity. Surface roughness is generally used to measure the index quality of a turning process. It has been an important response because it has direct influence toward the part performance and the production cost. Hence, choosing optimal cutting parameters will not only improve the quality measure but also the productivity. In this study, an ONSI-56 (Onsifocon A) contact lens buttons were used to investigate the triboelectric phenomena and the effects of turning parameters on surface finish of the lens materials. ONSI-56 specimens are machined by Precitech Nanoform Ultra-grind 250 precision machine and the roughness values of the diamond turned surfaces are measured by Taylor Hopson PGI Profilometer. Electrostatics values were measured using electrostatic voltmeter.

An artificial neural network (ANN) and response surface (RS) model were developed to predict surface roughness and electrostatic discharge (ESD) on the turned ONSI-56. In the development of predictive models, turning parameters of cutting speed, feed rate and depth of cut were considered as model variables. The required data for predictive models were obtained by conducting a series of turning test and measuring the surface roughness and ESD data. Good agreement is observed between the predictive models results and the experimental measurements. The ANN and RSM models for ONSI-56 are compared with each other using mean absolute percentage error (MAPE) for accuracy and computational cost.

Keywords: Artificial Neural Network, Electrostatic discharge, Monocrystalline Diamond Tool, ONSI-56, Response surface methodology, Single Point Diamond Turning, Surface Roughness.

ABBREVIATIONS

ANN   Artificial Neural Network

ANOVA   Analysis of Variance

AFM   Atomic Force Microscopy

BBD   Box-Behnken Design

BPNN   Back Propagation Neural Network

CL   Contact Lens

CVD   Chemical Vapour Diamond

DTW   Diamond Tool Wear

ESP   Electrostatic Surface Potential

FDA   US Food Drug Administration

HEMA   Poly (2-Hydroxyethyl Methacrylate)

HTHP   High Temperature High Pressure

ISO   International Standard Organization

MMA   Methyl Methacrylate

MAPE   Mean Absolute Percentage Error

PC   Poly Carbonate

PCD   Poly-Crystal Diamond

PE   Polyethylene

PHEMA   Poly Hydroxyethyl Methacrylate

PMMA   Poly Methyl Methacrylate

PP   Poly propylene

UHPM   Ultra-high Precision Machining

UPHDT   Ultra-high Precision Diamond Turning

RGP   Rigid Gas Permeable

RSM   Response Surface Method

SCD   Single Crystal Diamond

SEM   Scanning Electron Microscope

SPDT   Single Point Diamond Turning

ONSI-56   Onsifocon-A

NOMENCLATURE

F   feed rate

S   cutting speed

D   depth of cut

R_a Surface Roughness

δ the estimation error

n   the total number of measurements

i   the estimated measurement for a specific run

R^2 coefficient of determination

GLOSSARY OF TERMS

A

Aspheric - property of a surface or lens deviating slightly from a specific spherical shape and relatively free from aberrations.

Astigmatism - A defect in the eye or in a lens caused by a deviation from spherical curvature, which results in distorted images, as light rays are prevented from meeting at a common focus.

B

Biocompatible – the capability of coexistence with living tissues or organisms without causing harm.

Brittle - the tendency of a material to fracture without first undergoing significant plastic deformation.

C

Cornea – the transparent anterior part of the external coat of the eye covering the iris and the pupil and continuous with the sclera

Crystalline - of or like a crystal, clear, transparent.

D

Ductile - ability of a material to be able to undergo change without breaking.

F

Freeform – a form of lens surface not organized in a planned conventional way; without restrictions or preconceptions.

H

Hydrogel – a form of lens type which liquid constituent composition is water

Hydrophilic – a form of lens which holds high affinity for water.

Hydrophobic – a form of lens or substance having little affinity for water or tending not to dissolve in, mix or be wetted by water.

M

Monomers – a molecule of low molecular weight capable or reacting with identical or different molecules of low molecular weight to form a polymer.

Moulding – the act of creating a particular shape or form from a material.

Myopia – a condition in the eye in which parallel rays are focused in front of the retina objects being seen distinctly only when near to the eye.

N

Nanometric – a term to describe measurements in the scale of study equal to one billionth of a meter and also equal to 10 Angstroms.

O

Optics – lenses or instruments pertaining to the eye or sight.

P

Polymers – a substance of high molecular weight derived by either the addition of many smaller molecules, or by the condensation of smaller molecules with the elimination of water.

Precision – In mechanical study, it is the state of scientific exactness ir accuracy.

R

Roughness – the property of a lens having a coarse or uneven surface, as from projection, irregularities or breaks. A state of been not smooth.

T

Topography – the detailed mapping or charting of the features of a relatively small are, district, or locality.

Tribo-chemical – a form of wear mechanism affecting the properties of the surface of a material by the chemical action from other elements.

Tribo-electric – a form of wear linked with negative surface effects on a material caused by static build-up.

Tribo-thermal – A condition on the surface of a material influence its makeup by the action of an external heating source on its surface.

W

Wear – a condition of a surface which infers causing deterioration or degradation of that surface.

(Adapted from [1])

LIST OF PUBLICATIONS FROM THIS WORK:

Conference paper:

Muhammad M. Liman, Khaled Abou-El-Hossein, Odedeyi P. Babatunde and Abubakar I. Jumare "*Ultra-High Precision Diamond Turning of Contact Lens Polymer*", Proceedings of the 1st International Conference of Institute of Polymer Engineers, Abuja, Nigeria, 15th-17th December 2016. PP 8-10

Poster Publication:

Muhammad M. Liman, presented a technical poster on "Single point diamond turning of contact lens polymers", at UNESCO AFRICA ENGINEERING WEEK, held at Nelson Mandela Metropolitan University, Port Elizabeth, South Africa during 28th-29th September 2016

Table Of Contents

LIST OF FIGURES

LIST OF TABLES

1 INTRODUCTION

1.1 Background and Significance

In the years since polymers introduction, contact lens technology has been expanding at a rapid rate. There have been improvements in the manufacturing techniques, as well as an increase in the type of polymer used in lens manufacturing industries. Today, contact lenses can be manufactured through spin casting, cast moulding or lathe techniques. A commonly used ultra-high precision machining (UHPM) process in contact lens manufacture is single-point diamond turning (SPDT) [2].

Single-point diamond turning is an ultra-precision machining (UPM) process for producing high quality optical surfaces on metals, polymers, and crystals. At the present-day, the UPM process of single-point diamond cutting is regarded as an effective process for the generation of high-quality functional surfaces. It produces surfaces with minimal defects in the superficial surface layer from various materials, especially thermoplastic amorphous polymers and their composition for optical, photonic and bioengineering applications [3].

SPDT has always been an important machining process throughout the history. In 1901, Carl Zeiss Company used SPDT to produce aspheric surfaces but the quality was not good enough to be used in camera lenses [4, 5]. However, in 1929, lenses having high accuracy level surface finish could be manufactured by Bausch [6]. Later, Taylor and Robson [7] developed a polar coordinate aspheric generation machine to produce high-quality camera lenses.

In spite of advances in ultra-precision turning, it is not always easy to achieve a high-quality surface finish. Lots of parameters such as machine tools, cutting tools, workpiece material and machining process affect surface quality during turning. Too many investigations have been made to optimize parameters to have a better surface finish [8].

Since polymeric materials were introduced for optical applications, diamond turning of plastics have been studied intensely. The use of contact lenses for vision correction stresses high precision and surface integrity in the nanometric ranges for functionality. Moreover, optical aberrations on these lenses caused by geometrical deviations, surface roughness and sub-surface defects resulting

from the fabrication process could greatly influence their functionality. Consequently, Heinrich in his study stressed that the design, manufacture and metrology of contact lenses is a field severely dependent on the existence and advancement of precision engineering [9].

Several researches have been made about cutting behavior of polymeric materials. Notably, Smith [10] investigated the relationship between the glass transition temperature of the polymer and the surface roughness and claimed that ductile chip is formed due to adiabatic heating with the increasing cutting speed. Then, Gubbels [11], investigated the hypothesis after turning polymers (PS, PMMA and PC) with different cutting conditions. He found that glass transition temperature is not reached in diamond turning of polymers investigated. He showed that there can be little temperature increase in primary shear zone when cutting speed increases but it is not enough to reach glass transition temperature in PC. This research contradicts the study of Smith. Gubbels also studied about the wear mechanisms during turning plastics and he found that both tribo-electric and tribo-chemical wear significantly affect tool wear during turning polymers.

Saini et al. [12] made a research about determining optimum parameters for a better surface finish during turning PC. They changed several parameters to achieve high surface quality. They suggested that 0.5 μm/rev feed rate, 2 μm depth of cut and 3000 rpm gives best results during turning and 25.4 nm average surface roughness is achieved with an old diamond tool. Furthermore, Carr and Feger [13] made a study about the material removal mechanisms during diamond turning of polymers and revealed that material and visco-elastic properties play an important role to achieve a better surface quality. They also stated that every specific material need to be analysed to have a better understanding about diamond turning of polymers.

1.2 Research Motivation

In the global optical industries, the segment of contact lenses has witnessed a sweeping transformation from being once considered lifestyle products to common eye accessories sought as a convenient and fashionable replacement to glasses.

"Transparency Market Research estimates that the global contact lens market will expand at a 7.6% compound annual growth rate (CAGR) over the period between 2016 and 2024. Expanding at this pace, the market, which had a valuation of US$9.74 billion in 2015 in terms of revenue, is

projected to rise to US$18.70 billion by 2024. In terms of volume, the market is expected to rise to 2,135.0 mn units by 2024" [14].

Due to huge global contact lens market revenue and the growing need for high quality optical lens, an increase in the performance of the ultra-high precision of polymeric contact lens material would pioneer South Africa to lead to most promising growth opportunities.

1.3 Problem Statement

In spite of advances in UHPM of polymers, it is not always easy to achieve a high-quality surface finish. Contact lens manufacture requires high accuracy and surface integrity. Surface roughness is generally used to measure the index quality of a turning process. It has been an important response due to its direct influence toward the part performance and the production cost. Therefore, developing a predictive model based on ANN and RSM to evaluating the effects of cutting parameters on surface roughness and choosing optimal cutting parameters will not only improve the quality measure but also the productivity.

In contempt of high accuracy produced in UHPM of polymers, tool wear by electrostatic discharge is another phenomenon during polymer machining. Contrary to common belief, diamond tool wear during polymer machining can have hazardous effect on final quality of polymer parts. Electrostatic charging between diamond tool and polymer causes luminescence effect on the tool surface and the cutting tool edge gets damaged. For this reason, Olufayo and Abou-El-Hossein [15] made a study about the tribological wear in SPDT of contact lens polymers. They identified that the adhesion of the tool chip around the tool dictates the presence of an electrostatic force field known as tribo-electric charging, which is responsible for tool wear and poor surface finish.

To the best knowledge of the researcher, there is limited amount of research work in polymer machining, thus, the need to examine the commercially available contact lens materials for their electrostatic charging and discharging behaviors and if these have any effect on surface roughness. Furthermore, developing a predictive model based on ANN and RSM to find the optimum relationship between cutting parameters and electrostatic discharge will reduce manufacturing cost and increase production rates in the machining of contact lens polymers.

1.4 Aim and Objectives of the Research

In this research study, the overall aim is to machine ONSI-56 contact lens polymers to optical quality and analyze the surface roughness and electrostatic discharge for saving cost and time for high production rates.

In order to achieve the above aim, five main research objectives are set as follows:

- To review the existing literature to gain an understanding of the Ultra-precision diamond turning of contact lens polymers and identify any advantages and shortcomings of the technique.
- To measure electrostatic discharge (ESD) and surface roughness for varying cutting parameters (cutting speed, feed rate and depth of cut).
- To investigate the effects of cutting parameters on the ESD and surface roughness.
- To Develop an independent predictive model for ESD and surface roughness using Response surface methodology (RSM) and Artificial neural network (ANN).
- To compare the performance of RSM and ANN Models using mean absolute percentage error (MAPE).

1.5 Hypothesis

Null hypothesis:

- An artificial neural network (ANN) and response surface (RS) model cannot be developed to predict surface roughness and electrostatic discharge (ESD) on the turned ONSI-56.

Alternative hypothesis:

- An artificial neural network (ANN) and response surface (RS) model can be developed to predict surface roughness and electrostatic discharge (ESD) on the turned ONSI-56.

1.6 Structure of The Thesis

The thesis consists of five chapters. The comprehensive details of the thesis are illustrated as in figure 1.1, which also illustrate the underlying philosophy of the chapters and their logical flow.

Chapter 1. Presents the background and the significances of the research project, SPDT of contact lens polymers, explains the motivation, Problem Statement, Aim and objectives of the research work and structure of the thesis.

Chapter 2. Review polymeric materials, contact lens manufacturing methods, critically reviews the Ultra-precision diamond turning, Surface roughness and diamond tool wear of polymeric materials.

Chapter 3. Experimental Design and Procedure. Chapter 3 provides a detailed description of the experimental setup and system process flow. It exposes the implementation methodology and equipment used during the experiments.

Chapter 4. Result and Discussion, Chapter 4 presents the various results observed and discusses the observations. This chapter also includes the development of a response surface model, and neural network scheme for predicting the surface roughness values and electrostatic discharge.

Chapter 5. Conclusion and Recommendation, Chapter 5 concludes the findings in the research and highlights suggested recommendations for future improvement on the research.

Chapter 1
- Introduction
- Problem statement
- Aims & Objectives

Chapter 2
- Literature Review

Chapter 3
- Experimental Design &
- Procedures

Chapter 4
- Results &
- Discussions

Chapter 5
- Conclusion &
- Recommendatio
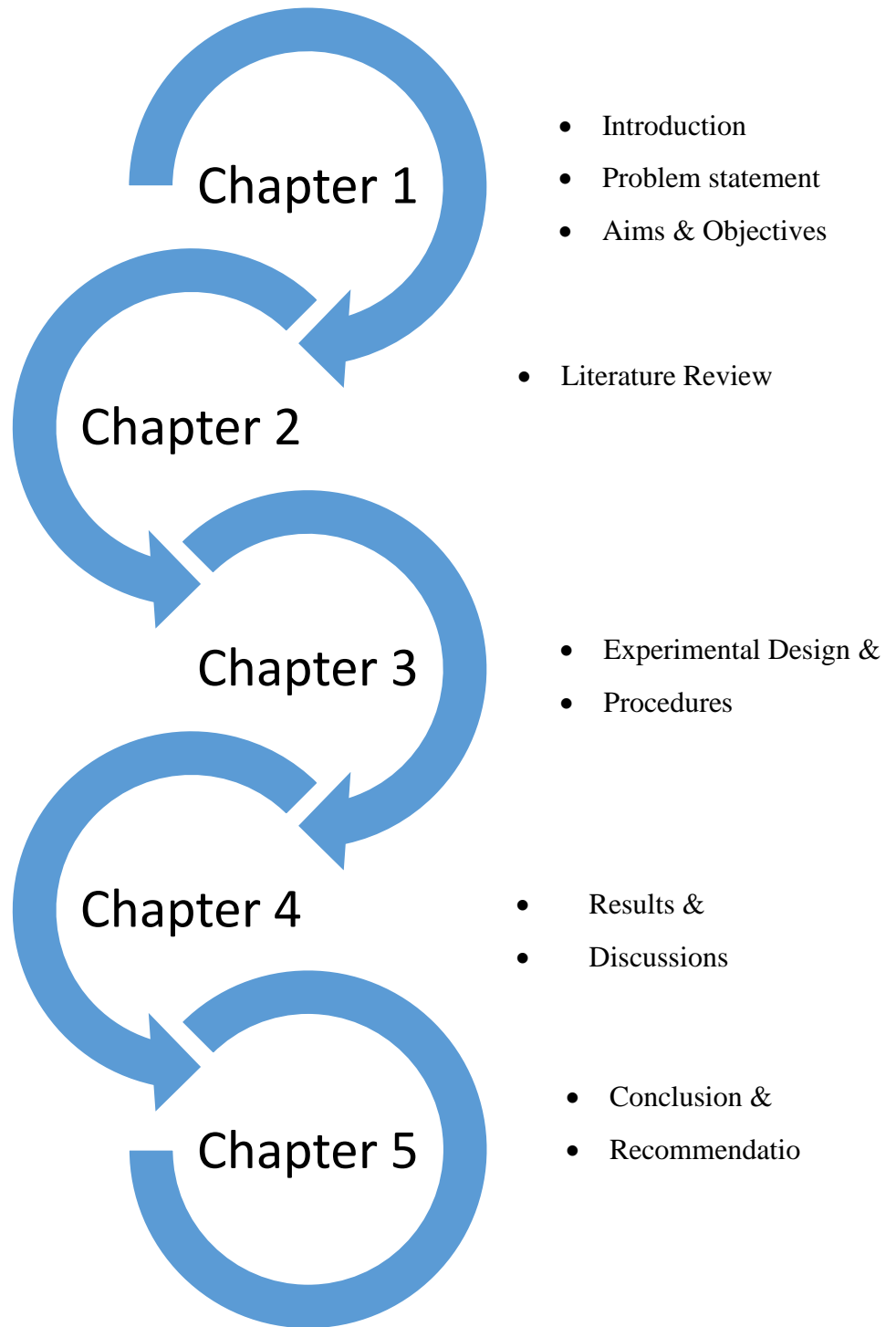
Figure 1.1:The Logical flow structure of the thesis

CHAPTER TWO

2 LITERATURE REVIEW

2.1 Introduction

In this chapter, a detailed review of polymeric contact lens materials, contact lens manufacturing techniques and ultra-high precision diamond turning using monocrystalline diamond tools are given together with the factors affecting surface roughness in diamond turning. In the following sections, the current research progress and the technical challenges regarding the study of diamond tool wear in polymer machining are introduced.

2.2 Polymeric materials

2.2.1 Polymer Fundamentals

All modern contact lens materials, since the introduction of polymethylmethacrylate (PMMA) have been based on polymer technology. In attempting to understand the optical performance of contact lenses, it is important to understand the properties these materials possess and how this is influenced by manufacturing conditions. A basic knowledge of polymer science is therefore necessary in order to allow an understanding of the bulk and surface characteristics of these materials.

Polymer is a word originated from the traditional Greek language *poly* which connotes "many" and *meres* meaning "parts.". Therefore, a polymer can be defined as a long-chain molecule that consist of a large number of *repeating units* of undistinguishable structure. Polymers can be found in nature such as proteins, cellulose, and silk, while many other polymers can be synthetically formed, examples of such are: polystyrene, polyethylene, and nylon. In some cases, naturally occurring polymers can also be produced synthetically. An important example is natural (Hevea) rubber, known as polyisoprene in its synthetic form [16].

Polymers can also be grouped as plastics (thermos & thermosetting), elastomers (rubber), fibre and hydrogels. This material has a unique property that emerged from the ability of certain atoms to link together to form stable bonds. Carbon has the ability to link together with four other atoms, such as hydrogen, oxygen, nitrogen, Sulphur, chlorine or itself. The origin of organic chemistry came as a result of the ability of carbon to act along this process.

A polymer is formed when many smaller units, called monomers, link together to form a long chain [17]. In Figure 2.1, the chemical reaction shown represents the conversion of monomer units to form a polymer chains. The fundamental requirement of a small molecule to be suitable as a monomer is the possession of two or more bonding sites, through which they can be linked together to form a polymer chain. Hence, functionality can be regarded as the number of bonding sites. Structural and functional groups (X and Y in Figure 2.1) are present along the polymer chain. This represent the way these functional groups connect with each other and their surrounding environment that influences the interaction of polymer chains and the resultant polymer properties. Polymers are regularly very long when compare with their cross sectional diameter. This gives this material another exceptional features, such as toughness or elasticity. Furthermore, these polymer chains are frequently arranged arbitrarily and are intertwined with other polymer chains. The level of interaction and entanglement gives stand out properties on the polymer, which can bring about a material transformation from that of a hard glassy material to that of an elastomeric material. A polymer can be given more elastomeric behavior with the incorporation of plasticizer. A plasticizer is a liquid (usually organic) with a high boiling point, which acts as an internal lubricant allowing polymer chains to move more freely.

$$CH_2 \!\!=\!\! CH + CH_2 \!\!=\!\! CH \rightarrow CH_2 \!-\! CH \!-\! CH_2 \!-\! CH$$
$$\quad\quad | \quad\quad\quad\quad | \quad\quad\quad\quad | \quad\quad\quad\quad |$$
$$\quad\quad X \quad\quad\quad\quad Y \quad\quad\quad\quad X \quad\quad\quad\quad Y$$
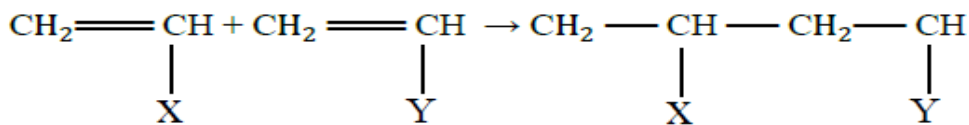
Figure 2.1 Schematic representation of monomer conversion to polymer (X and Y represent structural and functional groups)

2.2.2   Types of polymers

There are different types of polymers that are possible with a few examples shown in Figure 2.2. The simplest and most common type of polymer is one where all monomers are connected to form a long linear chain of n-monomers. For example, at certain points along the main chain, shorter chains can branch off. Or long chains could all be attached to a central monomer, forming a star pattern [18]. Meanwhile, the possible permutations do not stop here. Branches can be connected to other branches, which are linked to other branches all the way up in a very complex configuration. While it may seem like a simple thought experiment, all these possible
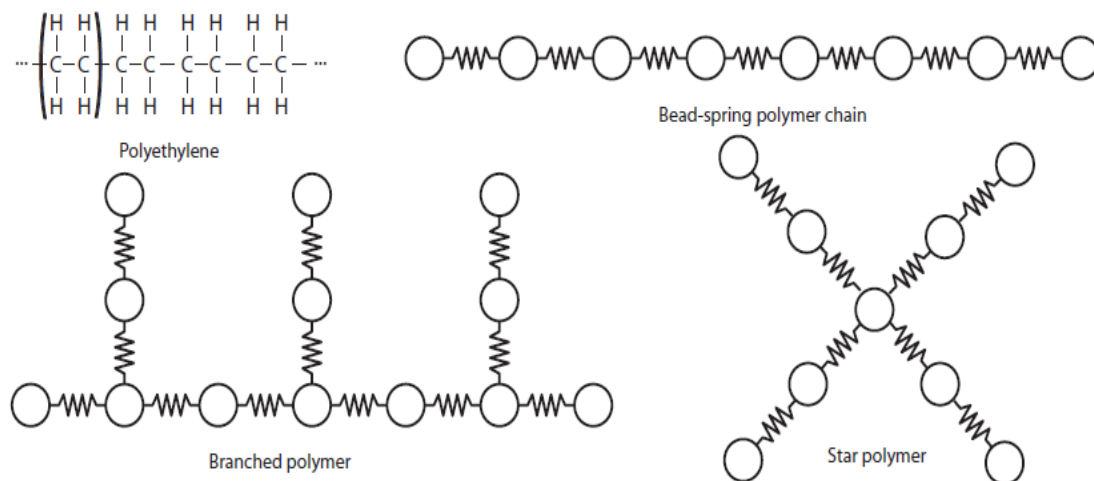
Figure 2.2: Examples of different types of polymers

branching shapes are not just the issue of theoretical interest. For a long time, Chemists have been synthesizing polymers with manageable designs, and some applications rest on the exclusive properties provided by the branching [18, 19].

2.2.3 Classification of polymers

There are two main classifications of polymers used for biomedical applications. They are, Homopolymers and copolymers. A homopolymer is a type of polymer in which all the monomer units are chemically and stereochemically identical, with the exception of the terminal units. Homopolymers can be linear (all monomers arranged in a linear sequence) or branched (non-linear) (Figure 2.3). Although chemically similar, linear and branched Homopolymers often have very different properties (e.g. high and low-density polyethylene). A copolymer is a type of polymer in which more than one type of monomer is present. For linear copolymers the monomers can be arranged in an alternating, block or random patterns, and can also form branched and graft structures (Figure 2.4). Complex three-dimensional structures can develop with a more extensive distribution of branched points, leading to highly ramified structures.

Linear homopolymer   **Branched homopolymer**

Alternating copolymer

—A—B—A—B—A—B—A—B—A—B—A—B—A—B—A—

Block copolymer

—A—B—B—B—B—B—B—A—A—A—A—A—B—B—B—
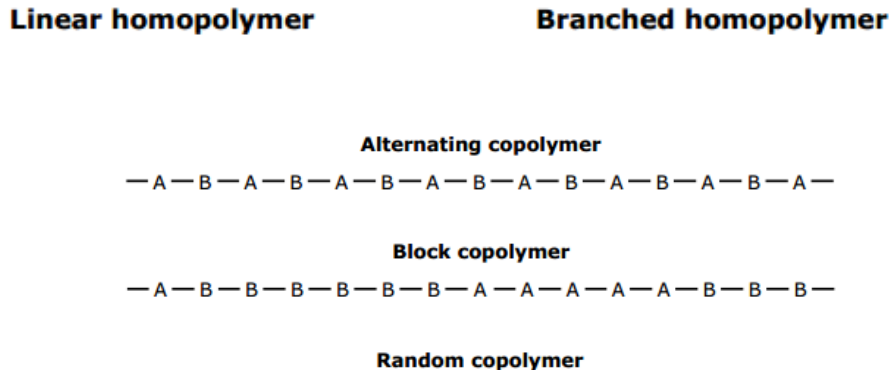
Random copolymer

Figure 2.3: Schematic representation of linear and branched homopolymer

Graft copolymer

—A—A—A—A—A—A—A—A—A—A—A—A—A—A—A—
    | | |
    B   B   B
    | | |
    B   B   B
    | | |
    B   B   B
    | | |
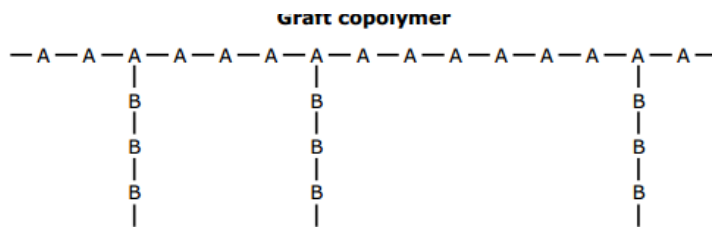
Figure 2.4: Schematic representation of alternating, block, random and graft copolymers

2.2.4 Principles of polymerization

There are two main types of polymerization reactions; step-growth (or condensation) and chain-growth (or addition) processes. In step-growth reaction, polymers are produced by the reaction of monomer units with each other, with the elimination of a small molecule such as water (Figure 2.5). Hydrogels are not typically formed through this method of polymerization but through chain-growth polymerization [17]. Chain-growth polymers are formed by the reaction of monomer units with each other, without the elimination of by-product molecules. Each monomer typically has at least one double bond and is described as unsaturated. The polymerization process is triggered with the production of free radicals (Figure 2.6(a)). These free radicals combine with the monomer, resulting in a free radical of the monomer (Figure 2.6(b)). The radical monomers combine with other monomers to form a radical compound (Figure 2.6(c)). Radical compounds can continue to propagate, resulting in a polymer chain thousands of monomers long. Polymerization does not

usually continue until all the monomers have been polymerized, as the highly reactive free radicals inevitably lose their reactivity. Termination usually occurs either by recombination (where two propagating polymer chains, each containing free radicals, meet and share the unpaired electron (Figure 2.6(d))) or disproportionation (when two radicals interact via hydrogen abstraction, leading to the formation of two reaction products, one of which is saturated and the other unsaturated (Figure 2.6(e))). Due to the reactivity of the free radicals other reactions can occur, including chain transfer and free radical combination with retarders or inhibitors [20].

$$CH_3-\overset{\overset{\displaystyle O}{\|}}{C}-OH \quad + \quad HOCH_3 \quad \longrightarrow \quad CH_3-\overset{\overset{\displaystyle O}{\|}}{C}-O-CH_3 \quad + \quad H_2O$$

Figure 2.5: Schematic representation of a condensation reaction

Figure 2.6 :Schematic diagram of the initiation, propagation and termination stages of polymerization (adopted from [17])

2.2.5 Polymers in medicine

To understand why current polymeric materials are used in medicine and to appreciate the advantageous properties they possess, it is logical to follow the evolution of polymer-based contact lens materials. Among other fields, polymers have a great influence in the medical field for purposes such as heart pacemakers, artificial valves, biodegradable sutures and biomedical contact

lenses. There are many types of polymers used for biomedical purposes. They are: Polymethyl methacrylate (PMMA), Poly (2-hydroxyethyl methacrylate) poly (HEMA), Polypropylene (PP) Poly (dimethyl siloxane) (PDMS), and Polyethylene (PE).

2.2.5.1 POLY (METHYL METHACRYLATE) (PMMA)

PMMA was the first polymer used in the manufacture of contact lenses, when it began replacing glass as the material of choice during the 1940s. PMMA is a hydrophobic, linear chain molecule that is glassy at room temperature. PMMA lenses are hard, rigid and is in many ways an excellent material for contact lens manufacture due to its toughness, dimensional stability, optical properties, ease of manufacture and physiological inactivity [17]. However, a known disadvantage of early PMMA lenses is that they did not allow oxygen to pass through to the cornea, which caused a damaging to the eye. Furthermore, the PMMA surface has relatively poor wetting properties and almost negligible permeability to oxygen, resulting in corneal hypoxia. Based on the need for biocompatible polymers, 2-hydroxyethyl-metacrylate (HEMA) soft lens hydrogel contact lens was then introduced leading to the evolution the more versatile contact lens industry with new biocompatible polymers. Soft lens hydrogels, known as water-loving polymers are hydrophilic in nature and possessed gas permeability.

2.2.5.2 POLY (2-HYDROXYETHYL METHACRYLATE) (HEMA)

A key development came in 1960 when Otto Wichterle and Drahoslav Lim based at Institute of Macromolecular Research in Czechoslovakia engineered a monomer similar to PMMA but with the addition of a hydroxyl group [21]. Due to initial problems with the cast moulding method of manufacture, a spin-casting method of production was developed, with the first soft contact lens manufactured in 1961. This new material was 2-hydroxyethyl methacrylate (HEMA). HEMA can be polymerized to make pHEMA due to its two double carbon bonds in much the same way as MMA is polymerized to make PMMA (Figure 2.7). As HEMA has this addition hydroxyl group, in the presence of water, hydrogen bonding occurs between the hydroxyl group and water molecules. The material is therefore much more hydrophilic and causes water to be drawn into the polymer matrix.

MMA monomer

CH3
|
CH2=C
|
C=O
|
O
|
CH3

HEMA monomer

CH3
|
CH2=C
|
C=O
|
O
|
CH2
|
CH2
|
OH
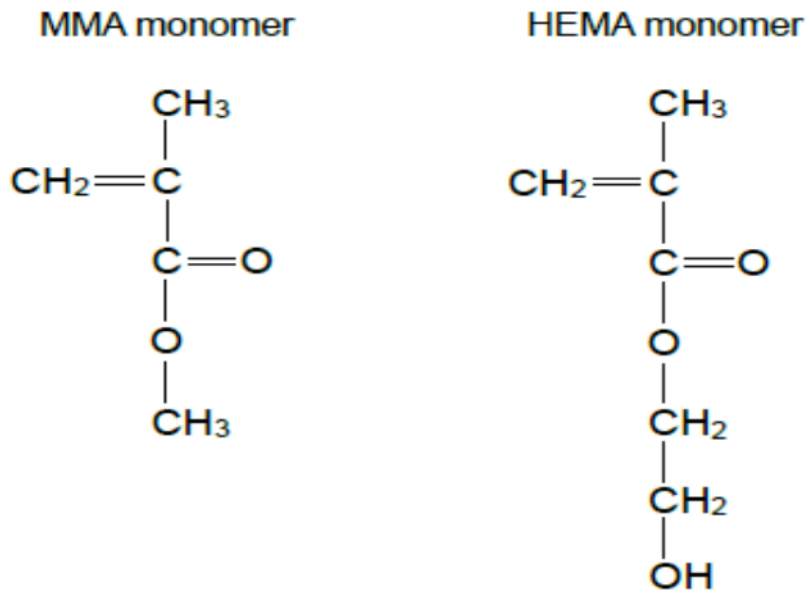
Figure 2.7: A Schematic diagram of MMA and HEMA Monomer [17]

2.3 Contact lenses

A contact lens (CL) is a prescription medical device manufactured from high-grade plastic polymers [22]. CL can be worn by people with eye disorders as an alternative to glasses. Contact lenses are considered medical device and can be worn for ocular rectification, aesthetic or therapeutic reasons. They provide a safe and effective way to visual conditions such as myopia, hyper myopia, presbyopia, and astigmatism. Contact lenses could be classified by their primary functions or material composition (Figure 2.8) [23]. Research into new types of polymers has now provided three types of material that can be used to make different kinds of contact lenses. These are called hard (created in the early 1960s), soft (created in the early 1970s) and gas-permeable (created in the late 1970s) lenses [22].

14
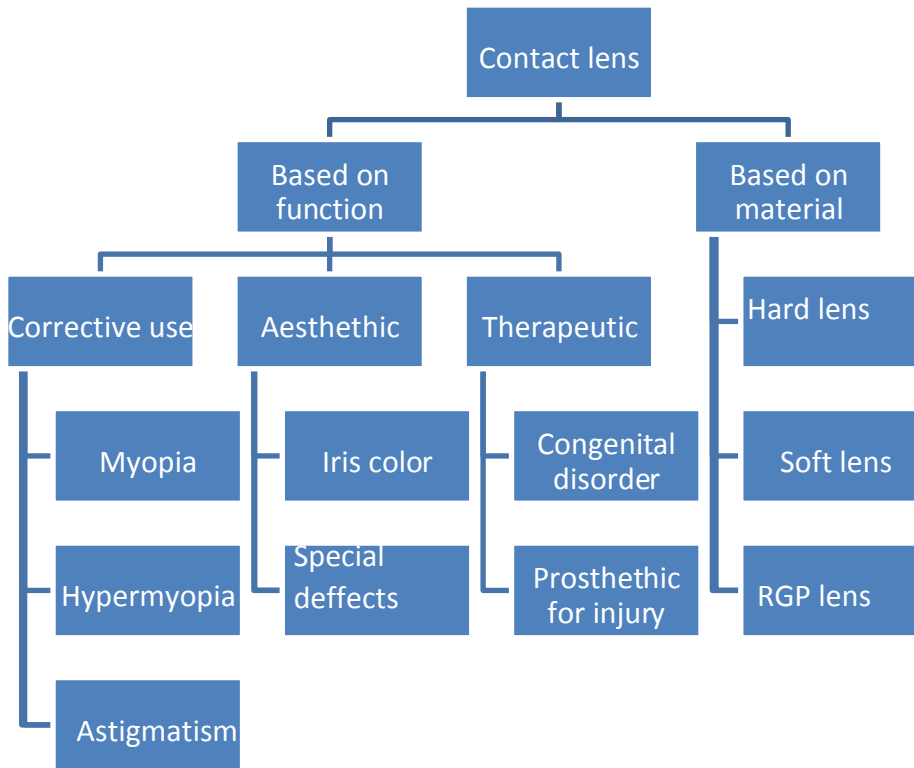
Figure 2.8:Flow chart of Contact Lens classification

A brief view of historical facts of the contact lens over the years is shown below [24]:

- 1508 Leonardo da Vinci illustrates the concept of contact lenses
- 1888 First contact lens manufactured from glass, by Adolph Eugene Fick
- 1936 Rohm and Haas create first contact lenses made from plastic
- 1948 Plastic contact lenses designed to cover only the eye's cornea
- 1965 Silicon elastomer lenses
- 1972 Introduction of soft contact lenses
- 1974 Introduction of RGP contact lenses
- 1988 Introduction of disposable soft contact lenses
- 1994 Introduction of one-day disposable soft lenses
- 1998 Silicone-hydrogel contact lenses first marketed
- 2010 Custom-manufactured silicone-hydrogel lenses become available

2.3.1 Contact lens classification

There are two general classification systems for contact lens materials which are the US Food and Drug Administration (FDA) classification system and the International organization for standardization (ISO) system for contact lens material classification.

2.3.1.1 FDA CLASSIFICATION SYSTEM

According to Leonard [17], In the United States all contact lens materials are issued with a USAN (United States Adopted Name) identity by the FDA (e.g. Onsifocon A) which is specific to the composition of the material. The material will also fall into one of the four groups for the USA Food and Drug Administration (FDA) classification scheme (Table 2.1), which offers a simple but effective subdivision of lens materials on the basis of water content and ionic character [25]. The main drawback of the FDA system is that materials composed of very different chemistry can be classified within the same material group.

Table 2.1**:** FDA Categorization of hydrogels contact lens materials.

FDA Categorisation	Group I	Group II	Group III	Group IV
Water content	Low	High	Low	High
Charge	Non-ionic	Non-ionic	Ionic	Ionic
	Low = ≤ 50% water	High ≥ 50% water	Ionic = charge	Non-ionic = No charge

2.3.1.2 ISO SYSTEM OF CONTACT LENS CLASSIFICATION

European standards have set out the ISO system for contact lens material classification (Table 2.2). Each contact lens material is classified by a six-part code: Prefix, stem, series suffix, group suffix, Dk range and surface modification code.

Table 2.2: The ISO system of contact lens material classification.

Prefix	This is one of two parts of the code administered by USAN. Use of the prefix is optional outside of the USA. For example, Etafilcon A has the USAN code 'Eta'.
Stem	Filcon for soft lenses (hydrogel-containing lenses having at least 10% water content by mass)
Series suffix	Also administered by USAN, a capital letter added to the stem to indicate the revision level of the chemical formula: A is the original (first) formulation, B the second and so on. Can be omitted if there is only one formulation.
Group suffix	
I	< 50% water content, non-ionic
II	$\geq$ 50% water content, non-ionic
III	< 50% water content, ionic
IV	$\geq$ 50% water content, ionic
Dk range	A numeric code which identifies the permeability in ranges which are considered significant in contact lens wear. 0:<1Dk, 1:1-15 Dk, 2:16-30 Dk, 3:31-60 Dk, 4:61-100 Dk, 5:101-150 Dk, 6:151-200 Dk.
Modification code	A lower case m, which denotes that the surface of the lens is modified, having different chemical characteristics from the bulk material.

2.3.2 Manufacturing of contact lenses

Contact lens manufacturing requires high accuracy and surface integrity. The manufacture of a conventional lens begins with a glass blank manufacturing and proceeds to the generation of the optical surface by various diamond shaping techniques such as polishing and grinding. Contact

lens manufacturing techniques moved from the lenses being handmade, grinding and polished, to modern day lathes where the lenses are cut with lasers to computer precision. There have been improvements in the contact lens manufacturing techniques, as well as an increase in the type of polymer used in the lens industries. There are three main methods of contact lens manufacture.

They are:

- cast moulding,
- spin casting and
- lathe lens manufacture.

2.3.2.1 CAST-MOULDED LENS MANUFACTURE

Lens manufacture by Cast-moulding involves the formation of a lens from the monomer mixture placed between two casts (Figure 2.9). The monomer is in liquid form and is introduced into a concave (female) mould, which defines the front shape of the lens. A male mould is then mated to the female mould which define the back surface of the lens. The mould is then either irradiated with ultraviolet (UV) light or placed in an oven, which initiates polymerization, resulting in the formation of a contact lens. The moulds are then disassembled and discarded and the lens is hydrated in saline, inspected, packaged and sterilized. Cast moulding method produces high quality lenses as it is the most economically viable for mass manufacture.
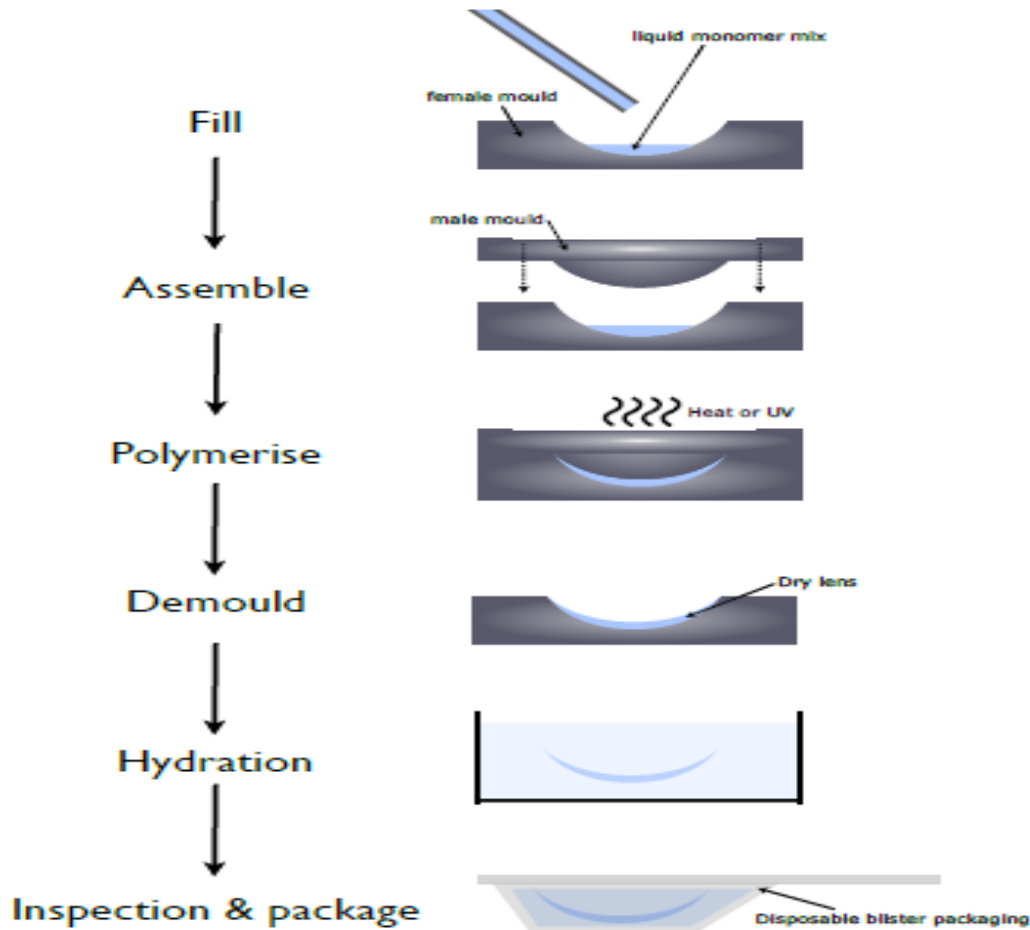
Figure 2.9: A schematic diagram of manufacture of contact lenses by a cast moulding process [17]

2.3.2.2 SPIN-CAST LENS MANUFACTURE

The spin-cast lens manufacturing method involves placing a liquid monomer in to a mold, the mold is then rotated at a computer-controlled speed, into which the mixture of monomers is injected. The monomer is then polymerized inside the rotating mold. The shape of the mould controls the front surface of the lens and the back surface is dependent on gravity, and the amount of liquid monomer in the cast. Spin-cast manufacturing is good because the lens optics can be varied by simply varying the speed of rotation or the shape of the mold.

2.3.2.3 LATHED LENS MANUFACTURE

In lens manufacture, lenses are formed from solid buttons of dehydrated polymeric material. The buttons are mounted in a lathe where the back surface is cut using a diamond tool. This newly

formed back surface is subsequently polished and a solvent then used to remove the polish. The back surface is attached to a chuck by means of melted wax and the front surface is then lathe cut and polished. Following lathing the lenses are hydrated and packaged in individual glass vials or blisters (disposable packaging). The lathing process is not well suited to mass production and is favoured for low-volume custom lenses.

At the present time, the ultra-precision machining process of single point diamond turning is regarded as an effective process for the generation of high quality functional surfaces [23]. It produces surface with minimal defects in the superficial surface layer from various materials such as thermoplastics amorphous polymers and their composition for optical, photonic and bioengineering applications [3].

2.4 Ultra-precision Single Point Diamond Machining

According to Li, in the field of precision engineering for the past several decades Ultra-precision single point diamond turning (SPDT) is one of the most important and effective technologies [26]. This is not only because the SPDT integrates many state-of-the art technologies of precision engineering, such as ultraprecision machine tool design, high speed and ultraprecision air spindle, high stiffness and ultraprecision hydrostatic slide ways, multi axis servo computer numerical control (CNC), fine polished monocrystalline diamond cutting tool, precision metrology, just to name a few, it was discovered that the SPDT technology has already been useful in a wide range of fields ranging from advanced science and technology for defense, energy, electronics applications to commercial and consumer products [26]. Ultraprecision SPDT is a skill that uses monocrystalline diamond tools and ultraprecision machine tools to manufacture mechanisms with sub micrometer form accuracy and less than a few tens of nanometers surface roughness [27].

In Davies et al work [28], they have recited Fortune's [29] statement that "Ultra precision manufacturing is doing for light what integrated circuits did for electronics" stress the importance of the precision of material removal possible using lasers. Hitherto, quite a lot of researchers have sought to define ultra-precision machining [30], a selection of which follows:

Taniguchi (1983) [31] : "Ultra-precision machining is the process by which the highest possible dimensional accuracy is achieved at a given point of time"

McKeown (1987) [32], "The role of ultra-precision machining in the manufacturing sector is to research, design, develop and commercialize processes, sensors, instruments, machines, control systems and materials in order to achieve further advances in technology, science and wealth creation".

Corbett et al. (2000) [30] : Nano-machining is "the study, development and processing of materials, devices and systems in which structure of a dimension of less than 100 nm is essential to obtain the required functional performance". In the 1980s, Taniguchi [31, 33] established a predictive map of development in precision machining, figure 2.10, which is still being practiced as we move towards 2020.
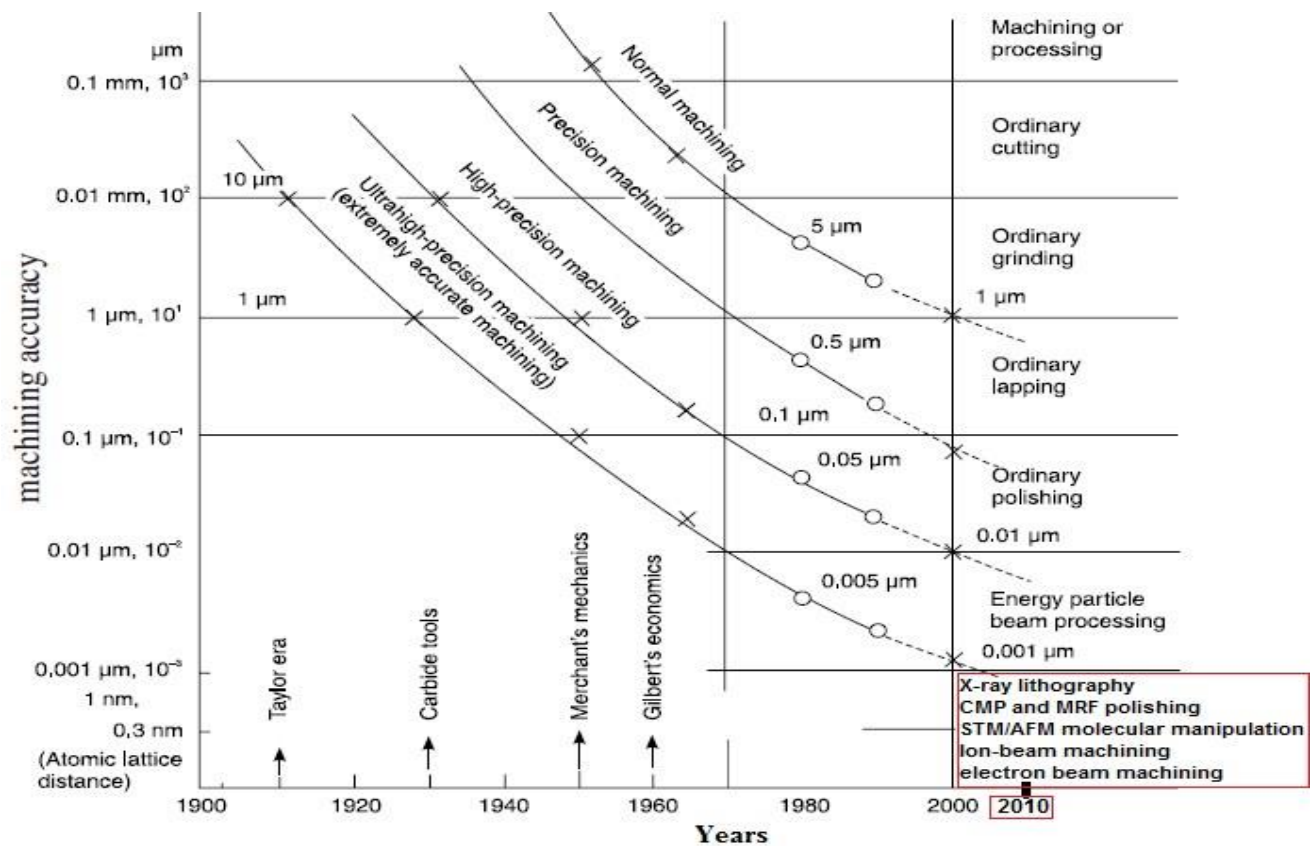
Figure 2.10 :Evolution of machining accuracy - Taniguchi's prediction's [31] updated beyond 2000 to include state-of-the-art manufacturing processes (shown in red box)

The initial work of diamond turning can be traced back to as early as the beginning of 20th century and later in World War II by Frank Cooke of Cooke Optical and several others companies [28,

34]. The development of diamond turning 1960s' was very crucial because of an increasing demand for high accuracy parts used for energy, computer, electronics and defense application [27, 34, 35]. The work was mainly completed by Y-12 (Union Carbide Nuclear Division, Oak Ridge, Tennessee) and Lawrence Livermore National Laboratory (L.L.N.L.) and these studies have become the foundation of the ultraprecision single point diamond turning technology of today. From 1960's to 1970's, the ultraprecision SPDT was mostly technologically advanced in national laboratories and a few companies and the products were used for advanced science and technology such as the optical components for NASA grazing-incidence x-ray space telescopes [26]. During this time, the main technology had been used in the diamond turning machine tool included air spindle, laser interferometer position feedback, capacitance gage, numerical control, three-axis or two-axis machining, brushless DC motor, pneumatic vibration isolators, and temperature control [36].

In the 1980's, diamond turning machine tool became commercialized and available because more and more sophisticated technology had been inculcated in diamond turning, the SPDT technology began to be widely used in industrial and commercial products. The new technologies used included hydrostatic slide ways and second rotary axis [26]. With additional demand for non-rotationally symmetric parts, such as toric lenses, a special device, which was later called fast tool servo (FTS), that was capable of small and high frequency synchronized movement with the main spindle was developed. Though the theoretical design of this device first appeared in 1976 [37], the first report of the realization of this device was in 1983 by Douglass [38] and later the device was also built by Patterson that was used on a diamond turning machine [39]. In this age the well-known products fabricated by SPDT included computer memory disk, scanner parts in photo copying machines, as well as many other early complex components.

In the last two decades ago, the SPDT technology has been rapidly advanced. The associated technologies have experienced momentous face-lifts with features such as high resolution glass scales, high speed CNC controls, high speed spindle, DC linear motor, and high precision on-machine measurement technique. The SPDT technology was quickly adopted in both industry and academia. The SPDT was an expensive process at the beginning of its appearance and was suitable for single piece or small volume production. When combining with mass production process such as injection molding and compression molding, the SPDT became appropriate for high quality low

22

cost consumer products and quickly popularized among related industries. To extend the ability of SPDT, many different technologies have also been added to the diamond turning machine, i.e. ultrasonic vibration turning [40], micro milling, raster fly cutting and grinding.

Presently, the complex multi-axis control system provides SPDT the ability to machining freeform device rather than just spherical and aspherical surfaces, both of which are axisymmetric. SPDT process has been expanded to single point diamond machining (SPDM) process, which includes several related processes as well as the more conventional single point diamond turning. The other related processes are fly cutting, fast tool servo, slow tool servo (STS)/ slow slide servo, and broaching.

2.5 Surface Roughness in Diamond Turning

Surface quality is one of the most identified customer requirements of machined parts, which is expressed as surface roughness. Surface roughness is one of the most important factors used in evaluating the quality of a lens. Thus, continuous perfection in precision machining has enabled the application of ultra-precision cutting [41], achieving high accuracy and good surface roughness. In other words, surface quality of machined components is one of the most important criteria for the assessment of turning processes.

Ultra-precision diamond turning technique is widely used in manufacturing high-precision optical lenses with a surface roughness within few nanometers range [27, 35]. The surface roughness obtained by diamond turning is determined by the type of cutting tool, the cutting conditions, the machine characteristics, machining environment and the work piece material [42].

SPDT, as an UPM process for producing high quality optical surfaces on metals, polymers and crystals [8] allows high precision aspheric optics to be produced rapidly and efficiently. However, the process is hindered by some types of errors that may occur on the machined surface – form, figure and finish or roughness (Figure 2.11). But it is difficult to say, at what point does finish error becomes figure error. Therefore, it is recommended to separate finish, figure and form error according to their causes, as this associates to the performance factors. Roughness arise due to the abnormalities, which are intrinsic in the production process (e.g. cutting tool, and feed rates). It also depends on the material's configuration and heat treatment. Figure error or waviness may

result from vibrations, chatter or workpiece deflections and strains in the material while form error is regarded as the general deviation of the surface from the intended shape, disregarding deviations due to roughness and figure error.
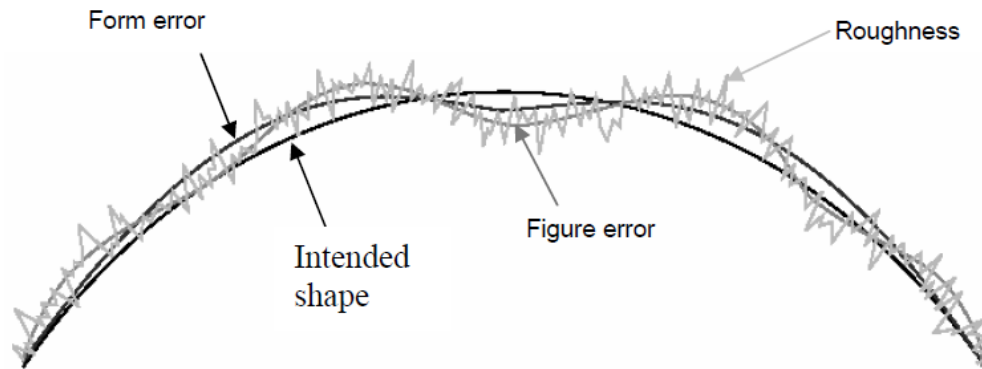
Figure 2.11**:** Three types of error arising from turning operation. Form, figure and finish [43]

Additionally, form error can be categorized into 3 types: eccentricity, higher order synchronous motion and asynchronous error motions in diamond turning [44]. Synchronous error motion is when a disturbance frequency is harmonic or multiple of the rotating spindle frequency. But when the disturbance frequency is independent, it is termed as asynchronous error motion. Reducing eccentricity can be addressed by proper bearing alignment and spindle balancing. Reducing synchronous and asynchronous errors requires attention to the airflow and geometry of the aerostatic bearing. Whereas, one way of reducing asynchronous error is to guarantee that the incoming air supply is free from pressure pulses and contaminants [8].

2.5.1   Effect of Material Characteristics on Surface Roughness

Previous researches indicate that the quality of a diamond turned surface is determined by both the process factors, which include feed rate, spindle speed, depth of cut in addition to relative tool-workpiece vibration due to machine vibration and material factors such as material anisotropy, swelling and crystallographic orientation of work materials [45]. Diverse features of materials may significantly affect the cutting process also. Tensile strength, degree of crystallization and molecular weight are also effective properties, which may govern the accuracy level of machining process [46].

Lee *et al.* [47] noted that the variation of the crystallographic orientation of the workpiece material can influence such a vibration that can lead to change in the surface modulation frequency formed in machined surface. Then, Carr and Feger [13] studied the effect of molecular weight on surface roughness. They showed that increasing molecular weight causes greater surface roughness for different PMMA grades and based on that, they inferred that cutting of polymers occurs in the thermal flow regime.

Gubbels [11], indicated that crosslink density is not a unique parameter for the determination of surface roughness, contrary to what Carr and Feger [13] mentioned that crosslinked materials cannot be turned to a high optical quality because of their brittle behaviour. Gubbels experimented different PMMA grades with changing crosslink densities and reported that PMMA grades with higher cross linked density still have optical quality and low Ra value [11]. Similarly, Zhang and Xiao [48] mentioned that viscous deformation of a polymer plays a vital role in obtaining superior surface quality. They also revealed that glass transition temperature, fracture toughness and molecular mobility are the most essential polymer properties for an optimal machining condition.

2.5.2   Effect of Temperature on Surface Roughness

Although, based on the knowledge of the researcher, there have been few studies about the relationship between cutting temperature and surface roughness, temperature rise during diamond turning may play an essential role in determining the final surface quality of a machined component. This is because temperature rise in the cutting zone may result in considerable tool wear and the change in deformation characteristics of materials, which will be diamond turned [48].

Smith [10] stated that more thermal softening arise as a result of an increase in cutting speed and better surface quality is probable when the polymer attained a thermal softening point. However, with regards to Gubbels' [11] thermal model, argued that increase in cutting speed is not that effective for a significant temperature rise in the primary shear zone. Besides, in his study revealed that with increased cutting speed, most of the heat generated during the cutting action is conveyed to the chips through heat conduction and material transport.

Lubricants also determine the efficiency of machining operations due to their lubrication and cooling properties. Kamruzzaman *et al.* [49] declared that the use of high-pressure coolant caused substantial decrease in tool wear, surface roughness and cutting forces as well as significant increase in tool life by means of temperature reduction and the change in tool-work and tool-chip interactions. Wang *et al.* [8] also stated that oil-air lubrication is more effective in reducing cutting temperature than wet and dry cutting and also helps eluding environmental pollution and reducing running and maintenance costs.

Herbert [50] experimented chip-tool interface temperature change under different cutting conditions by using a tool-work thermocouple system. He analyzed the temperature increase with the varying cutting speeds and diverse cutting fluids and revealed that temperatures increase with the increasing speed from 0.1 m/s to 1 m/s. When the results of dry cutting, cutting with oil lubricant and cutting using just water as the cutting fluid are compared, cutting with water yield the best result because water is the best heat conductor among the others. Nonetheless, water causes some severe problems such as corrosion on the machine tool and workpiece and insufficient lubrication.

2.5.3   Effect of Vibration on Surface Roughness

Vibration is a crucial phenomenon that significantly affect surface roughness generation in UPM [51, 52] as relative tool-workpiece vibration accounts for the form error in the resulting part [44]. Researches are available in offline and in-process metrology to develop new technologies in order to compensate for these errors. Tool-workpiece vibration in SPDT is usually apparent even in special machines incorporated with vibration isolation systems. Vibration in ultra-precision machine centers can lead to various form and surface errors thereby influencing the form of the resulting part. The reason of machine vibration can be attributed to a combination of the machine spindle and linear drives as well as other external impacts such as disturbances in the compressed air supply or disturbances transmitted through the ground. In a typical production environment, it is seldom not technically or economically feasible to completely isolate the machine tool from outside disturbances.

In manufacturing industry, vibration is an important parameter that affects the cutting process. Machining vibration is influenced by different sources such as structure of machine, type of tool,

work material, etc. Forced and self-excited vibrations are the known main types of the machining vibration. Unbalanced machine tool components, misalignment, bad gear drives are the main motives for forced vibration. Whereas, self-excited vibration is produced from the interaction of the chip removal method and the machine tool structure, which worsens surface quality of the machined part [53, 54].

Asiltürk [55] examined the effect of depth of cut, feed rate, nose radius, cutting speed and vibration on the surface roughness of AISI 1040 steel. He developed an ANFIS predictive model based on vibration monitoring using only the general mean vibration amplitude. Then, Sohn et al. [56] claimed that vibration is the second most important factor after feed rate, supposing good tool edge quality and proper material selection. They specified that gradual reduction of feed rate is not a practical means of getting good surface roughness since environmental and material effects control the machining operation and lower feed rates than 2 µm using a 0.5 mm radius tool do not enhance the surface quality either. On the other hand, Abuthakeer et al. [57] studied the self-excited vibration analysis of the spindle bearing. They investigated the natural frequency and vibration response of the system with the varying machining parameters – feed rate, depth of cut and cutting speed. Accelerometers were used for sensing vibration due to their versatility and ability to measure deformations and forced vibrations compared to microphones.

Similarly, Lee et al. [58] underlined the material induced vibrations because depth of cut is in micrometer in diamond turning and that is smaller than the grain size, which makes cutting process perform in a single grain. Therefore, the quality of the machined surface is greatly affected by the change of material microstructure. Chen and Chiang [53] used the rubber-layered laminates to reduce the vibration amplitude in tool-tip in diamond turning of Al6061-T6 aluminum alloy. They experimented styrene and butadiene rubber (SBR) and silicone rubber (SI) as rubber materials. They found 5.77% and 13.22% better surface roughness values by using SBR and SI respectively. The best surface roughness achieved was 0.13µm.

2.5.4 Optimization of Parameters Affecting Surface Roughness

Increasing demand for better surface quality and dimensional accuracy has necessitated the need for optimal use of cutting parameters, measuring techniques and experimental design methods in machining process. Final surface quality of a workpiece in an ultra-precision machining process

can change depending on tool parameters (nose radius, rake angle, clearance angle), cutting parameters (feed rate, depth of cut, cutting speed) and all other process parameters such as coolant, tool-workpiece interaction, machine vibration. However, achieving optimum parameters in manufacturing process is not an easy task due to nonlinear structure of the machining process. There are so many variables which can significantly affect the process. Nevertheless, the main purpose is to obtain a low surface roughness and less tool wear at a maximum production rate, minimal operational cost and high product quality [12].

To achieve that, experimental design methods, statistical methods and mathematical models have been used to analyze the experimental results. Thus, empirical relations have been found to relate surface roughness with the cutting variables. In literature, many studies have been conducted to optimize surface roughness by varying machining parameters and by implementing different experimental methods. For instance, Özel and Karpat [59] investigated the effect of depth of cut, feed rate and insert radius on surface roughness in turning of AISI 1030 steel bars by using Taguchi method. Çalı [8] studied the effect of cutting parameters and rake angle during single point diamond turning of silicon by using 23 factorial design method to optimize parameters achieving best average surface roughness of 1 nm. In the study of Aslan et al. [60], an orthogonal array and analysis of variance method were used to optimize the cutting parameters such as cutting speed, feed rate and depth of cut and final surface roughness of turned AISI4140 steel and flank wear of Al_2O_3 ceramic tool coated with TiCN were examined as quality objectives. Al-Ahmari [61] used response surface methodology and neural networks to compare and evaluate the relationship between cutting parameters and surface roughness by developing empirical models on turning of austenitic AISI 302.

Moreover, Kopac et al. [62] studied the effect of cutting speed and feed rate variations on recorded noise amplitude and found that cutting speed do not have much effect on sound vibration compared to feed rate. Huang and Chen [63] developed a multiple regression model to predict the in-process surface roughness of Aluminum 6061T2 in a turning operation by using feed rate, depth of cut and spindle speed and vibration as independent variables (input), obtained via an accelerometer on tool holder as predictors. Greater prediction accuracy level of 1.55% was obtained by using the vibration information than that of the model, which has no vibration information. Equally, Xu et al. [64] conducted another experimental study on the diamond turning of silicon, germanium and

28

aluminum alloy (Al 6061). Moore Nanotech 250UPL lathe and New view 7300 interferometers were used for that experiment. A tool of 0° rake angle has been chosen for aluminum and -25° for germanium and silicon due to different machining characteristics of the materials. The best average and rms surface roughness values measured for aluminum were 1.6 nm and 1.2 nm respectively. For silicon, the best values were 0.46 nm rms and 0.37 nm average surface roughness. As for germanium, 0.58 nm rms and 0.42 nm average surface roughness values were found to be the best. Meanwhile, Khatri et al. [65] studied the effect of machining parameters on surface roughness during diamond turning of polycarbonates. They also tried to find out the profile error to optimize tool path. During experiments, the best achieved average surface roughness value was around 50 nm. Goel et al. [66] also observed the surface roughness and waviness during machining of polycarbonate. They concluded that surface roughness and waviness are increasing with machining time. Surface roughness value of 9 nm was the best achieved from the tests. Gubbels [11] also investigated different polymeric materials and machined polymers in different cutting conditions. However, the optical quality of polycarbonate could not go under the accuracy level of 10 nm average surface roughness.

2.6 Diamond tool wear in polymer machining

Diamond has many outstanding properties, such as high hardness, great toughness, high capability up to a nanometric tool cutting edge, high thermal conductivity, low friction, and high wear resistance. Accordingly, it is employed as an efficient tool in ultra-precision machining (UPM). However, diamond tool wear (DTW) in UPM is an inevitable physical phenomenon and even a little DTW will produce a direct impact on nanometric surface roughness [67]. In contempt of high accuracy produced in UHPM of polymers, diamond tool wear is an inevitable physical phenomenon and even a little diamond tool wear will produce a direct impact on nanometric surface roughness. Gubbels [11] in his research on diamond turning of glassy polymers (PC and PMMA) identifies two dominant wear mechanisms, namely: Tribo-chemical wear and Tribo-electric wear.

2.6.1   Tribo-chemical wear in polymer machining

Chain scission of monomers which procedures some highly reactive radicals can be used to explain the phenomenon of Tribo-chemical wear in diamond turning. This chemical reaction could be

29

observed by a "chipped" effect on the diamond surface. In their research Gubbels et al. accounts wear patterns observed on PC and PMMA to chemical causes [68].

At room temperature, diamond is inert. It will not react chemically with other elements such as oxygen and Fe and not be etched by acids. However, under a high temperature, it is activated. At a temperature in the range 800–1100K, molten potassium nitrate is a commonly used as etchant for diamond. Over 900 K, diamond will have a reaction with oxygen to form CO or CO_2 [67].

In 1949, Pauling [69] presented the theory of d-electron band responsible for physical and chemical properties. Paul et al. [70] attributed chemical wear of diamond tools to unpaired d-electrons of metals. Carbon atoms are drawn from diamond lattices and then diffuse into the workpiece, graphitize, or react with workpiece to form carbides or with oxygen to form CO or CO_2. In cutting steel or iron, diamond graphitizes and diffuses [71, 72] or maybe forms iron carbide (Fe_3C) [73]

Furthermore, Gubbels et al. [68] also stated that the chain scission results in highly reactive radicals, additional to form chemical wear in diamond turning of polymers. In the monomer shown below in Figure 2.12, the ester bond in methyl methacrylate break off to combine with carbon atoms of the diamond tool under extreme temperatures resulting into a gradual degradation of the diamond tool tip (Figure 2.13).

$$C(diamond) + O_2 \rightarrow CO_2$$

$$2C(diamond) + O_2 \rightarrow 2CO$$
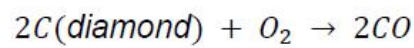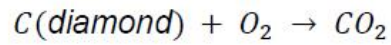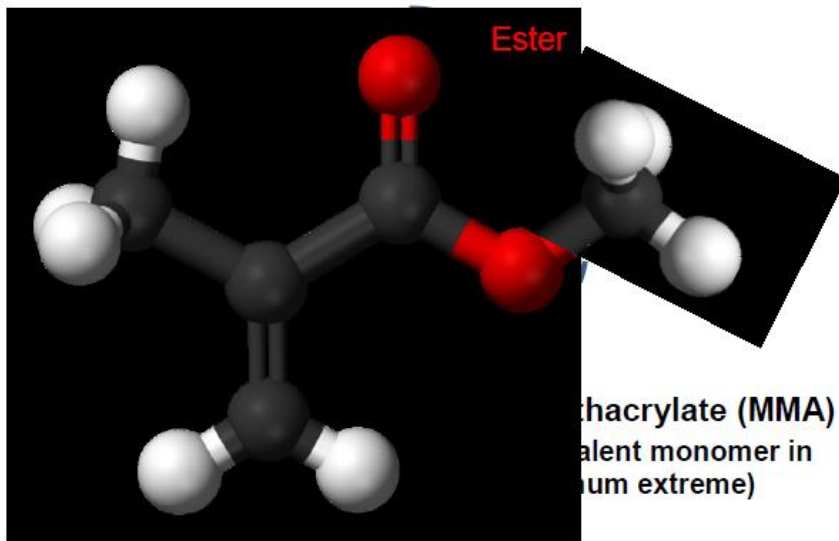
Figure 2.12: Methyl methacrylate (MMA) ester bond [23]
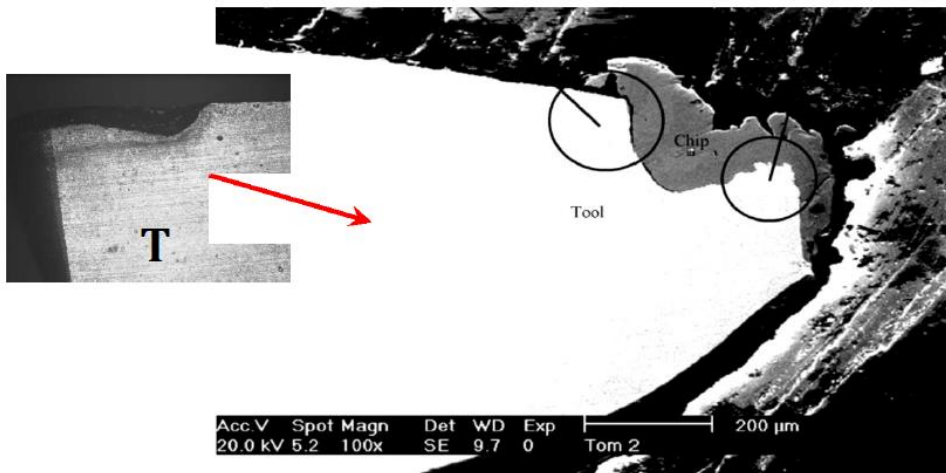
Source: Abou-El-Hossein &Yahya,

Figure 2.13: Chemical wear on a diamond tool

2.6.2   Tribo-electric wear in polymer machining

Ultra-high precision diamond turning is known to be an acceptable and suitable manufacturing method with the capability to produce freeform optics of various conventional surface profiles by

31

various researchers [28, 74]. However, during polymers machining, Olufayo and Abou-El-Hossein have identified that the adhesion of the tool chip around the tool dictates the presence of an electrostatic force field (Figure 2.14). This phenomenon known as tribo-electric charging is responsible for tool wear and poor surface finish [15].
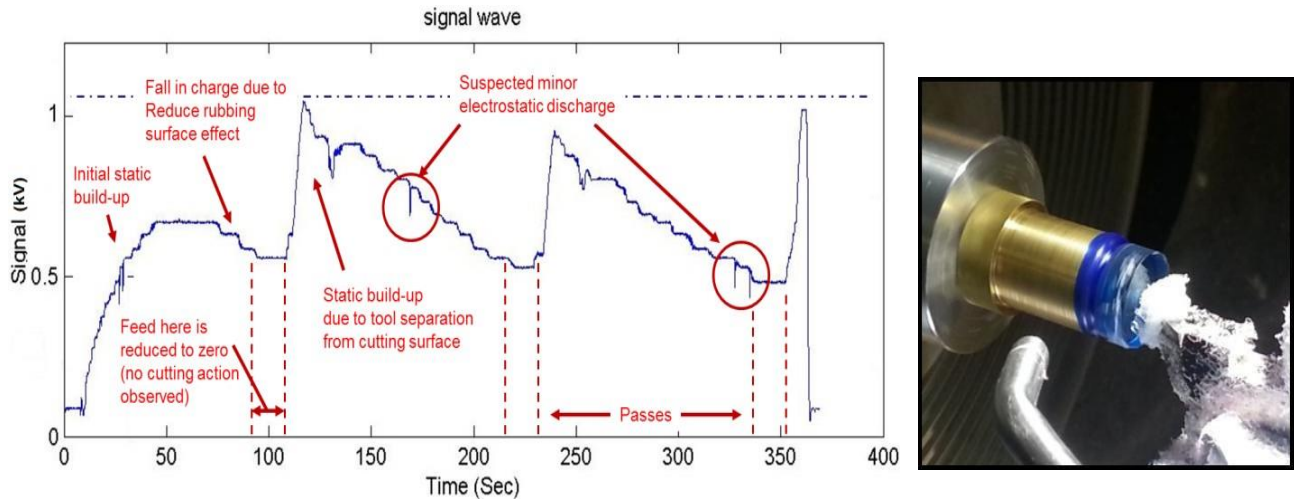
Figure 2.14**:** Basic cycle chart of static during SPDT of CL polymers and diamond chip build up [15]

The process of a charge being build up between two insulating materials due to contact or rubbing can be regarded as contact electrification tribo-charging [15]. This process can lead to surface charge accumulation resulting in an electric discharge which can be troublesome in industrial production, laboratory research and civil working activities [75, 76].

According to Zhang et al [67], Static electricity is a common phenomenon in nature. In cutting the electric insulating materials, static electricity may be takes place. The electric field can generate electrostatic discharge between two surfaces or induce lightning, plasma, and luminescence. It causes or facilitates DTW, namely triboelectric wear [11]. In industrial applications of UPM of contact lens, tribo-electric wear might occur and may become a key problem. Brezoczky and Seki [77] experimentally tested an electrostatic attractive force in diamond rubbing on hard amorphous carbon films, which creates tribo-electricity at a nanometric distance and leads to tribo-electric wear. Gubbels et al [11, 68]. measured electrostatic voltage between diamond tool and polymers (PC and PMMA) during machining and observed light emission induced by electrostatic discharge, as shown in Figure 2.15. Figure 2.16 presents tribo-electric wear of diamond tools when cutting

polymers. It was established that triboelectric wear is one DTW mechanism but does not dominate in diamond turning of polymers[70] . During wet cutting of PC, the wear is less without luminescence, but the wear pattern is the same as observed during dry cutting and cutting PMMA. The assertion that tribo-chemical wear is performed is in contrast to the work of Paul et al. [70], since PMMA and PC do not have unpaired d-electrons. Therefore, further research needs to be conducted for clarification.
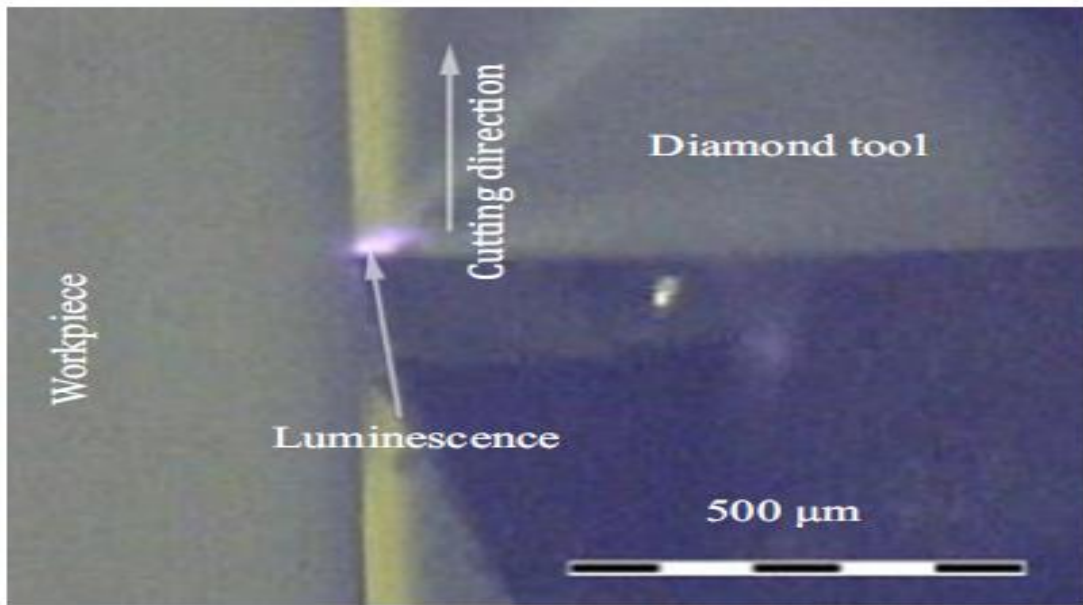
Figure 2.15: Light emission when diamond turning of PC [68]
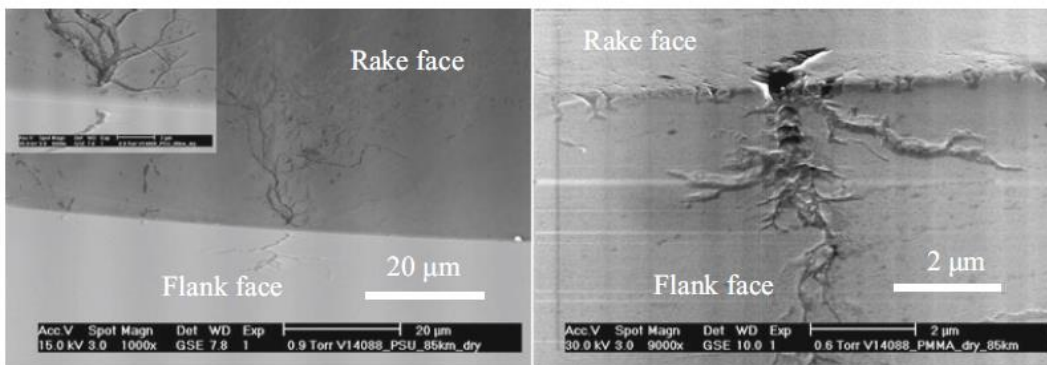
Figure 2.16: Tribo-electric wear of diamond tools when cutting polymers [11]

In 2008, McCarty and Whitesides [78] in their work, they projected that contact electrification in polymers is largely due to the partition of the hydroxyl ions from water adsorbed between the two contacting surfaces. This was challenged by Liu and Bard [79] after some times by presenting an evidence of PTFE undergoing tribo-electric charging by free electrons during contact electrification with PMMA.

Another renowned but rarely understood part of contact electrification is the effect of the environmental conditions such as humidity or atmospheric pressure. Hogue et al. [80] explored the influence of atmospheric pressure on contact charging between two insulators and put forward an established model to describe this phenomenon.

Several experiments that were conducted to investigate contact charging in higher humidity showed that water is capable of influencing the electrostatic charging behavior of polymers. In the case of Polymers, in the presence of high humidity polymers react differently, with some polymer surfaces swelling while others experienced the formation of an adsorption layer of water. A few of the polymers with swollen surfaces experienced an additional ion transfer from or into the bulk phase [81]. Therefore, it is recommended that further research needs to be carried out for clarification relating to the electrostatic charging and discharging characteristics for a wide variety of contact lens polymers.

2.7 Conclusion

In ultra-precision diamond machining (UPDM), diamond tool wear is a key factor directly and indirectly influencing surface quality of polymeric contact lens materials. In industrial applications of UPDM of lens, tribo-electric wear might occur and may become a key problem. Due to limited amount of research in this field of polymeric contact lens materials, hence, further research needs to be conducted. However, in this study, an ONSI-56 (Onsifocon A) contact lens buttons will be used to investigate the triboelectric phenomenon and the effects of turning parameters on surface finish of the lens materials.

CHAPTER THREE

3 EXPERIMENTAL DESIGN AND PROCEDURE

3.1 Introduction

In this chapter, major components used for diamond turning of ONSI-56 contact lens polymer will be explained. Firstly, experimental design methods will be introduced to find a correlation between surface roughness and process parameters. Response surface methodology (RSM) based on Box-Behnken design and Artificial neural network (ANN) will also be introduced. Comparisons among these methods will be figured out. Then, a brief description of single point diamond turning of ONSI-56 setup will be made. Later, main characteristics of diamond tool setup and system will be introduced. Lastly, the preparation of workpiece setup, electrostatic sensor setup, LabVIEW data acquisition will be mentioned and surface roughness and electrostatic discharge measurement methods will be explained.

3.2 Design of experiment

Design of experiments (DoE) is a mathematical methodology used to determine the most relevant factors in a process and provide interpretation of the results and also predict the possible results for high accuracy. It gives very producible results by minimizing the number of runs with the minimum cost [82]. DoE is also a method of systematically obtaining and organizing knowledge so that it can be used to improve operations in the most efficient manner possible and to meet specified objectives. The method has been used widely in the industry and research field for process optimization [83]. Its objective is to provide an efficient means of experimental method and analysis of experimental results [84].

The DoE techniques enable designers to determine simultaneously the individual and interactive effects of many factors that could affect the output results in any design and also provides a full insight of interaction between design elements. Experimental design is an effective tool for maximizing the amount of information gained from a study while minimizing the amount of data to be collected and is applicable to both physical processes and computer simulation models [85].

Designing experiments is centered on factors, responses, a model and runs. Design of Experiment helps designers to determine if and how a factor affects a response [86]. In machining processes,

DoE is used to generate the necessary combination of the machining parameters or conditions as inputs (independent variables) and the corresponding surface roughness as output (dependent variable). Separate set of tests are for each set of combination of machining conditions (speed, feed rate, and depth of cut) are required in order to establish an adequate functional relationship between the independent and the corresponding dependent variables. The combination matrix of these three parameters is of critical importance in determining the outcome of the machining process.

Determination of optimum parameters lies in the proper selection and introduction of suitable design of experiments (DoE's) at the earliest stage of the process and product development cycles.

DoE is extremely helpful in discovering the key variables influencing the quality characteristics of interest in the process. A designed experiment is a test or sequence of tests in which purposeful changes are made to the input variables of a process so that we may observe and identify corresponding changes in the output response.

3.2.1 Common design techniques

There exist numerous DoE techniques that have been used for different experiment purposes. The following list gives the commonly used design types [87]:

1. For comparison:
   - One factor design
2. For variable screening:
   - 2 level factorial design
   - Taguchi orthogonal array
   - Plackett-Burman design
3. Response surface methodology (For transfer function identification and optimization):
   - Central composite design
   - Box-Behnken design
4. For system robustness:
   - Taguchi robust design

36

The designs used for transfer function identification and optimization are called Response Surface Method (RSM) designs. In this study, the experiments were planned and conducted according to a Box-Behnken type response surface design using Design Expert software by considering three turning parameters (cutting speed, feed rates and depth of cuts).

3.3 Response Surface Methodology

Response surface methodology (RSM) is a collection of statistical and mathematical technique that can be used to model and analyze engineering problems in which several independent variables influence a dependent variable or response and the goal is to optimize the response [88]. RSM can be used for a variety of purposes such as analyzing of experimental, ordinal, or categorical data. Thus, it can be considered to be helpful in predicting the surface roughness and electrostatic discharge [89]. Box- Behnken Design (BBD) is one of the most popular RSM and DoE techniques used for optimization. With the combination of parameters in diamond turning of polymers, RSM Box-Behnken can be applied to polymer machining concept in response areas such as surface generation and tribological wear determination.

Box–Behnken design, is often preferred, since interaction parameter estimates are not completely confounded and in many cases, these designs are considerably smaller than 3^{p-s} fractional factorial designs [90]. Box-Behnken designs are formed by combining 2^k factorials with incomplete block designs. Figure 3.1 shows the three variable Box – Behnken design. It can be noticed that the Box-Behnken design is a spherical design with all points lying on a sphere of radius $\sqrt{2}$. Also the BBD does not contain any point at the vertices of the cubic region created by the upper and lower limits for each variable [91].

A BBD also requires only three-levels and is a more efficient alternative to the full three-level factorial. The study employs three levels (+1, 0 and -1 as high, medium and low levels respectively) and three factors, viz: cutting speed, feed rate, and depth of cut, were considered due to their combined and or individual effects on the surface roughness or on the ESD of the machined ONSI-56 contact lens. In this case, referred to as independent variables.

37
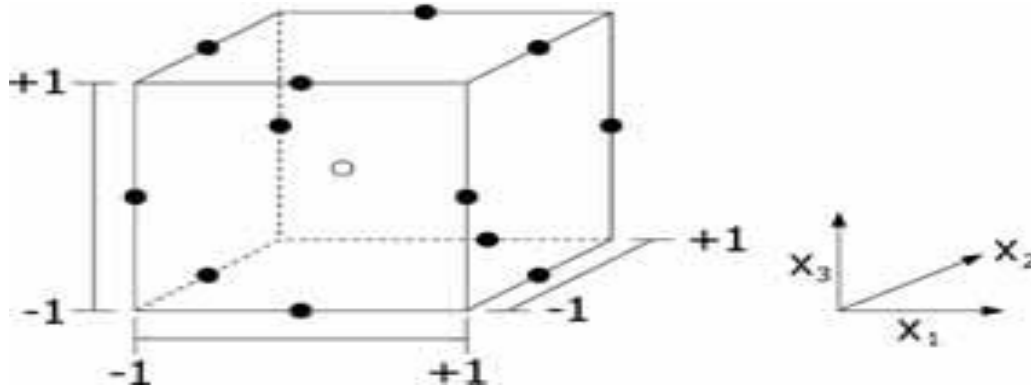
Figure 3.1: A three dimensional representation in X_1, X_2, X_3 space of a 3 Level, 3 Factor BBD [91]

In this research study, the overall main objective is to machine ONSI-56 contact lens polymer to optical quality and predict the surface roughness and electrostatic discharge for saving cost and time for high production rates. Therefore, most important factors in this machining process need to be highlighted. Different experimental methods such as multiple regression techniques, artificial neural network, full factorial designs and RSM Box-Behnken have been used to analyze the effect of machining parameters and predict the surface roughness during cutting process. Box-Behnken and Artificial Neural Network have some advantages over other methods. Box-Behnken designs can reduce the number of runs significantly and provide useful information about the process parameters. The advantages of the Box-Behnken design over other designs are such that it employs fewer design points hence it less expensive. With respect to ANN, artificial neural network is very effective if there are too much parameters to control. Complex relationships between input and output parameters can be modeled accurately and reliable and robust models can be obtained. Due to their advantages, Box-Behnken design and Artificial neural network approach will be used in this experimental study.

Finally, the relation between surface roughness of machined ONSI-56 contact lens button and cutting parameters like cutting speed, depth of cut and feed rate will be determined by using mathematical models which is obtained from DoE methods. Lastly, an analysis of variance (ANOVA) will be performed using Design Expert software to explore the significance level of parameters on surface roughness and ESD of ONSI-56 contact lens polymer. All results from experimental methods and all data collected from ANOVA studies will be given in Chapter 4.

38

3.4 Artificial Neural Network Approach

An Artificial Neural Network (ANN) is a mathematical model that tries to simulate the structure and functionalities of biological neural networks [92]. The main element of ANN is artificial neuron whose shape and size can change according to its function. A typical Artificial neural networks architecture basically consists of the input layer neurons, hidden layer neurons, the outputs and the connection weights. Basic building block of every artificial neural network is artificial neuron, that is, a simple mathematical model (function). Such a model has three simple sets of rules: multiplication, summation and activation. At the entrance of artificial neuron, the inputs are weighted that means, every input value is multiplied with individual weight. In the middle section of artificial neuron is sum function that sums all weighted inputs and bias. At the exit of artificial neuron, the sum of previously weighted inputs and bias is passing through activation function that is also called transfer function (Figure 3.2)
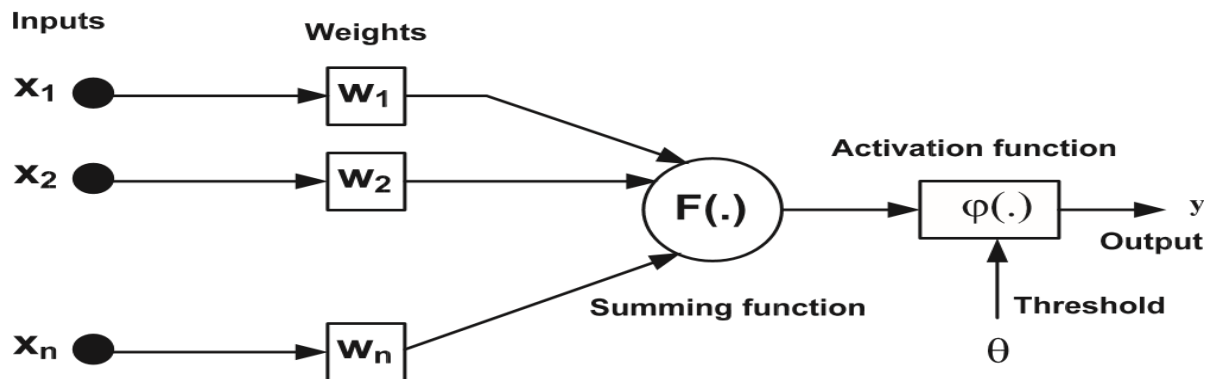
Figure 3.2: Working principle of an artificial neuron [93]

The most powerful feature of ANNs is their ability to learn [94]. the ANN uses learning algorithms that change its connection weights and cause the network to learn the solution to a problem. The connection strength between the neurons is stored as a weight-value for the specific connection. The system learns new knowledge by adjusting these connection weights. The learning ability of a neural network is always determined by its architecture and by the algorithmic method chosen for training. There are formally two types of learning in artificial neural networks. The supervised and unsupervised learning.

3.4.1 Supervised learning, as the name implies, refers to learning with a supervisor or teacher. The teacher represents the ANNs input-output pairs, providing the network with a desired response to the training inputs. The network will learn by adjusting its weight until the desired output known by the teacher is reached. In this way, the difference between the actual response of the network and the desired response known to the teacher is iteratively calculated. The most popular algorithm of this kind of network is the Back Propagation Network. This algorithm iteratively minimizes the network error by filtering back in the opposite direction information about the error through the system. In this way, the connection weights between the layers are adjusted, thus improving the performance of the network.

Back propagation neural network is the most popular algorithm that has been used in most research and many industrial applications, especially in control applications. The technology is used for decision making, diagnosis, control and predictions [94].

3.4.2 Unsupervised learning: In this method, there is no external teacher who manipulates the network weights from outside the network, in contrast to supervised learning. The training set of unsupervised learning consists of input training patterns only. The network learns to adapt the inputs based on the experiences collected through the previous training patterns. Subsequently, the network forms its classification and organization from the input pattern. The Self-Organizing Maps (SOM) or Kohonen network is the most popular algorithm for this particular type of learning.

In this study, neural network toolbox from Matlab (8.1.6) software with a 3-layer feed-forward Back propagation network with sigmoid hidden neurons and linear output neurons will be used to predict surface roughness and electrostatic discharge. The same data set which is prepared for Box-Behnken design will be used as input data set of the ANN. Thus, feed rate, depth of cut, and cutting speed are used as input layer parameters. The surface roughness will be used as output layer of the ANN. A single hidden layer of different number of neurons will be implemented. The behaviors of networks with varying number of neurons would be tabulated in Chapter 4. The prediction values for testing data which has never been trained before, would also be tabulated and compared in Chapter 4.

3.5 Ultra-High Precision Diamond Turning of Contact Lens Polymers

Ultra-high precision machining (UHPM) of polymers is an aspect of polymer machining still at its early stages since polymeric materials were started to use in optical applications such as contact lenses, diamond turning of plastics have been intensely used. At present, diamond turning can be readily applied to a wide range of metallic alloys, polymeric materials, and precious crystals. A commonly used ultra-high precision machining process in contact lens manufacture is Single point diamond turning (SPDT) [2].

Single Point Diamond Turning is an ultra-precision machining process for producing high-quality optical surfaces on metal, polymers, and crystals. At the present day, the ultra-precision machining process of single point diamond cutting is regarded as an effective process for the generation of high quality functional surfaces. It produces surfaces with minimal defects in the superficial surface layer from various materials especially from the thermoplastic amorphous polymers and their composition for optical, photonic and bioengineering applications [3]. In diamond turning, work piece is pulled onto a vacuum chuck, whose surface quality is within a few fringes, the spindle rotates with high precision with the help of air bearings, the tool is numerically controlled and a laser interferometer monitors its movements. A submicron level dimensional accuracy and nanometer level surface roughness can be achieved by diamond turning with a single point cutting tool.

In this research, Precitech Nanoform® 250 ultra-grind four-axis diamond turning machine is used as shown on Figure 3.4 and the specifications of the machine are given on Appendix A. This precision machine is equipped with 4-axis capability, vacuum chuck, ultra-high precision air-bearing spindle, granite base, oil hydrostatic slides and optimally located air isolation mounts. Therefore, the research experimental tests were carried out on Precitech Nanoform® 250 ultra-grind machine. The machine is sufficient for machining of flat, spherical, aspheric or diffractive optical surfaces.

Figure 3.3: Nanoform® 250 ultra-grind Precision Diamond Turning Lath at Precision Engineering Laboratory, Nelson Mandela Metropolitan University

3.5.1 Mono-crystalline Diamond Tool Setup

Diamond is a nearly ideal tool material for ultraprecision machining of polymers due to its high hardness, strength, thermal conductivity, and its ability to be honed to a very sharp edge and retain this edge while machining. Table 3.1 summarizes the properties of diamond. Its only shortcoming is that diamond has chemical affinities with certain materials like iron and the fact that it breaks down under high temperatures [44].

In Ultra-high precision Diamond turning, the selection of cutting tool is very important. Final surface quality is affected by several error sources such as tool setting, tool waviness, fixturing, and environmental conditions [8]. However, proper selection of tools can decrease such kind of errors and production costs can also be decreased by choosing appropriate turning parameters. As mentioned in the literature, tool parameters can also affect the final surface roughness of machined

parts. Therefore, suitable tool parameters were chosen according to experiments reported in the literature, manufacturer's suggestions, and wealthy experience of my supervisor to ensure that the turning parameters chosen do not damage the tool.

Table 3.1**:** Properties of Diamond [95]

Symbol	C
Atomic Number	6
Atomic Weight	12.011
Hardness	7000 Knoop Hardness (WC=2100 Knoop Hardness)
Density	3.51 g/cm3
Most Common Valence	+4
Electron Configuration	$1s^2 2s^2 2p^2$
Melting Point	>3550 0C
Bonding Type and Energy	Covalent; 713 *kJ/mol*
Mechanical Properties	E= 1035 GPa
Electrical Conductivity	10^{-14} [$(\Omega\text{-m})^{-1}$]
Thermal Conductivity	2000-2500 W/m-K
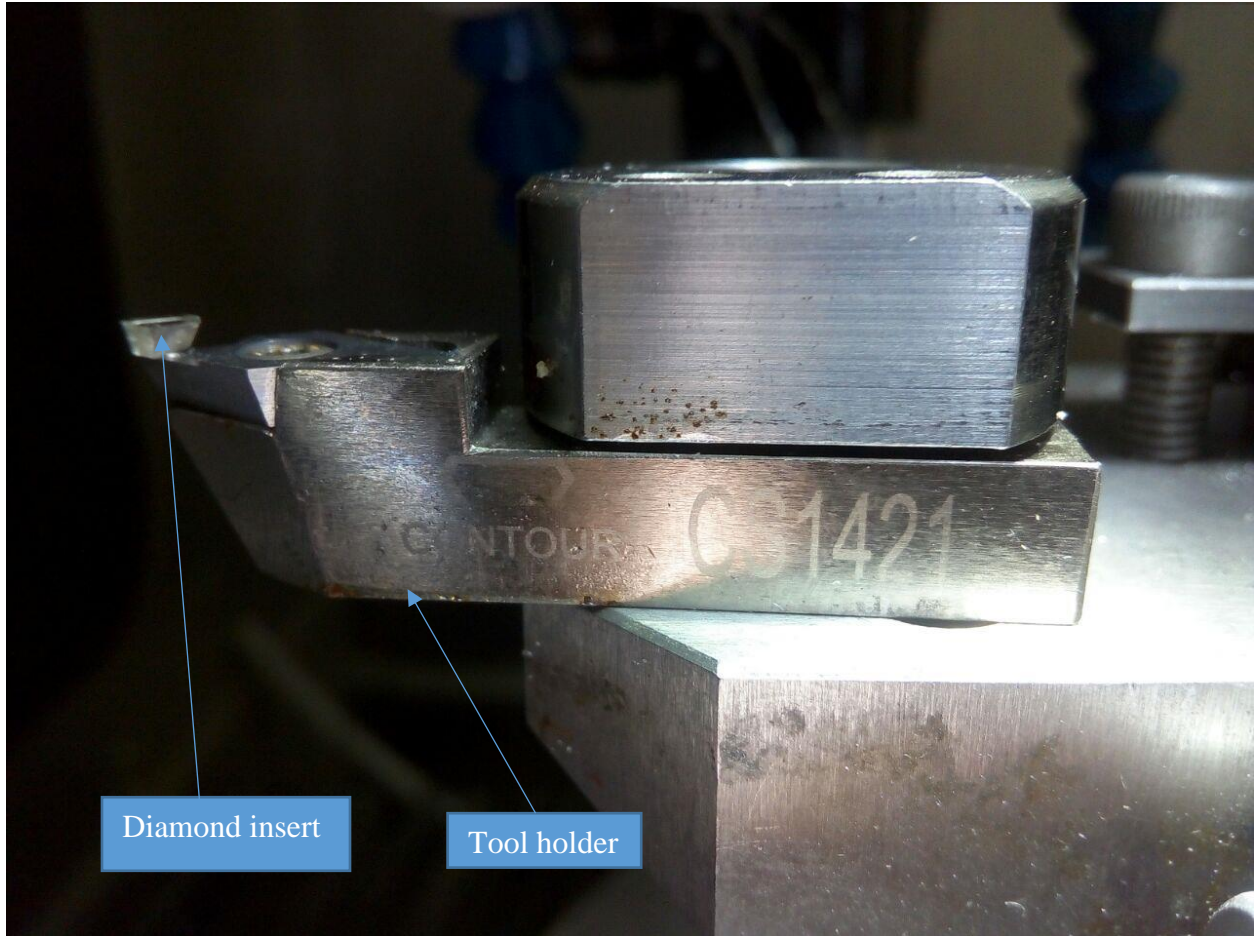
Figure 3.4**:** Mono-crystalline diamond tool mounted on a tool holder for ONSI-56 Machining

In this study, mono-crystalline diamond tool was used to machine ONSI-56 specimens with 0.5mm nose radius. In manufacturer's catalog, the suggested rake angle is 0, hence, this tool rake was used throughout the experiment. The monocrystalline diamond tool is mounted on a tool holder (Figure 3.5) by means of M5 screws. The sample tool number on the tool is shown in Figure 3.5.

3.5.2   Work-piece

Before implementing this experiment, first of all a hydrophilic rigid gas permeable contact lens buttons called ONSI-56 (Onsifocon A) 12.70 mm x 4.40 mm was purchased from Lagado's flagship Corporation Company (Figure 3.6). Experimental tests were conducted using ONSI-56 commercially available contact lens buttons. The ONSI-56 (Onsifocon A), is a contact lens polymer of trifluoroethyl methacrylate polymer with tris (trimethylsiloxy) methacryloxypropylsi lane 3-trimethoxysilylpropylmethacrylate methacrylic acid 1,3-bis (3-methacryloxypropyl) tetra

kis (trimethylsiloxy) disiloxane ethylene glycol dimethacrylate 2-hydroxyethylmetbacrylate N-vinylpyrrolidone [96]. "ONSI-56 has increasingly become the material of first choice as both a problem solver in overcoming lens comfort issues and as a problem preventer by offering patients excellent oxygen delivery and a superior hydrophilic surface" [96]. Table 3.2 shows the physical properties of ONSI-56 contact lens polymers.

Figure 3.5: The ONSI-56 (Onsifocon A) Contact lens bonnets used for this experiment

Table 3.2: The physical properties of **ONSI-56** (Onsifocon-A) [96]

Typical Property	Test Value
Hardness	D/86 (Shore Hardness Units)
Water content	<1.0%
Wetting Angle	7.25' ± 1.55 (sessile drop method)
Oxygen Permeability	56.2 ANSI units
Dimensional Stability	Stable
Refractive Index	1.452
Specific gravity	1.206
Flexural strength	3952 psi

3.5.3   Data Acquisition System

The electrostatic discharges encountered by a cutting tool wen diamond turning of contact lens polymers are important as they reflect the quality and condition of the tool, machine, fixture, and the finished surface. The use of an electrostatic sensor is critical and allows for easy monitoring electrostatic effects and the cutting process. The data acquisition system (DAQ) used for this study is NI myDAQ (Figure 3.7). NI myDAQ is a low-cost portable data acquisition (DAQ) device that uses NI LabVIEW-based software instruments, and is used to measure electrostatic signals in this experiments. A PC using 'National Instruments' (NI) LabVIEW software is used to collect the electrostatic discharge data. The NI LabVIEW allows the manipulation of the incoming signal to provide a graphical overview of the changes in the statics of the contact lens material. Figure 3.8 shows the experimental process flow diagram.
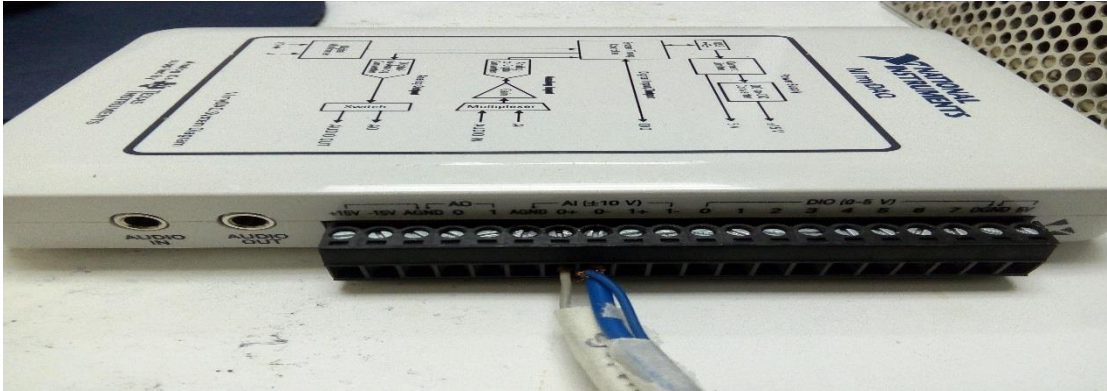
Figure 3.6**: NI** myDAQ, at the Precision Engineering Laboratory, Nelson Mandela Metropolitan University
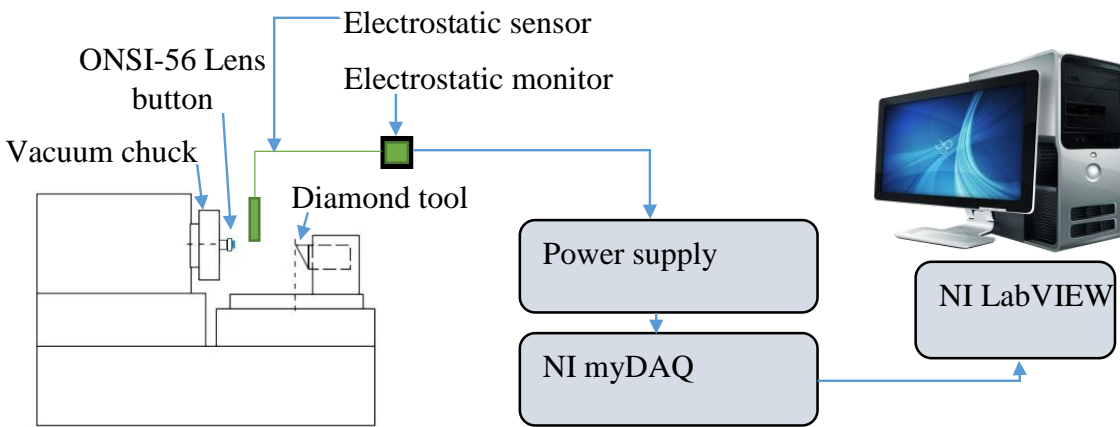
Figure 3.7: Experimental process flow diagram

3.5.4   Data Acquisition Software: NI LabVIEW 2015

The National Instruments LabVIEW is an acronym for Laboratory Virtual Instrument Engineering Workbench. It is a visual programming language used in this study for electrostatic data acquisition and monitoring. The NI LabVIEW consist of a front panel for viewing the ESD signal output in real time and a block diagram section for developing the G-code programming for the data acquisition (Figure 3.9). The programs created by LabVIEW are called VI, or virtual instruments.

For data acquisition, the NI myDAQ Assistant was used to match the physical channels from the USB or PCI data acquisition system to input channels in the VI. For reading the saved measurements from the data acquisition program, the same program is used by replacing the NI myDAQ Assistant VI with the Read LVM File VI.
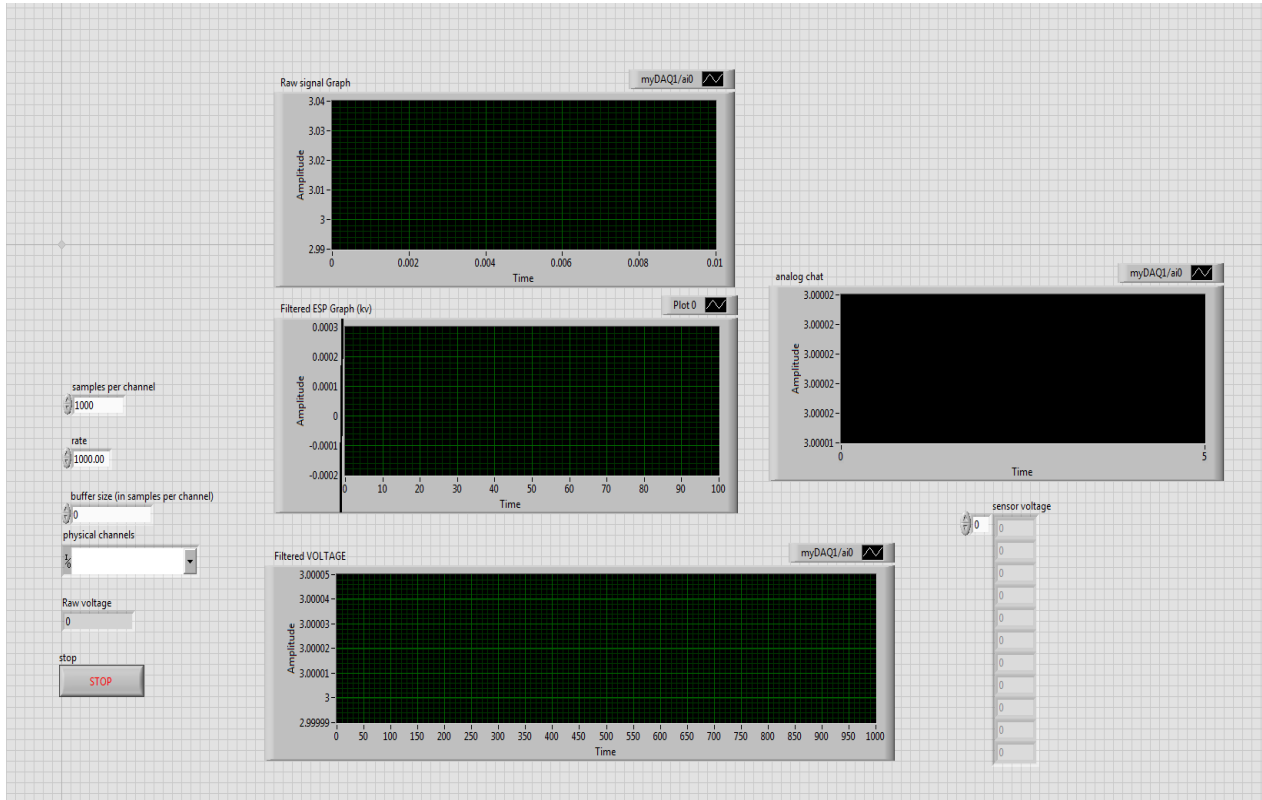
Figure 3.8**: NI** LabVIEW programme (front panel) for ONSI-56 Machining

3.5.5   Electrostatic Sensor Setup

Electrostatic sensor consists of the sensor head and sensor amplifier (Figure 3.10). The relation between the output voltage of the electrostatic sensor and detected charged electricity depends on the distance between the sensor head and measured object. Table 3.4 shows the relation between the output voltage of the electrostatic sensor and detected charged potential based on installed distance. The ESDs on the polymeric contact lens material were measured using an SMC IZD10 electrostatic sensor and ESD monitor configuration. The IZD10 sensor has a measuring range of +/-20Kv. The electrostatic sensor is connected to an electrostatic monitor which provides an output scaled using Equation (3.1) and ranges between 0V and 5kV. This output is connected to a computer running NI LabVIEW software through NI myDAQ. The sensor and the NI myDAQ are

48

powered by an S-100-24 supply. The input of the power supply was set at 220V with the output voltage stepped down to 24V with reference to ground.
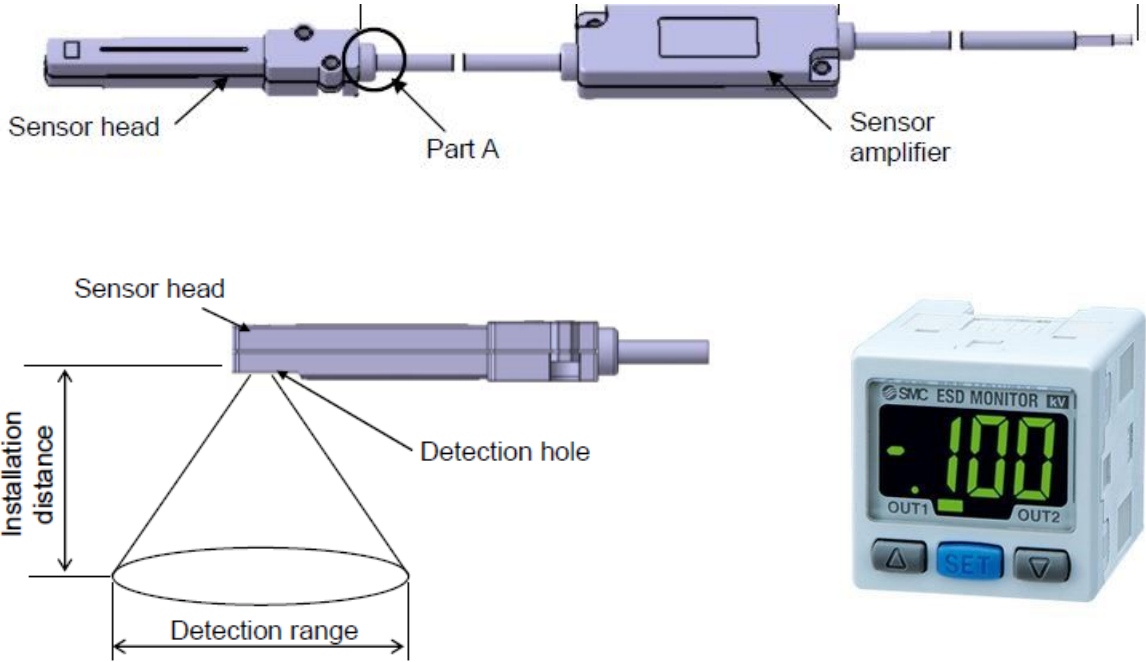
Figure 3.9: Electrostatic sensor head, sensor amplifier and ESD Monitor [97]

Table 3.3: Sensor installation distance and detection range

Installation distance (mm)	Detection range (mm)
10	45
20	85
25	100
30	120
40	150
50	200

The output measurement varies according to the installation distance as shown in Figure 3.11. In this study, the electrostatic sensor and the monitor were calibrated with the aid of the manufacturers separation manual (Appendix C), based on the detection range of 100 mm, an installation distance of 25 mm was selected as it can provide accurate representation of charge potential on the material surface considering 12.70 mm diameter contact lens buttons used. Figure 3.5 shows how the output of the electrostatic sensor varies with the actual charged potential observed on the material surface at installation distance of 25 mm during the calibration of the sensor.
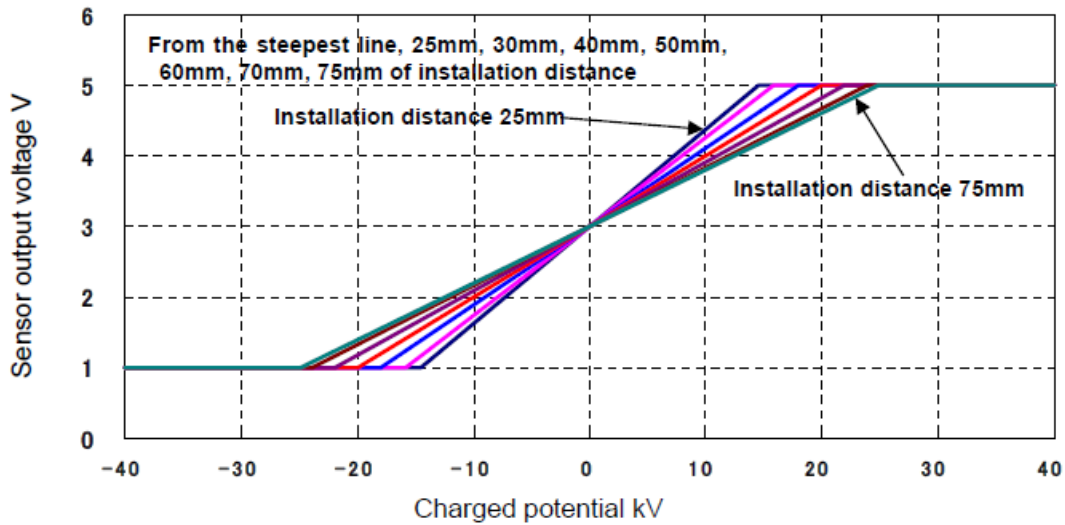
Figure 3.10: Relationship between sensor output and charge potential on installation distance [97]
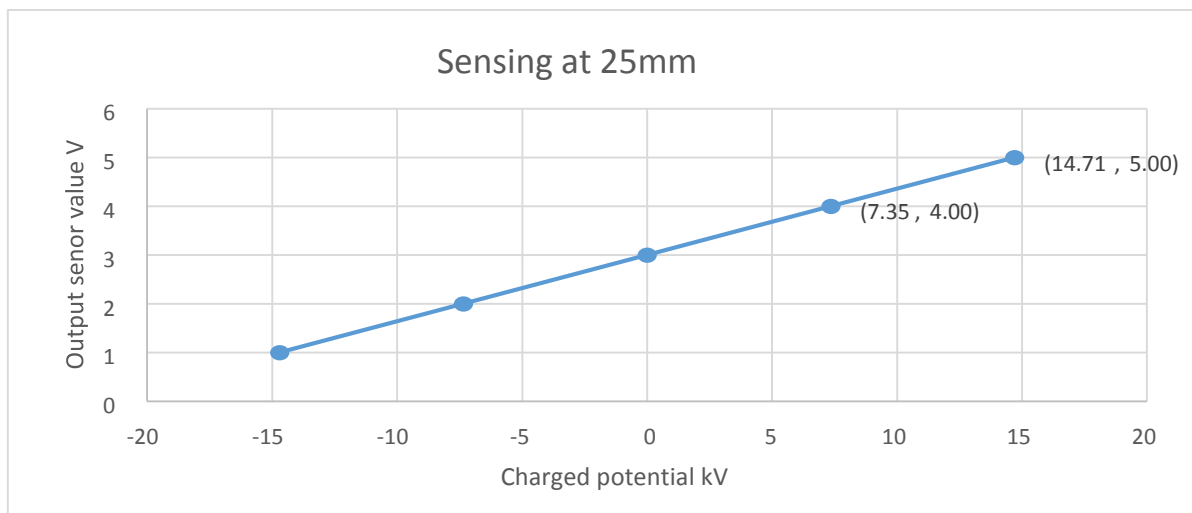
Figure 3.11: Electrostatic sensor Output versus actual charged potential

Figure 3-11 Shows how the output of the electrostatic sensor varies with the actual charged potential observed on the material surface. From Figure 3.11, the y-intercept is 3V while the gradient is 0.136.

$$y_0 = 0.136y_a + 3 \tag{3.1}$$

Where y_0 represents the electrostatic sensor output and y_a represents the actual ESDs observed by the electrostatic sensor. Equation (3.1) is manipulated such that y_a is the subject of the formula.

$$y_a = 7.353y_0 - 22.059 \tag{3.2}$$

Equation (3.2) is used in LabVIEW to scale the sensory output and provide the actual ESDs.

In this experiments, oscilloscope was used to check the continuity of voltage signals between the NI myDAQ and the sensor over time. During the sensor calibration, an oscilloscope measuring device provide graph of signals voltage over time. The Y-axis of the oscilloscope represents the voltage while the x-axis represents the time. The oscilloscope was adjusted so that the repetitive signals was observed as continuous waveform on the screen.

3.5.6   Cutting Parameters in the UHPM of Contact Lens Polymers

In this study, the turning parameters (cutting speed, feed rates and depth of cuts) were chosen based on [8, 11, 15]. As mentioned in the literature, tool parameters can also affect the final surface roughness of machined parts. Therefore, suitable tool parameters are chosen according to experiments in literature, manufacturer's suggestions, and wealthy experience of my supervisor to ensure that the turning parameters chosen do not damage the tool.

These turning parameters were chosen to encompass the research material and provide results with reasonable readings of electrostatic discharge. Parameters that were known, from previous research, to provide unfeasible data were ignored hence forming the ranges provided in table 3.5 below. The turning parameters were imported to Design of experiments software and process the runs combination using Box-Behnken Response surface methodology.

Table 3.4: Turning Parameters used for the experiments

Turning Parameters	Low	High
Cutting Speed (rpm)	200	4000
Feed rate (mm/min)	2	12
Depth of cut (µm)	10	40

During tests, turning parameters shown in table 3.5 were used. Very low cutting parameters within close ranges were utilized to suit parameters needed in high end optics. This was a balance obtained between surface integrity and tribo-electric effects in polymer cutting.

3.6 Measurement of Surface Roughness

3.6.1 Contact lens surface topography

Surface topography is a property which describes the shape and features of the polymer surface. It is known to be an important property for contact lens materials, particularly with respect to optical quality, adhesion and biocompatibility [17]. Surface topography can be characterized directly using an instrument such as an Atomic force microscopy (AFM) or indirect by imaging using an instrument such as scanning electron microscope (SEM). Very few materials possess a surface which is atomically fat, with the majority of materials exhibiting surface features such as steep gradients, pores and imperfections. These features constitute the topography of the surface and can have a considerable impact on a material's performance [98]. Soft matter when relaxed will form surface undulations, known as capillary waves, as a result of the inherent entropy of the system balancing the increased energy of the greater surface area [99]. This effect is particularly important in soft hydrogel materials as they have a compliant nature and relatively low surface energy. For polymeric materials such as ONSI-56, the molecular size [100] and the presence of two or more phases at or near the polymer surface can also influence the topography of the surface [98]. Other factors such as material processing (e.g. the transfer of a defect from the mould to the surface profile of the moulded item) or rheological effects during manufacture [101] can also influence surface topography. The surface topography of a biomaterial has been shown to influence several key factors. Figure 3.13 shows the main components of the surface topography.

Adhesion

The adhesion between one surface and another depends on factors such as the degree of chemical interaction between the two components, the proximity and the area of contact. The last two factors are dependent on the topography of the two surfaces to be joined [98].

Optical finish

The optical finish of the contact lens is directly linked to its surface topography [102].

Biocompatibility

The surface topography has been shown to strongly influence its interaction with biological components [103]. In the context of contact lens materials, surface topography has been shown to influence factors such as optical performance [104], bacterial adhesion [105] and tear film deposition [106]. Several types of instrumentation are available for analysis of surface topography. These can be split into contact and non-contact techniques.
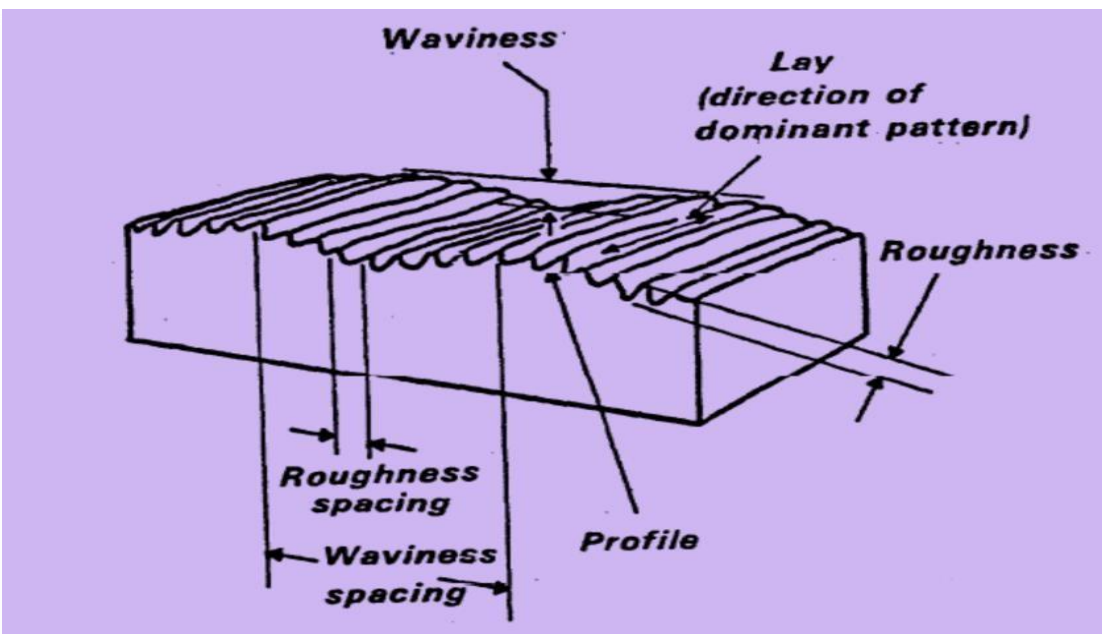
Figure 3.12: Surface characteristics and Terminology (adapted from [107])

During machining, it is inevitable to have some defects and the impurities on the surface of the machined parts. Workpiece material properties, machine vibrations, surface damage due to chip formation and inaccuracy of spindle and tool holder can cause such defects on the surface and the surface roughness is the results of all these irregularities [108].

In this study, Taylor Hobson PGI Dimension XL surface Profilometer shown in Figure 3.14 is used to measure the surface roughness of the finish-turned ONSI-56 contact lens buttons.

The Taylor Hobson PGI Dimension XL features [109]:

- 300 mm diameter capability
- Fast stylus trace speed of 100 mm/s
- Automated 3D measurement
- Automated centre and level
- Class leading accuracy and repeatability
- Enhanced roughness measurements of up to 0.2 nm resolution
- Steep slope surfaces of up to 85 degrees
- Taylmap advanced analysis with excellent report building tools.
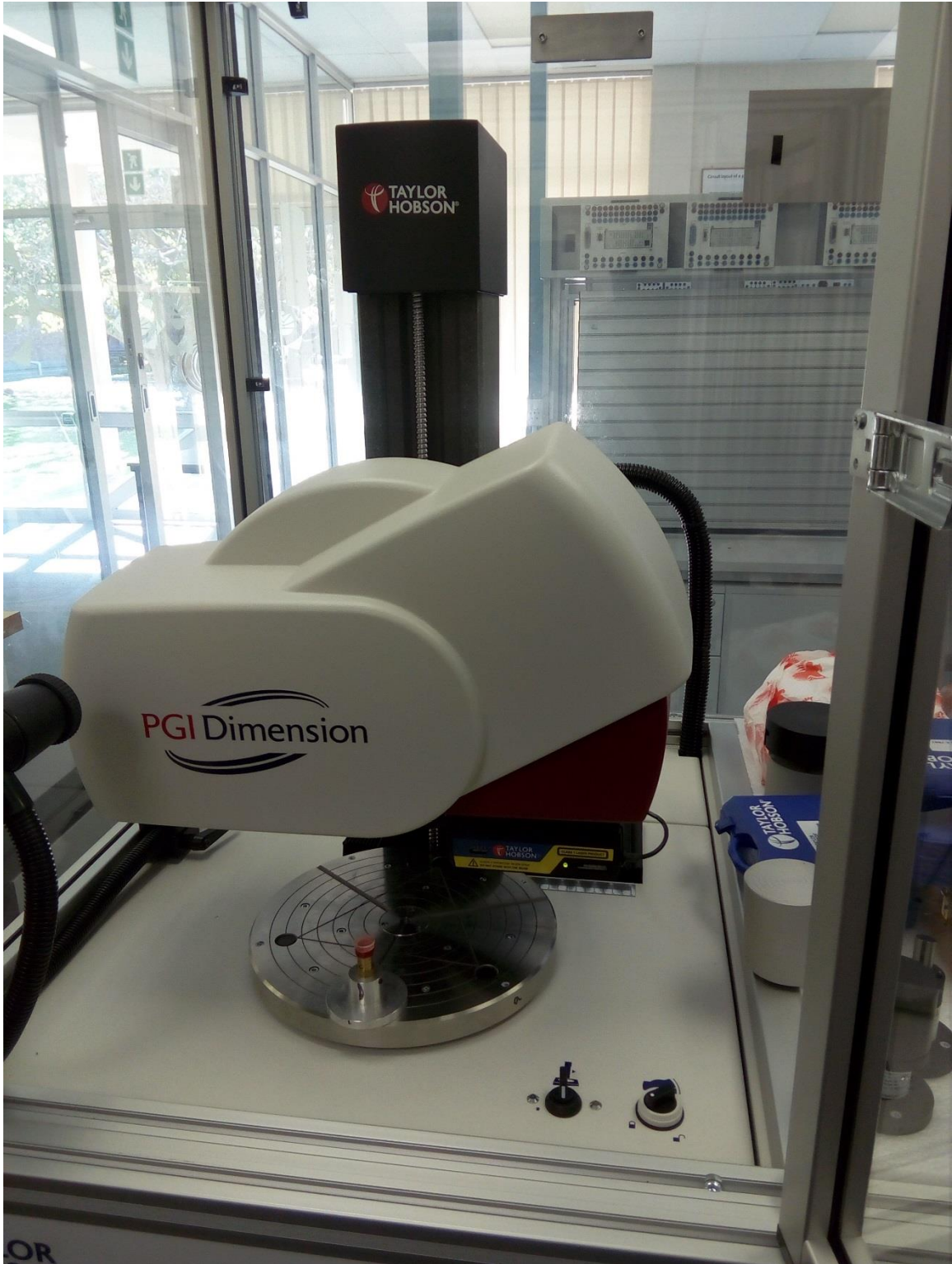
Figure 3.13**:** Taylor Hobson PGI Dimension XL Surface Profilometer at the Precision Engineering Laboratory, Nelson Mandela Metropolitan University

3.7 Experimental Setup

Experimental tests were carried out on the Precitech® Nanoform Ultragrind 250 ultra-high precision lathe. The tests were performed in dry operation as the polymer materials were soluble. The electrostatic sensor was mounted on a magnetic clamp at a distance of 25mm from the machining area.

Experimental tests were conducted using commercially available ONSI-56® Onsifocon-A contact lens buttons. The lens button dimensions are of 12.70 mm diameter and 4.40 mm thickness. This buttons were block-mounted unto a copper arbour for machining using low temperature optical wax. Figure 3.15 shows the blocking equipment and a contact lens button sitting on a copper arbour.

The blocking process was implemented by:

- Heating a strip of wax into a molten state.
- A copper arbour was warmed (to allow the wax to hold)
- The copper arbour was then dipped into the molten wax and the lens button was placed onto the wax
- The arbour was then placed onto the blocking machine which was used to centre the lens button onto the arbour.

Figure 3.14: ONSI-56 contact lens button and wax
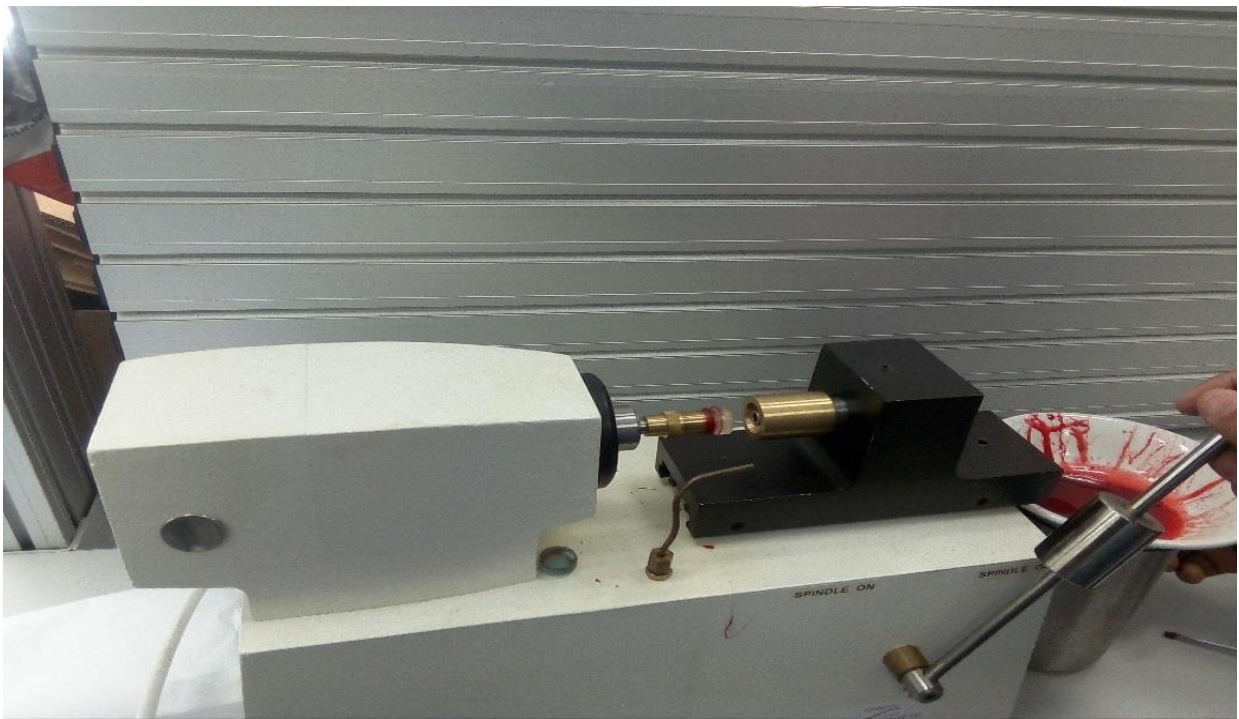
Figure 3.15**:** Blocking equipment

Before the start of the machining, tool setup such as tool centring (Figure 3.16) and spindle balance (Figure 3.17) experiments were performed to ensure the tool edge was centred and the vacuum

chuck was correctly positioned to prevent unwanted oscillations that would result in noise and less than optimal cutting results.
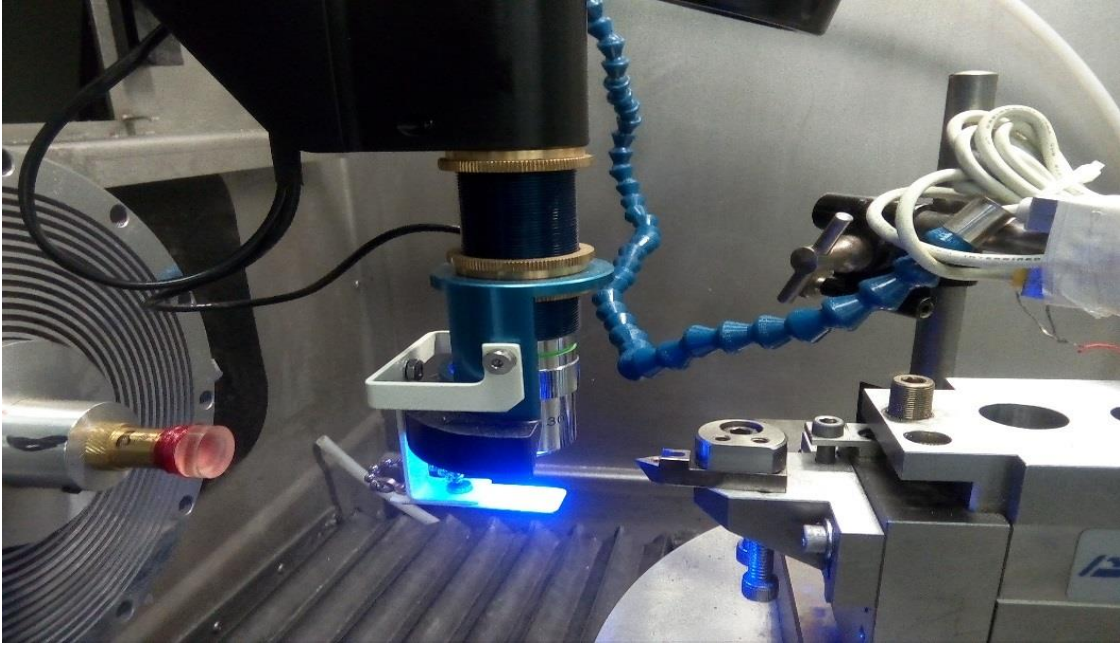
Figure 3.16: Tool centring for ONSI-56 experiment
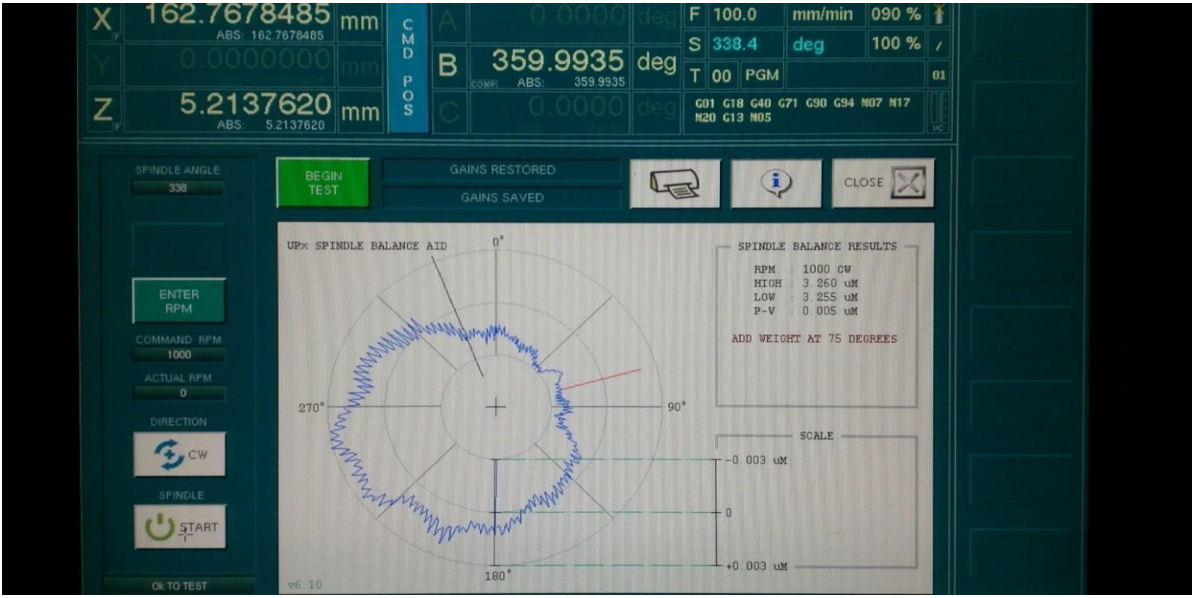
Figure 3.17: Spindle balancing platform DIFFSYS

3.7.1 Experimental Procedure

Figure 3.18 shows the experimental setup; the experiments began in the following steps:

- Step 1: The Copper arbour holding the contact lens button was mounted onto the machine spindle. Prior to experimental runs, contact lens buttons were lapped several times to flatten the surface area for measurement. Following lapping operation, the UHPM machine was wiped using anti-static foam cleanser and lenses were cleaned with a wet optical cloth to remove residual static charge generated during lapping.
- Step 2: The program was loaded onto the single point diamond turning machine interface with the updated parameter values for speed, feed and depth of cut.
- Step 3: The LabVIEW program (Figure 3.19) was initialized with continuous sample measurement and 1000 samples to read at a rate of 10 kHz to adequately monitor and capture the ESP data which was saved as a text file in Microsoft excel. During each cutting, Electrostatic data were acquired using NI myDAQ.
- Step 4: Additional experimental passes were run to ensure repeatability. After each experiment, the contact lens button was removed from the single point diamond turning machine and transferred to the Profilometer for surface profile measurements (Figure 3.20).
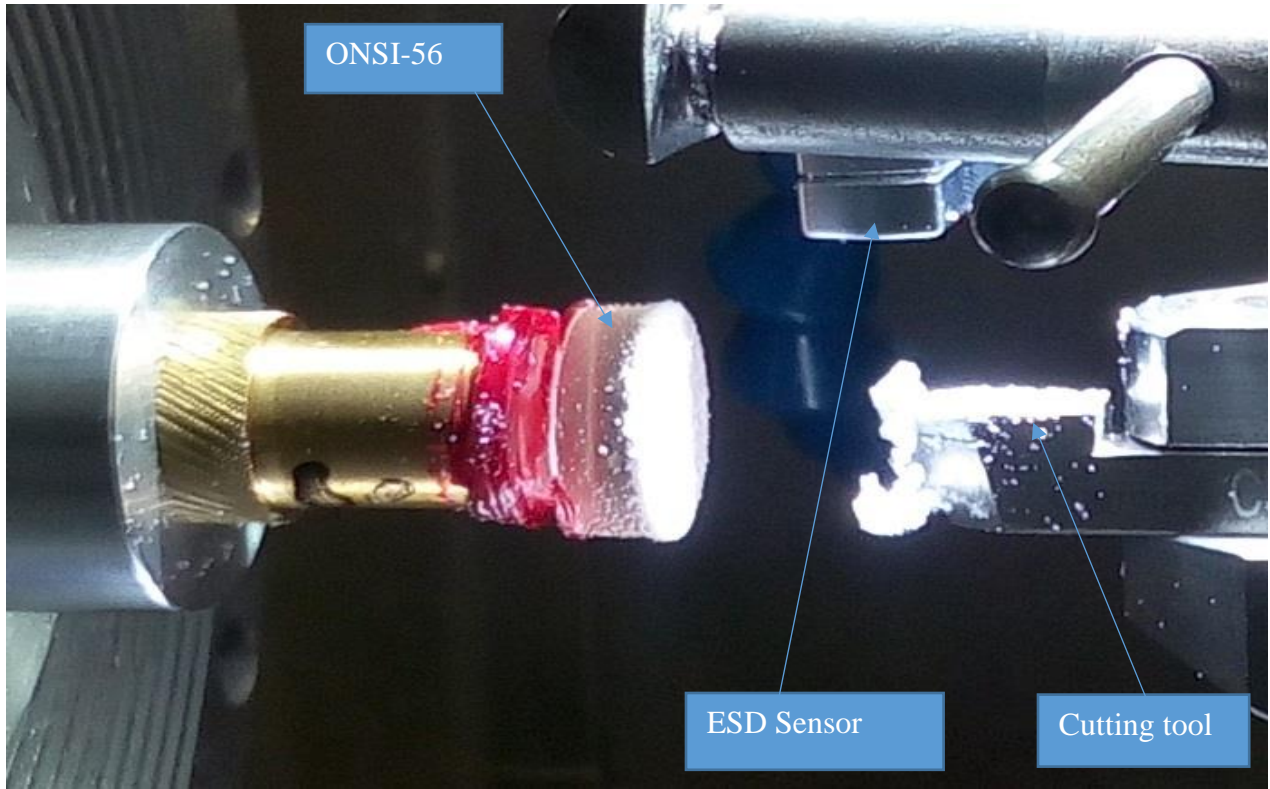
Figure 3.18: Setup for Diamond turning of ONSI-56 contact lens polymer
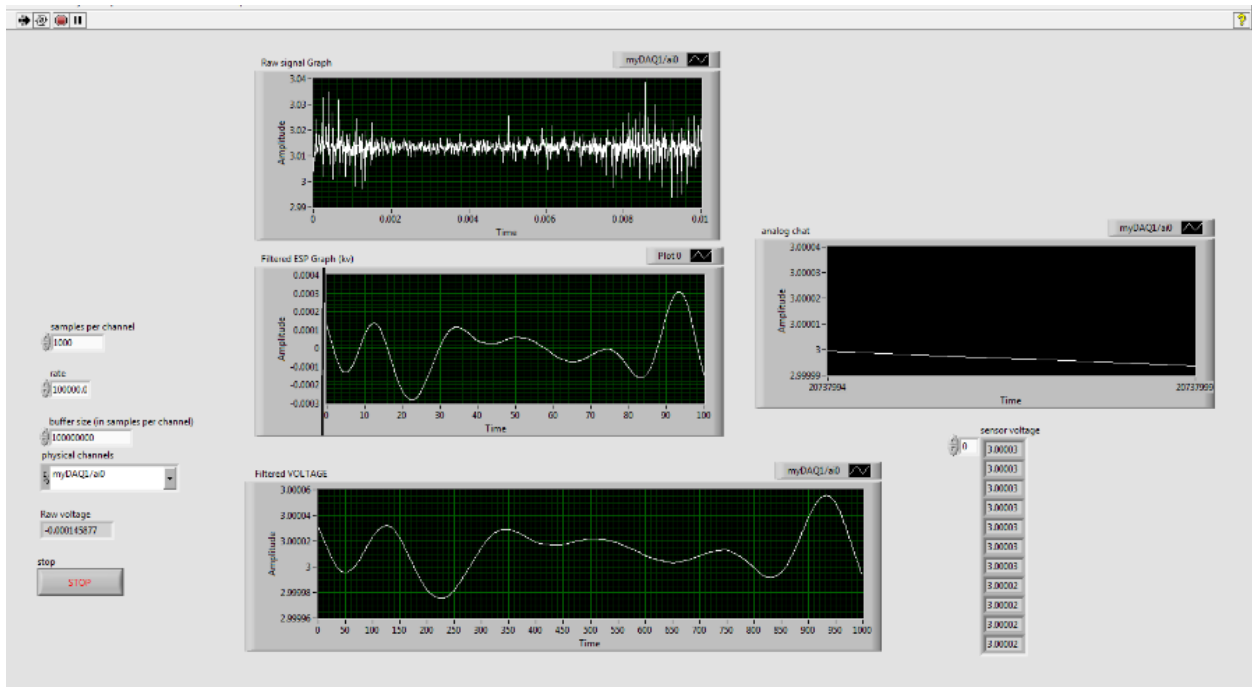
Figure 3.19: **NI** LabVIEW programme (front panel) showing electrostatic discharge during ONSI-56 Machining
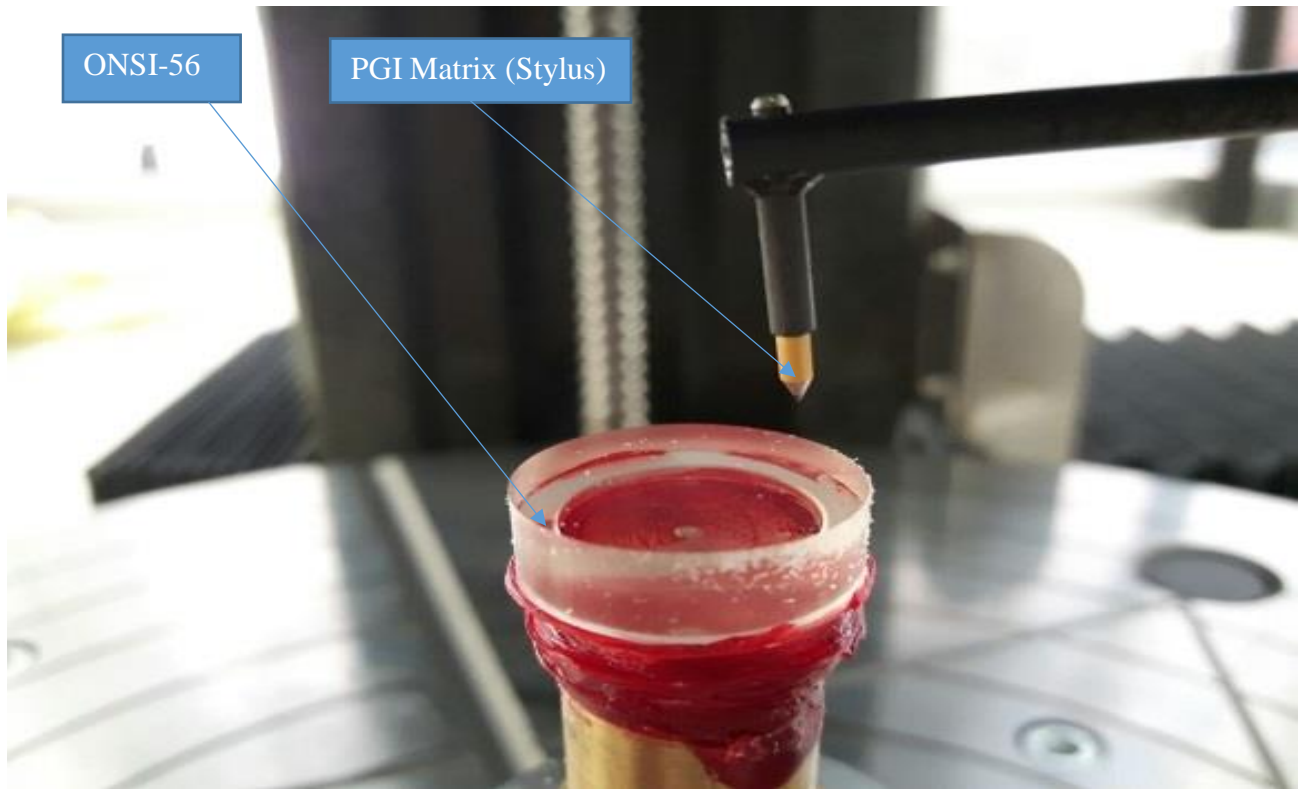
Figure 3.20**:** Surface roughness measurement of ONSI-56 lens button with Taylor Hopson optical profiler

3.8 Conclusion

In this research, the overall aim is to machine ONSI-56 contact lens polymers to optical quality and analyze the surface roughness and electrostatic discharge for saving cost and time for high production rates. The next chapter is aimed at investigating the surface roughness and ESD in the UHPM of contact lenses, and evaluating the effects of cutting parameters such as feed rate, cutting speed and depth of cut. Chapter 4 details the result and analysis.

CHAPTER FOUR

4   RESULTS AND DISCUSION

4.1 Introduction

The first section of this chapter details the surface roughness experiments, and the response surface methodology (RSM). The RSM model was used for predicting the surface roughness values and to investigate the influence of cutting parameters on the developed model and finally, artificial neural network (ANN) approach was employed for prediction of surface roughness. The second section explained the electrostatic discharge (ESD) experiments, RSM model for predicting the ESD data acquired during the study. ANN predictions, training and testing of feedforward back propagation neural network for predicting the ESD values are discussed. The analysis in this chapter was made possible using Design Expert 7, Matlab, and LabVIEW 2015 softwares.

4.2 Surface Roughness Experiments

Contact lens manufacture requires high accuracy and surface integrity. Surface roughness is generally used to measure the index quality of a turning process. It has been an important response because it has direct influence toward the part performance and the production cost. Hence, choosing optimal cutting parameters will not only improve the quality measure but also the productivity. This research work is therefore aimed at developing a predictive surface roughness model and investigate a finish cutting conditions of ONSI-56 contact lens polymer with a monocrystalline diamond cutting tool. Artificial neural network and Response surface methods were used to model the surface roughness of ONSI-56 contact lens polymer.

4.3 Response Surface Modelling

4.3.1   Response Surface Methodology Approach for Prediction of Surface Roughness

Response surface methodology (RSM) is a collection of statistical and mathematical technique that can be used to model and analyze engineering problems in which several independent variables influence a dependent variable or response and the goal is to optimize the response [88]. Box–Behnken design (BBD), the effective RSM with the lowest number of experiment was used to plan the experiment using Design Expert 7 software. Thus, RSM can be used for a variety of

purposes such as analyzing of experimental, ordinal or categorical data. therefore, it can be considered to be helpful in predicting the surface roughness [89].

Box-Behnken design of experiment used in this research contains three-level three input factors with full replication as shown in table 4.1. The experimental data consist of 15 experimental runs. Box-Behnken experimental design method is performed to obtain a mathematical model and find the relationship between cutting parameters and surface roughness. During machining, the highest, middle and the lowest values of machining parameters are used. Feed rate, depth of cut and spindle speed are selected to define a relationship between surface roughness and machining parameters. The experiments were implemented based on the setup discussed in chapter 3.

Table 4.1: Box-Behnken Experimental Results

Run Order	Cutting Speed (rpm)	Feed Rate (mm/min)	Depth of Cut (µm)
1	2100	2	10
2	2100	7	25
3	200	2	25
4	4000	7	40
5	2100	2	40
6	2100	7	25
7	200	7	40
8	200	7	10
9	4000	2	25
10	2100	7	25
11	4000	7	10
12	2100	12	40
13	2100	12	10
14	200	12	25
15	4000	12	25

Runs 6 and 10 are repeat of run 2

After each experimental run, the surface roughness values for ONSI-56 was measured using Taylor Hobson PGI Dimension XL Surface Profilometer. The measurement results for all runs are tabulated in Table 4.2 below. Figure 4.1 shows the series plots of the measured surface roughness. The best and the poor surface roughness profile chart from the Surface Profilometer for ONSI-56 Contact lens buttons are given in figure 4.2 and figure 4.3

Table 4.2**:** Surface Roughness Experimental Results

Run Order	Cutting Speed (rpm)	Feed Rate (mm/min)	Depth of Cut (μm)	Surface Roughness Ra (nm)
1	2100	2	10	18.8
2	2100	7	25	6
3	200	2	25	46
4	4000	7	40	21.1
5	2100	2	40	20.2
6	2100	7	25	15
7	200	7	40	447.6
8	200	7	10	370.5
9	4000	2	25	18.2
10	2100	7	25	23.9
11	4000	7	10	28.3
12	2100	12	40	20.6
13	2100	12	10	28.1
14	200	12	25	1184.1
15	4000	12	25	36.6

Figure 4.1: Series plots of Experimental surface roughness
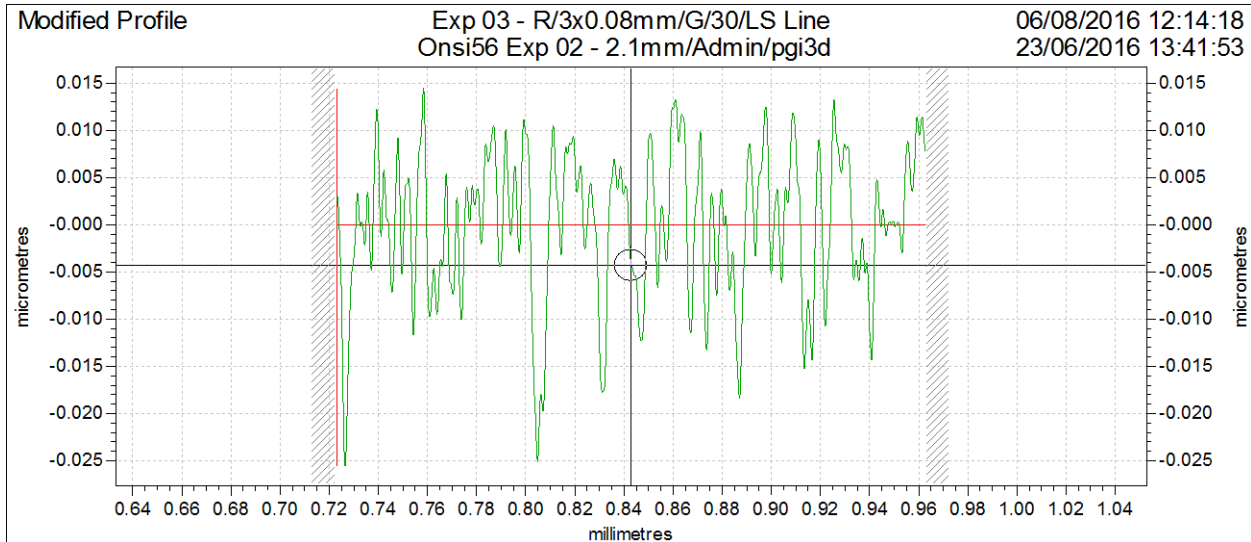
Figure 4.2: Surface profile chart for Ra 6 nm
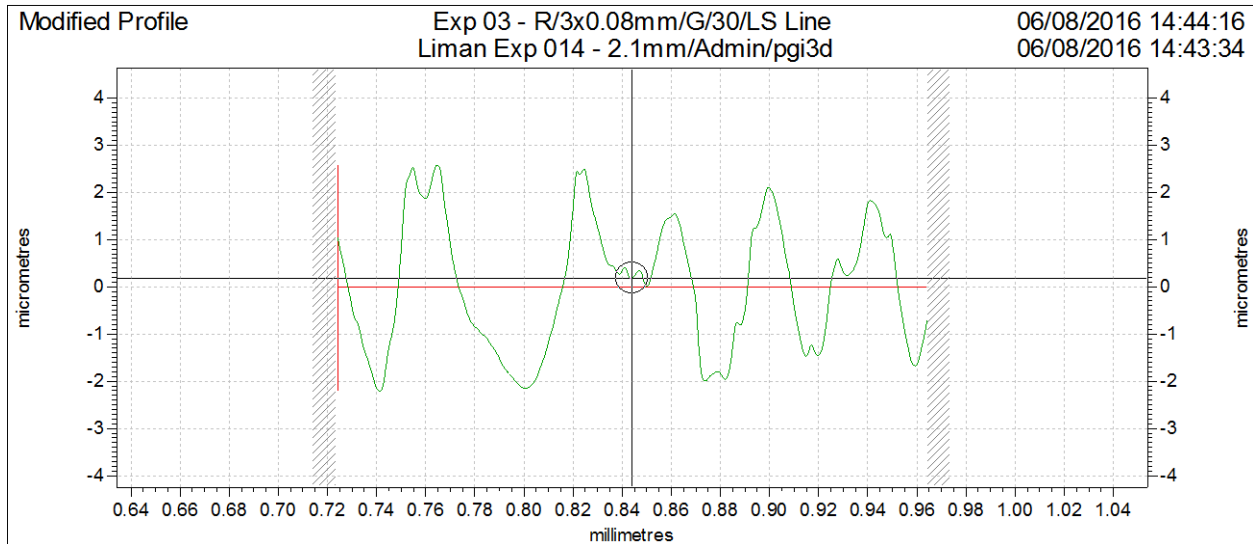
Figure 4.3**:** Surface profile chart for Ra 1184.1 nm

4.3.2   Determination of Appropriate Polynomial Equation to Represent RSM Model

According to the literature from Section 2.5.4, various modeling techniques have been investigated and applied to predict surface roughness and the influence of cutting parameters on surface roughness. Prediction model allows the machinist to determine the values of the cutting performance before machining and thus allows the machining process to become more productive, competitive, minimize machine error and technical specification satisfaction [110]. The procedures for developing the surface finish models in this study have been well comprehensive by Alao [111]. According to Alao and Konneh [112], the development of RS models includes checking the response data for any transformation need, fitting of the input and output variables to know whether the relationship between them is linear, linear and two-factor interaction (2FI), second-order or higher-order function and investigating the p-values. Design Expert software (7.1.6) version was used for analyzing the output data for ONSI-56 contact lens polymer. To obtain an adequate model equation, response transformation check is necessary. This transformation is carried out using Box–Cox plotting technique available in Design Expert software.

4.3.3 Response Transformation Check

Based on the experimental results in table 4.2, the response surface roughness ranges from 6 nm to 1184.1 nm. The ratio of maximum to minimum is:

$$\frac{1184.1}{6} = 197.35 \tag{4.1}$$

A ratio greater than 10 usually indicates a transformation is required [113]. Therefore, a transformation is required for a ratio of 197.35. For this analysis, Box-Cox plotting technique is used for the selection of the transformed scale model as shown in figure 4-4.
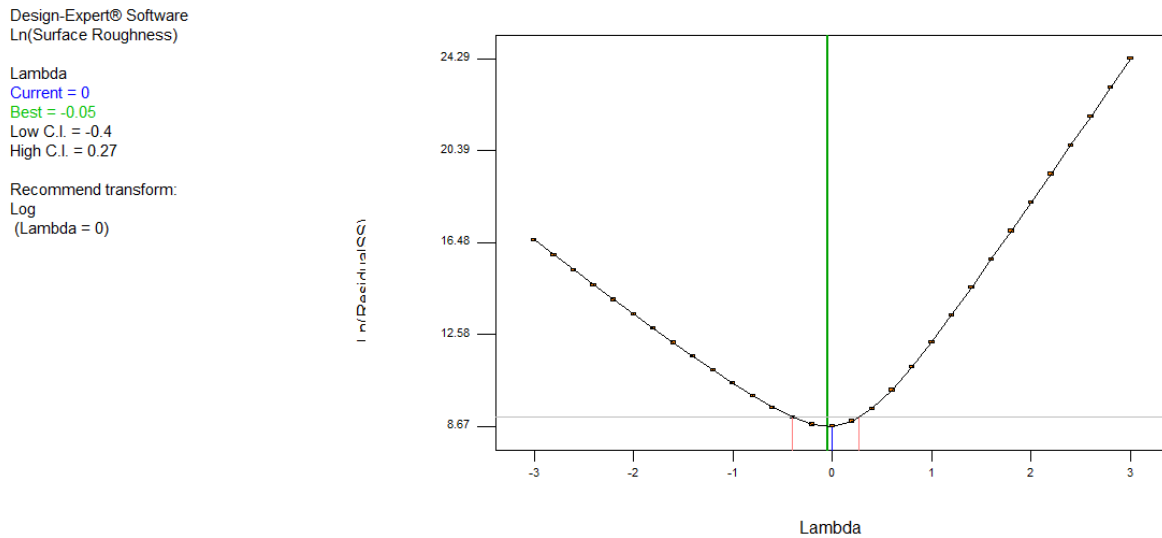
Figure 4.4: Box-Cox plot for transformed scale R_a model

Based on the Box-Cox plot (Figure 4-4), natural log transformation was recommended, which produced a model of the form:

$$y' = \text{Ln} \, (y + k) \tag{4.2}$$

Generally, natural log transformations is used for three purposes [114]: stabilizing the response variance, making the distribution of the response variable closer to the normal distribution, and improving the fit of the model to the data. This last objective could include model simplification,

say by eliminating interaction, or higher-order polynomial terms. Sometimes a transformation will be reasonably effective in simultaneously accomplishing more than one of these objectives.

In this research, a natural log transformation is used to determine a suitable polynomial equation to represent the relationships between the input parameters (cutting peed, feed rate and depth of cut) and the surface roughness (output response) by carrying out sum of squares sequential model and lack of fit test shown in table 4.3 and 4.4. The result from the sequential model indicate linear vs mean and quadratic vs 2FI approach, However, the lack of fit test suggests a linear and quadratic equation approach.

Table 4.3**:** Sequential Model Sum of Squares for surface roughness

Source	Sum of squares	df	Mean Square	F Value	p-Value Prob>F	Remark
Mean vs Total	207.52	1	207.52			
Linear vs Mean	14.98	3	4.99	3.69	0.0465	suggested
2FI vs Mean	1.72	3	0.57	0.35	0.7915	
Quadratic vs 2FI	10.43	3	3.48	6.36	0.0369	suggested
Cubic vs Quadratic	1.74	3	0.58	1.17	0.4905	Aliased
Residual	0.99	2	0.49			
Total	237.37	15	15.82			

Table 4.4: Lack of Fit Tests for surface roughness

Source	Sum of squares	df	Mean Square	F Value	p-Value prob>F	Remark
Linear	13.89	9	1.54	3.12	0.2662	Suggested
2FI	12.17	6	2.03	4.10	0.2089	
Quadratic	1.74	3	0.58	1.17	0.4905	Suggested
Cubic	0.000	0				Aliased
Pure Error	0.99	2	0.49			

4.3.4 Surface Roughness (Ra) Model Determination

Table 4.5 shows the statistical summary for each transformed scale model that was output by Design Expert Software. A linear and quadratic model were suggested, even though a linear model has lower R^2 and adjusted-R^2 (Adj-R^2) values than a quadratic and cubic models. This is because the cubic model is aliased, which means that the effects of each variable that caused different signals become indistinguishable. For a linear relationship, the R^2 and Adj-R^2 values are 0.5016 and 0.3657, respectively. It is clear that the 2FI model is not adequate for the experimental data. The transformed scale quadratic model, with the R^2 and Adj-R^2 values are 0.90850 and 0.7438 respectively which were therefore selected to fit the experimental data.

Table 4.5: Statistical summary for each model

Source	Std. Dev	R-Squared	Adjusted R-Squared	Predicted R-Squared	PRESS	Suggestion
Linear	1.16	0.5016	0.3657	0.1003	26.86	Suggested
2FI	1.28	0.5592	0.2287	-0.6425	49.04	Not adequate
Quadratic	0.74	0.90850	0.7438	-0.0084	30.11	Suggested
Cubic	0.70	0.9669	0.7681		+	Aliased

4.4 Analysis of Variance (ANOVA) for the Acquired Model

ANOVA of experimental data is always done to analyze statistically the relative significance of the models and its terms on the response. ANOVA is an analytical technique that is used to identify the importance of a model and its parameters, using Fisher's F-test and Student's t-test [115]. Student's t-test was used to determine the significance of the regression coefficients using a p-value standard. Table 4.6 shows the ANOVA results for the acquired transformed scale quadratic model. As can be seen, the model is significant as is evident from its F-value (F_{Model} = 5.52) and low probability value (p = 0.0373). A p-value lower than 0.05 indicates that the model is statistically significant, whereas a value higher than 0.1000 indicates that the model is not significant [116]. The Model F-value of 5.52 implies the model is significant. There is only a 3.73% chance that a "Model F-Value" this large could occur due to noise.

Table 4.6: ANOVA results for the acquired quadratic model

Response   1   Surface Roughness

Transform: Natural log   Constant: 0

ANOVA for Response Surface Quadratic Model

Analysis of variance table [Partial sum of squares - Type III]

Source	Sum of Squares	df	Mean Square	F Value	p-value Prob > F	
Model	27.12	9	3.01	5.52	0.0373	significant
A-Speed	12.58	1	12.58	23.02	0.0049	
B-Feed	2.39	1	2.39	4.37	0.0910	
C-Depth	0.015	1	0.015	0.027	0.8760	
AB	1.62	1	1.62	2.97	0.1452	
AC	0.058	1	0.058	0.11	0.7573	
BC	0.037	1	0.037	0.067	0.8062	
A^2	10.18	1	10.18	18.64	0.0076	
B^2	0.065	1	0.065	0.12	0.7434	
C^2	0.54	1	0.54	1.00	0.3638	
Residual	2.73	5	0.55			
Lack of Fit	1.74	3	0.58	1.17	0.4905	not significant
Pure Error	0.99	2	0.49			
Cor Total	29.86	14				

In this case A, and A^2 are significant whereas all other model terms are insignificant. Therefore, due to many insignificant model terms, the model can be improved by eliminating the terms that are not very significant even though table 4.7 shows high coefficient of determination R^2 value of 0.9085 and Adj-R^2 value of 0.7438

Table 4.7: Summary of regression coefficient (R^2)

Std. Dev.	0.74	R-Squared	0.9085
Mean	3.72	Adj R-Squared	0.7438
C.V. %	19.87	Pred R-Squared	-0.0084
PRESS	30.11	Adeq Precision	7.146

4.4.1 Surface Roughness (Ra) Model Modification

After the significance of the parameters has been evaluated, the model was improved by eliminating the terms that are not very significant. The ANOVA results for the modified model describing the relationship between the surface roughness and cutting parameters is shown in table 4.8

Table 4.8: ANOVA results for the modified model (only the significant terms)

Source	Sum of squares	Degrees of Freedom	Mean Square	F- Value	p-Value Prob>F	Characteristics
Model	26.43	4	6.61	19.29	0.0001	*Significant*
A-Speed	12.58	1	12.58	36.71	0.0001	
B-Feed	2.39	1	2.39	6.96	0.0248	
AB	1.62	1	1.62	4.74	0.0544	
A^2	9.84	1	9.84	28.73	0.0003	
Residuals	3.43	10	0.34			
Lack of Fit	2.44	8	0.30	*0.62*	*0.7440*	*Not significant*
Pure Error	0.99	2	0.49			
Corr. Total	29.86	14				

The ANOVA have been performed to check whether the modified model is adequate as well as to check the significance of the individual model coefficients. The Model F-value of 19.29 in table 4.8 implies the model is significant. There is only a 0.01% chance that a "Model F-Value" this large could occur due to noise. Values of "Prob>F" less than 0.05 indicate the model terms are significant. From the modified ANOVA table 4.8, it is clear that the p values for the cutting speed (A), feed rate (B) and the square of speed (A^2) are less than 0.05, indicating that these model terms are the most significant factors that influence the surface roughness. This implies that these factors have very large effects on surface roughness. However, the p value for the interaction between speed and feed (AB) is slightly greater than 0.05 indicating its partial or low significance on the R_a modified model. However, equation 4.2 and 4.3 reveals the interaction effects of cutting speed and feed rates. While the depth of cut has no significant effect on the surface roughness. The "Lack of Fit F-value" of 0.62 implies the Lack of Fit is not significant relative to the pure error. There is a 74.40% chance that a "Lack of Fit F-value" this large could occur due to noise. Non-significant lack of fit is good -- we want the model to fit. The lack of fit test of F value of 0.62 is not significant, indicating that all the data fit the model adequately.

In order to predict the surface roughness, the second-order regression equation can be expressed as:

$$y = \beta_o + \sum_{i=1}^{3} \beta_i x_i + \sum_{i=1}^{3} \beta_{ii} x_i^2 + \sum_i \sum_{j=1} \beta_{ij} x_i x_j + \varepsilon \quad (4.3)$$

The dependent variable, y, is the response and the independent variable, x, is the factor. β is the coefficient estimated from RSM analysis. After determining the significant coefficients (at 95% confidence level), the final model was developed using these coefficients and the final mathematical model to estimate surface roughness is given in equation 4.4 and 4.5

$$lnR_a = 4.47216 - 0.002085S + 0.25009F + (4.4979 \times 10^{-7})S^2 - (6.70913 \times 10^{-5})SF \quad (4.4)$$

The equation can be rewritten as

$$R_a = e^{\left[4.47216 - 0.002085S + 0.25009F + (4.4979 \times 10^{-7})S^2 - (6.70913 \times 10^{-5})SF\right]} \quad (4.5)$$

Where: R_a = Surface roughness, F = Feed rate and S = Cutting speed

As can be seen from table 4.9. The "Pred R-Squared" of 0.6438 is in reasonable agreement with the "Adj R-Squared" of 0.8394. For models to be adequate and accurate, it is suggested that Adj-R^2 should be greater or equal to 0.70 [117]. Thus, Adj-R^2 of 0.8394 indicate that the model is very significant. Then, "Adeq Precision" measures the signal to noise ratio where a ratio greater than 4 is desirable. Hence, the ratio of 13.634 indicates an adequate signal. At the same time a relatively lower value of the coefficient of variation (CV=15.74) indicates improved precision and reliability of the conducted experiments. This model can therefore be used to navigate the design space (surface roughness) for ONSI-56 contact lens polymers.

Table 4.9**:** Summary of regression analysis results

Std.Dev.	0.59	**R²**	0.8853
Mean	3.72	**Adj-R²**	0.8394
C.V. %	15.74	**Pred-R²**	0.6438
PRESS	10.64	**Adeq-Precision**	13.634

The coefficient of determination (R^2) is defined as the ratio of the explained variation to the total variation, and is a measure of the degree of fit [118]. Consequently, Joglekar [119] suggested that a good model fit should yield an R^2 of at least 0.80. This means that the modified response model evaluated in this study can explain the reaction very well, with an R^2 of 0.8853 and an Adj-R^2 of 0.8394 at a confidence level of 95% as shown in table 4.9. In addition, the model is very significant as is evident from its F-value ($F_{Model} = 19.29$) and very low probability value (p = 0.0001) from table 4-8. A p-value lower than 0.05 indicates that the model is statistically significant, whereas a value higher than 0.1000 indicates that the model is not significant [116].

4.4.2   Model Accuracy Check

To obtain an adequate model, an accuracy check is necessary. The RS model accuracy was checked by comparing the predicted and experimental surface roughness. Table 4.10 shows the prediction accuracy for RS model. The RSM results demonstrate that the proposed model in this study is suitable for predicting the surface roughness with an R^2 of 0.8853. Figure 4.5 shows the performance of RS model.

Table 4.10**:** Comparison of measured and predicted R_a of RSM values

Run order	Measured Ra (nm)	RSM Predicted Ra (nm)	Residual (nm)	Error (%)
1	18.8	27.39	-8.59	45.69
2	6	17.29	-11.29	188.17
3	46	94.63	-48.63	105.72
4	21.1	25.03	-3.93	18.63
5	20.2	10.07	10.13	50.15
6	15	17.29	-2.29	15.27
7	447.6	307.97	139.63	31.19
8	370.5	307.97	62.53	16.88
9	18.2	27.39	-9.19	50.49
10	23.9	17.29	6.61	27.66
11	28.3	25.03	3.27	11.55
12	20.6	29.96	-9.36	45.44
13	28.1	29.96	-1.86	6.62
14	1184.1	1002.25	181.85	15.36
15	36.6	22.87	13.73	37.51
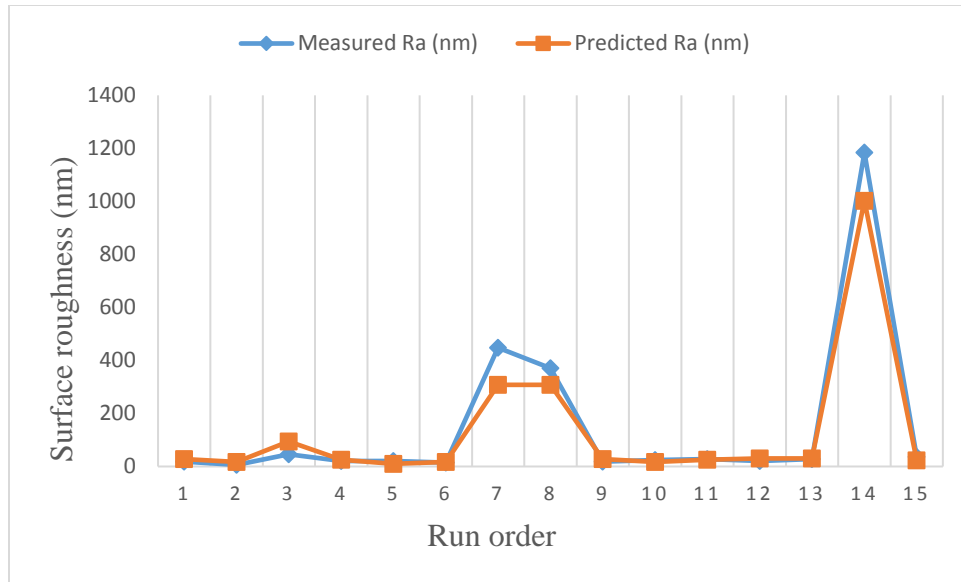
Figure 4.5: Comparison of measured and predicted surface roughness of RS model

In addition, a normal plot of residuals between the normal probability (%) and the internally studentized residuals and the plot of residuals versus the predicted response was also obtained. In this way, the residuals can be checked to determine how well the model satisfies the assumptions of ANOVA, and the internally studentized residuals can be used to measure the standard deviations separating the experimental and predicted values [120]. Figure 4.6 shows the relationship between the normal probability (%) and the internally studentized residuals. The straight line means that there was no apparent problem with normality. The normal probability plot of the residuals for the surface roughness shown in Figure 4.6 reveals that the residuals are falling on the straight line, which means the errors are distributed normally [121]. Figure 4.7 shows a plot of residuals versus predicted in surface roughness modelling. This indicates that the model possesses adequate normality of residuals and no constant error.
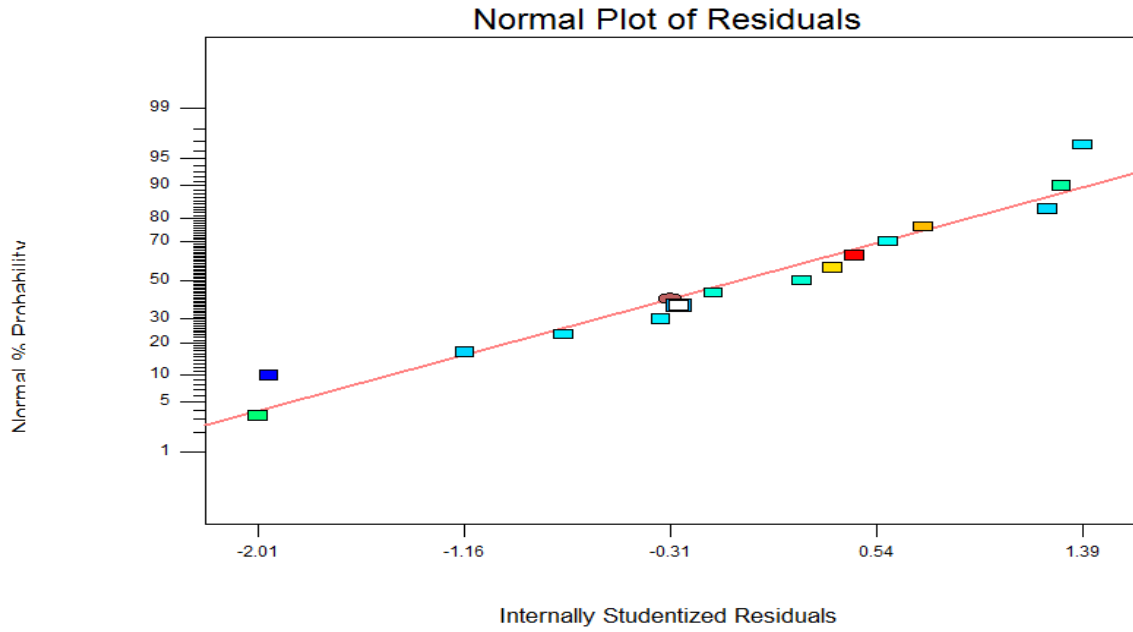
Figure 4.6: Normal Probability plot of residuals in Surface Roughness modelling
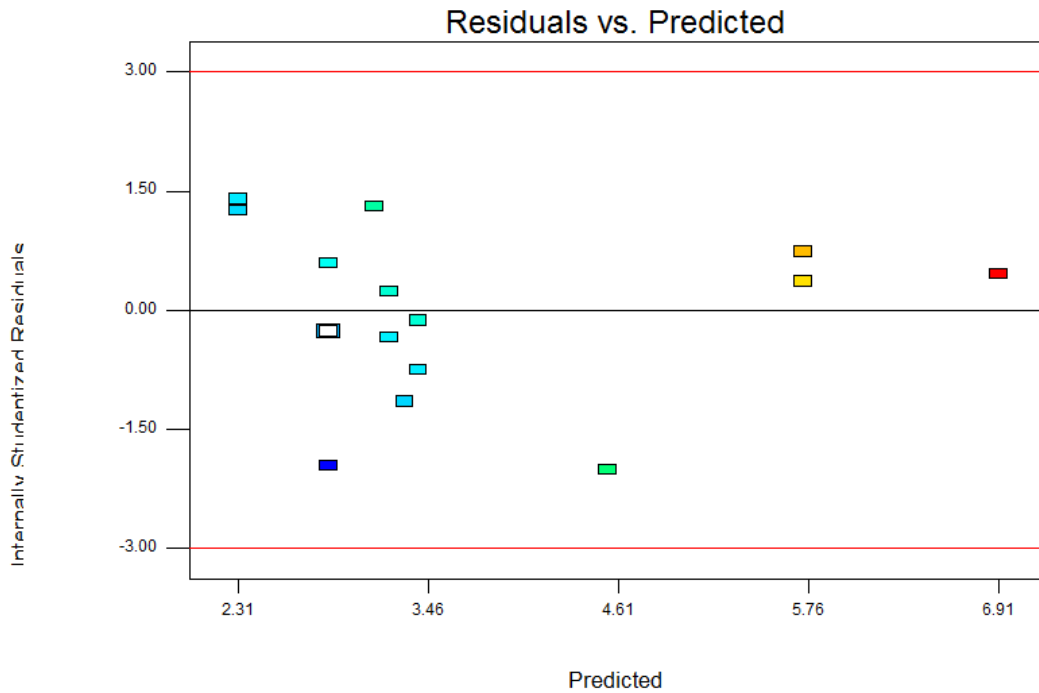
Figure 4.7: Probability plot of residuals vs. Predicted in Surface Roughness modelling

4.5 Influence of Cutting Parameters on Surface Roughness

In determining the cutting parameters influential to the surface roughness, the results from the modified ANOVA table (Section 4.4.1) were studied. By checking the p values and F values from ANOVA, it is clearly seen that all the model terms are significant with cutting speed having the highest degree of significance followed by the square of the cutting speed and the feed rate. However, interaction between cutting speed and feed rate has the lowest degree of significance on the surface roughness (R_a).

4.5.1   Effect of Cutting Speed

The effect of cutting speed on the transformed scale of R_a is depicted in figure. 4.8. It can be observed that the transformed scale of R_a decreases quadratically with an increase in cutting speed up to 3500 rpm and then slightly increases quadratically as cutting speed changes from 3500 to 4000 rpm at high feed and high depth. This implies that moderate spindle speed improves the R_a.
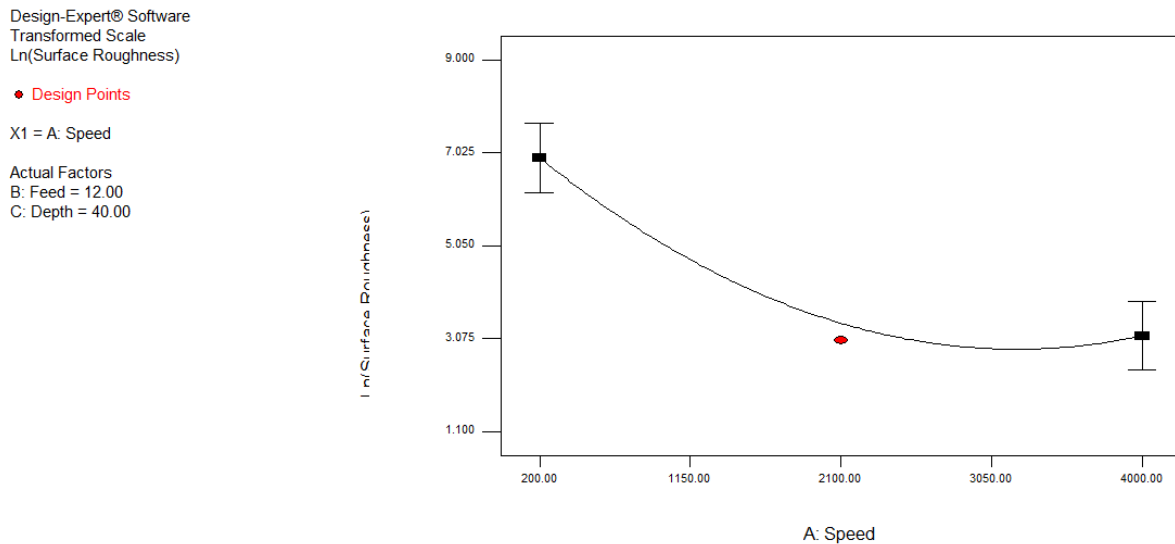
Figure 4.8**:** Variation of R$_a$ with cutting speed

It can also be seen that the roughness improves with increase in cutting speed. The results are, however, in agreement with the results of Gubbels [11] concerning the increase of surface quality with increasing cutting speed. From the experimental results, the best surface roughness is obtained at the feed rate of 7 µm/rev, cutting speed of 2100 rpm and depth of cut of 25 µm.

4.5.2　Interaction Effects

There exists an interactive effect between cutting speed and feed rate in equation 4.4 and equation 4.5 (Section 4.2.5). The authentication of this interaction is shown in figure 4.9. As can be seen from the figure, there is an interaction between the cutting speed and feed rate and these two parameters combined together to influence R_a.
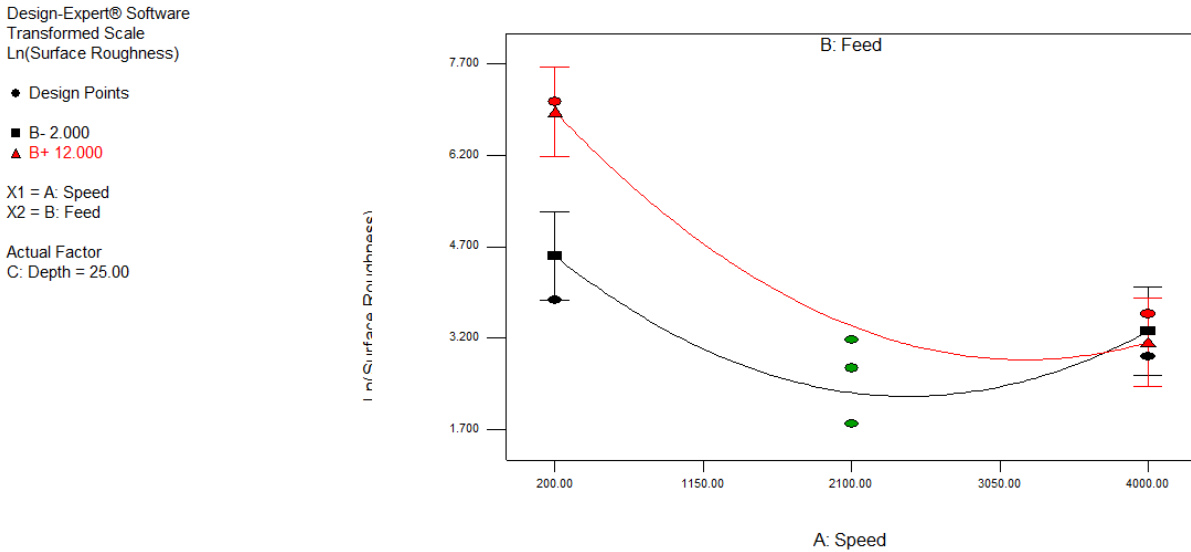
Figure 4.9: The interaction between feed rate and cutting speed

Also, figure 4.10 shows the 3D view of the interaction between cutting speed and feed rate while figure 4.11 shows the contour plot for the combined influence of cutting speed and feed rate at 25 μm depth of cut on R_a. From this figures, it can be observed that moderate cutting speed and feed rate improves the surface roughness R_a while depth of cut has no influence on the transformed scale of R_a. Adj- R^2 for R_a model is 83.9%, indicating the model terms in table 4.9 (Section 4.4.1) can contribute about 83.9% in the variability observed in the reduction of R_a model.
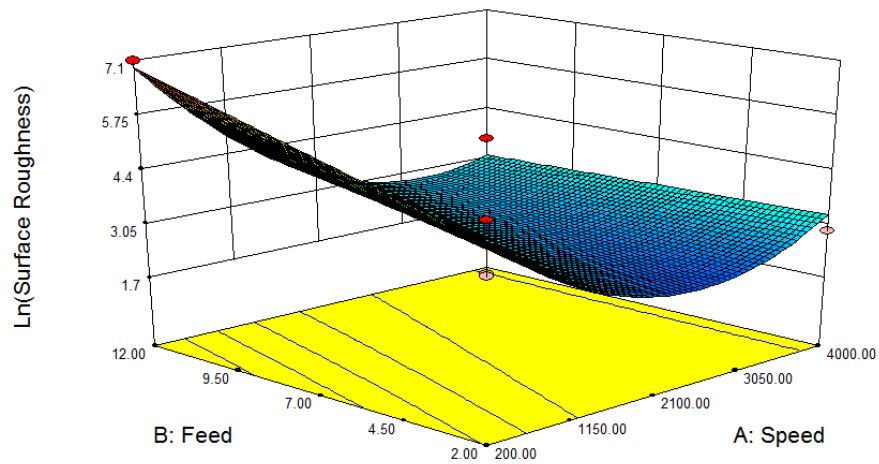
Figure 4.10**:** The 3D surface model of surface roughness with respect to speed and feed
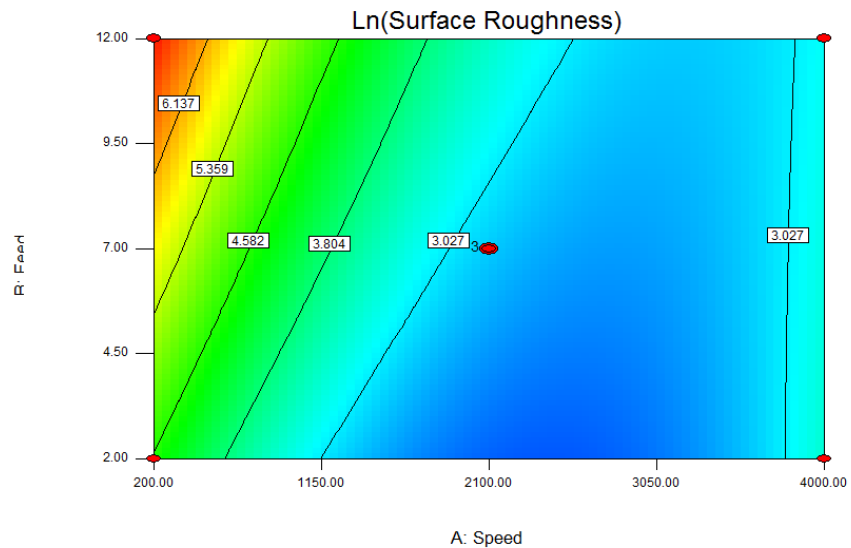
Figure 4.11**:** Contour effect of feed and speed for surface roughness

4.5.3   Effect of Feed Rate

ANOVA in table 4-8 (Section 4.4.1) indicated the influence of feed in diamond turning of ONSI-56 contact lens polymer. In literature, it is also indicated that feed rate is a significant cutting parameter in different cutting conditions. Cutting material changes, process variables change,

environmental conditions change but the effect of feed rate is always prominent [8]. Figure 4.12 shows the distribution of surface roughness with varying feed rate from 2 µm/rev to 12 µm/rev. This plots show that small feed rate gives better surface roughness and increasing feed rate diminishes the quality of the surface.
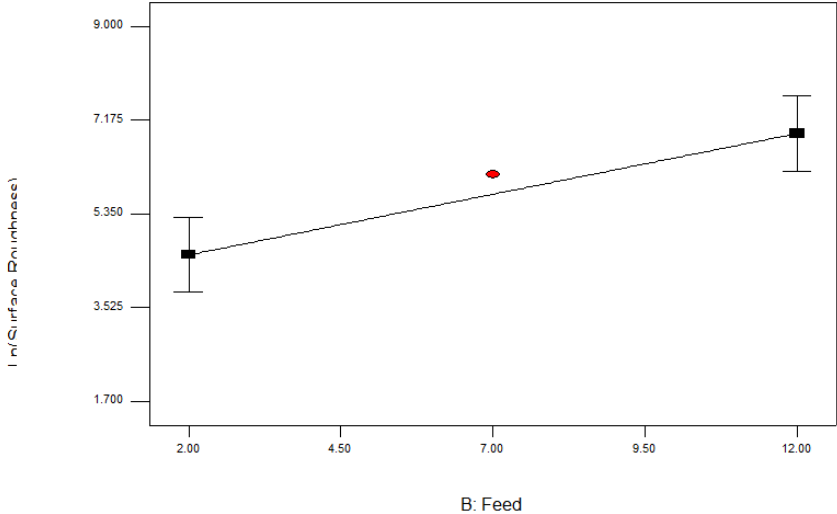
Figure 4.12: Variation of R_a with feed rate

4.6 Artificial Neural Network Model for Prediction of Surface Roughness

Artificial network networks are widely used in many applications such as control, forecasting, medicine, speech, data compression, pattern recognition, and power systems [122]. Neural network models provide an alternative approach to analyze the data, as they can reason patterns in the data. Artificial intelligence methods could have been used in the stages of optical lens manufacturing. Single point diamond turning is one of the basic manufacturing techniques used in the optical industry. Contact lens manufacturers must minimize cost and process time, and additionally, the product must comply with the required dimensions and high quality criteria for a better competition [122].

In this study, ANNs structure, 3-1-1, 3-2-1, 3-3-1 and 3-4-1 were tested for modeling and predicting surface roughness in SPDT. This means 1 node output layer, 1,2,3 and 4 node hidden layer, and 3 node input layer for input variables. This fully connected hierarchical network structure has an input layer, a hidden layer, and an output layer. The back-propagation learning algorithms Levenberg–Marquardt (LM) was used to update the parameters in feed forward single hidden layers. Neurons in the input layer correspond to cutting speed, depth of cut and feed rate. The output layer corresponds to surface roughness. Some parameters (i.e. the number of training and testing data, learning rate, number of hidden layers, and processing function used) affect the accuracy, reliability, and effectiveness of the neural network. The data are divided into two categories: training data and testing data. The training data are a random set of ten input samples from a total of 15 experimental findings. The testing data are the remaining five experimental findings, which does not intersect with the training data. Table 4.11 shows the input and target data set for the ANN modelling.

Table 4.11: Input and target data set for ANN modelling

Run order	Cutting speed (rpm)	Feed rate (mm/min)	Depth of cut (μm)	Ra (nm)
1	2100	2	10	18.8
2	2100	7	25	6
3	200	2	25	46
4	4000	7	40	21.1
5	2100	2	40	20.2
6	2100	7	25	15
7	200	7	40	447.6
8	200	7	10	370.5
9	4000	2	25	18.2
10	2100	7	25	23.9
11	4000	7	10	28.3
12	2100	12	40	20.6
13	2100	12	10	28.1
14	200	12	25	1184.1
15	4000	12	25	36.6

The inputs and output were normalized before training the network since the parameters were in different ranges, these parameters were normalized within 0–1 ranges in order to prevent the simulated neurons from being driven too far into saturation.

4.6.1   Normalization of Data

The inputs and the output were normalized between 0 and 1 using equation 4.6. The 0 and 1 correspond to the lowest and highest value in the subset respectively (Table 4.12). The normalization was done to achieve standardization of the data and reduce redundancy before feeding them into the network for training.

$$Y_t = \frac{(Y_0 - Y_{min})}{(Y_{max} - Y_{min})}$$
(4.6)

Where $Y_t=$ Normalized value of Y_0, Y_0- observed value, Y_{min}- minimum observed value in the subset and Y_{max}- maximum observed value in the subset.

Table 4.12: Normalized input and target data set for ANN Modeling

Run order	Cutting speed (rpm)	Feed rate (mm/min)	Depth of cut (µm)	Ra (nm)
1	0.50	0.00	0.00	0.01
2	0.50	0.50	0.50	0.00
3	0.00	0.00	0.50	0.03
4	1.00	0.50	1.00	0.01
5	0.50	0.00	1.00	0.01
6	0.50	0.50	0.50	0.01
7	0.00	0.50	1.00	0.37
8	0.00	0.50	0.00	0.31
9	1.00	0.00	0.50	0.01
10	0.50	0.50	0.50	0.02
11	1.00	0.50	0.00	0.02
12	0.50	1.00	1.00	0.01
13	0.50	1.00	0.00	0.02
14	0.00	1.00	0.50	1.00
15	1.00	1.00	0.50	0.03

The ANN model is designed depending on the normalized values above. The back-propagation based weight tuning was applied to model and predict the surface roughness. The network is trained by using Matlab (8.1.6) neural network toolbox. The training parameters used in the neural network are presented in table 4.13. Consequently, Liu et al. [123] proved that the sigmoidal function is easy to converge and provides fast learning speed using ANN model. Therefore, sigmoidal function is selected for the ANN model (equation 4.7).

$$f = \frac{1}{1+ e^{-x}}$$

(4.7)

The error during the learning referred to as mean squared error (MSE) is calculated as follows:

$$MSE = \left(\frac{1}{N}\Sigma_i|t_i - o_i|^2\right)$$ (4.8)

Where: N = number of samples, t = target value and o = output value

Table 4.13: Training parameters used

The number of layers	3
The number of neurons on the layers	Input: 3, Hidden: 1,2,3 and 4, Output: 1
Learning rule	Levenburg-Marquatt
Activation function	Log-sigmoid
Mu	0.001
Error goal	5.0002×10^{-5}
The normalization of data	0-1
The number of iteration	10,000

The back-propagation algorithm is used to adjust the weights of the hidden layer neurons. In this study, number of hidden layer neurons is varied from 1 to 4. Table 4.14 shows the MSE for different number of hidden neurons. The performances of these networks which have different number of neurons in hidden layers are shown in figure 4.13. As depicted by this figure, the best test results are obtained from the network which has 4 hidden neurons in the hidden layer. Therefore, single hidden layer with 4 neurons was selected for the prediction of surface roughness. Table 4.14 shows single hidden layer structure with 4 nodes produced the least MSE.

Table 4.14: Mean square error using different number of hidden neurons

Number of Hidden Neurons	Mean square error (MSE)
1	6.0698×10^{-5}
2	6.9635×10^{-5}
3	12.0436×10^{-5}
4	5.0002×10^{-5}
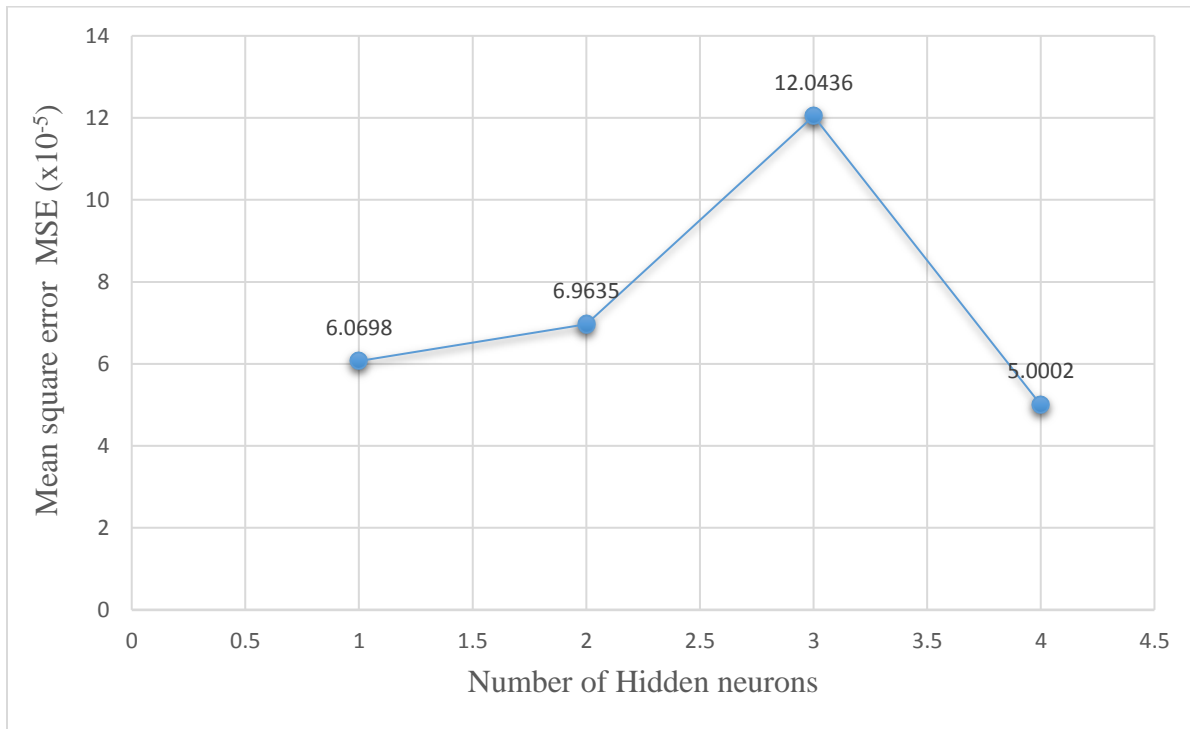
Figure 4.13**:** Performance of ANNs with different hidden layer neurons

The MSE of training of the selected ANN was about 5.0002×10^{-5} and its training took almost 7 epochs to complete. The MSE of all the three groups when the early stopping technique was applied during the training of the neural network are presented in figure 4.14.
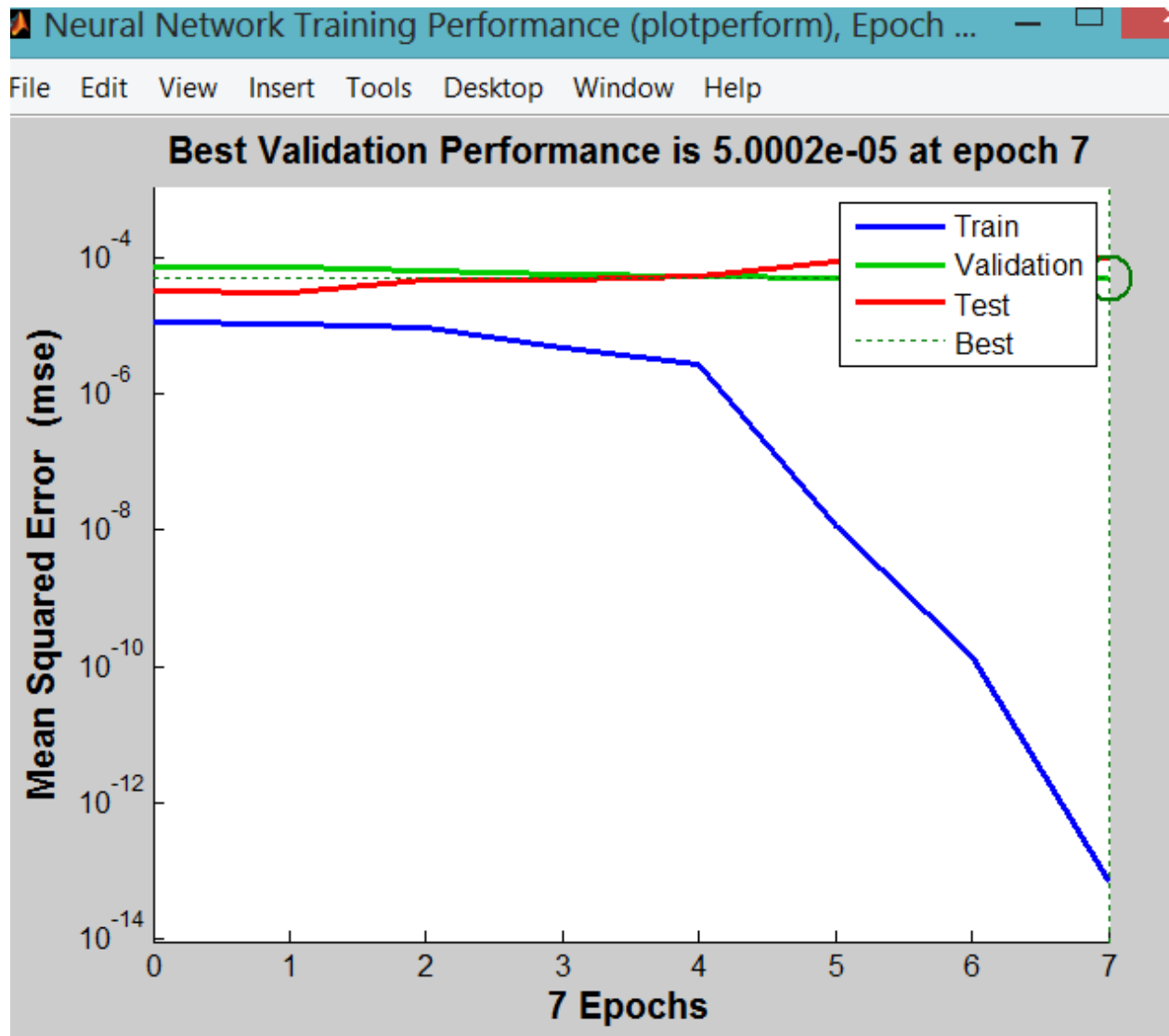
Figure 4.14**:** Results of the neural network training

From the figure it is evident that validation and testing group MSEs are higher than that of the training group, as expected. Moreover, they have similar values which indicates that the proposed neural network possesses good generalization ability, thus being able to model the surface roughness.

To compare the results clearly, a post-process operation is performed by using 'postreg' command of MATLAB. Postreg command post-processes the network training set by performing a linear regression between each element of the network response and the corresponding target. Where R is the regression value (R = 1 means perfect correlation) [124]. The post-regression results of 4

hidden neurons in the hidden layer is illustrated in the figure 4.15. The post-regression results show that the R values for training, validation and testing shows better prediction of surface roughness (R = 1).
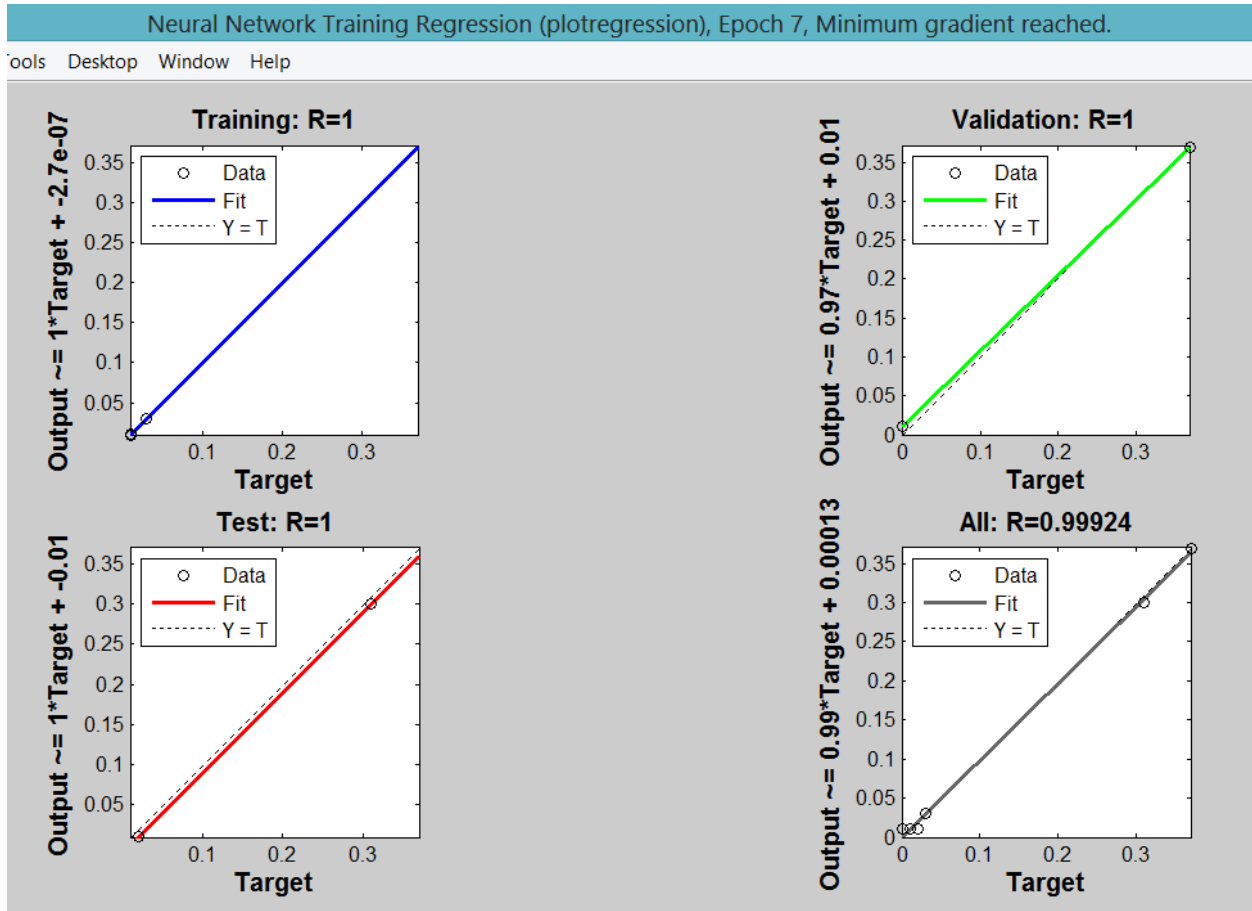
Figure 4.15: Post-regression results of 4 hidden neurons in single hidden layer

Training of the neural network model was performed using 10 experimental data out of 15 data as explained in Section 4.4. The trained network model was tested using five experimental data points (experiment 11-15), which were not used in the training process. The results predicted from the ANN model are compared with those obtained by experimental test in table 4.15 for 5 experimental test sets. It can be seen from table 4.15 that ANN prediction is in good agreement with the experimental results.

Table 4.15**:** Comparison of ANN results with experimental findings (Experiment 11-15)

Run	Measured Ra (nm)	ANN Predicted Ra (nm)	Error (%)
11	28.3	30.99	9.51
12	20.6	10.34	49.81
13	28.1	29.34	4.41
14	1184.1	990.37	16.36
15	36.6	32.46	11.31

Then, Figure 4.16 compares the neural network surface roughness prediction with experimental test results for experiment 11-15 data sets.
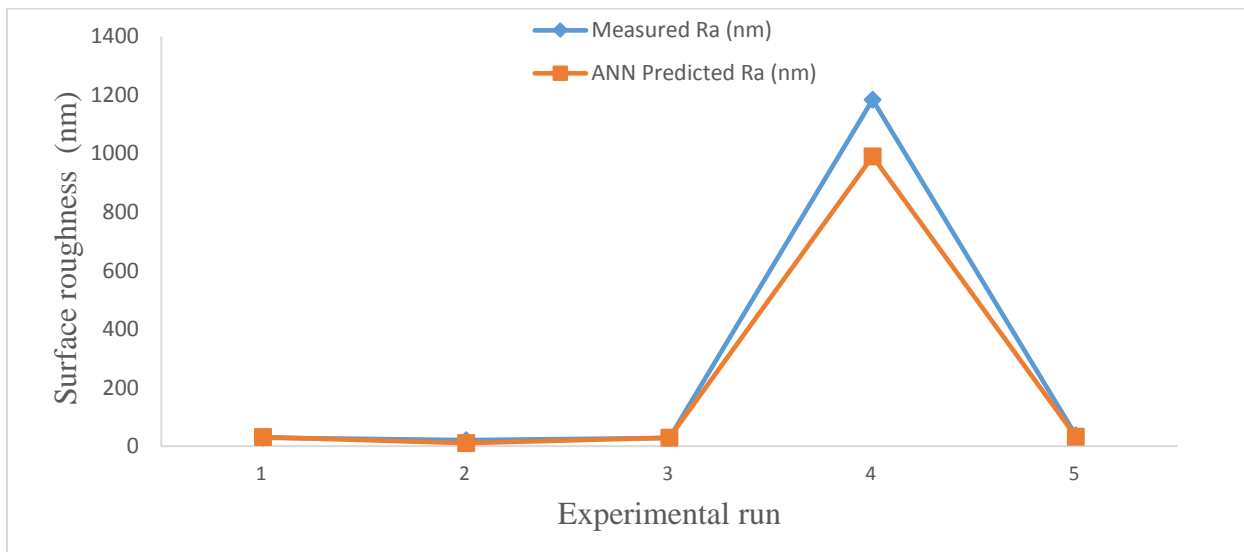
Figure 4.16**:** Comparison of the measured surface roughness and predicted surface roughness of ANN model

It is found that the developed ANN model has good interpolation capability and can be used as an efficient predictive tool for surface roughness. Increasing the number of nodes increases the computational cost and decreases the error [110]. In this study, ANN structure shown in Figure 4.17 is used for modeling and predicting surface roughness in turning operations. This fully connected hierarchical network structure has an input layer, a hidden layer, and an output layer.
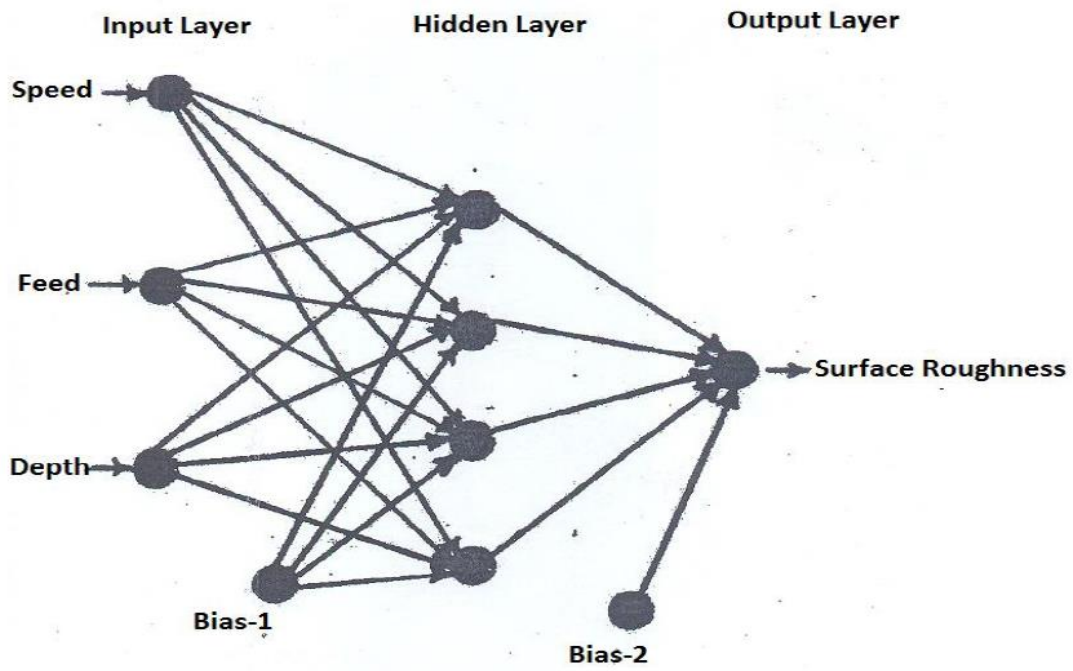
Figure 4.17: ANN Structure

4.7 Comparison of ANN and RS Models for Surface Roughness

In this section, the comparison between RSM and ANN modeling will be carried out. Both methods have been performed for the diamond turning of ONSI-56 polymer and prediction models have been obtained. In order to compare the modeling results of RSM and ANN with the experimental results. Five random factors (experiment 11-15) ware used. The performance criteria considered is the mean absolute percentage error (MAPE)

$$MAPE = \left(\frac{1}{n}\sum_{i=1}^{n}\left|\frac{R_{a,i}-R^{P}_{a,i}}{R_{a,i}}\right| \times 100\right)$$
(4.9)

Where

MAPE = mean absolute percentage error, n = the total number of measurements, i = the estimated measurement for a specific run, $R_{a,i}$ = the measured surface roughness for a specific run, $R^{p}_{a,i}$ = the predicted surface roughness for a specific run

Table 4.16 shows the comparison results according to accuracy values of RS model and neural network model. Equation 4.7 is used to calculate the MAPE for each model.

Table 4.16**:** Comparison of RSM and ANN with experimental results (experiment 11-15)

Run order	Experimental R$_a$ (nm)	RSM Predicted R$_a$ (nm)	ANN Predicted R$_a$ (nm)
11	28.3	25.03	30.99
12	20.6	29.96	10.34
13	28.1	29.96	29.34
14	1184.1	1002.25	990.37
15	36.6	22.87	32.46
MAPE		*23.29*	*18.28*

The prediction error of the ANN model for the surface roughness is 18.28%. The error rate has been calculated as 23.29% by RS model. Therefore, RS model has also made reasonable predictions of surface roughness. The results of the ANN model indicate it is much more robust

and accurate in estimating the values of surface roughness when compared with the response surface model.

	11	12	13	14	15
Experimental Ra (nm)	28.3	20.6	28.1	1184.1	36.6
RSM Predicted Ra (nm)	25.03	29.96	29.96	1002.25	22.87
ANN Predicted Ra (nm)	30.99	10.34	29.34	990.37	32.46
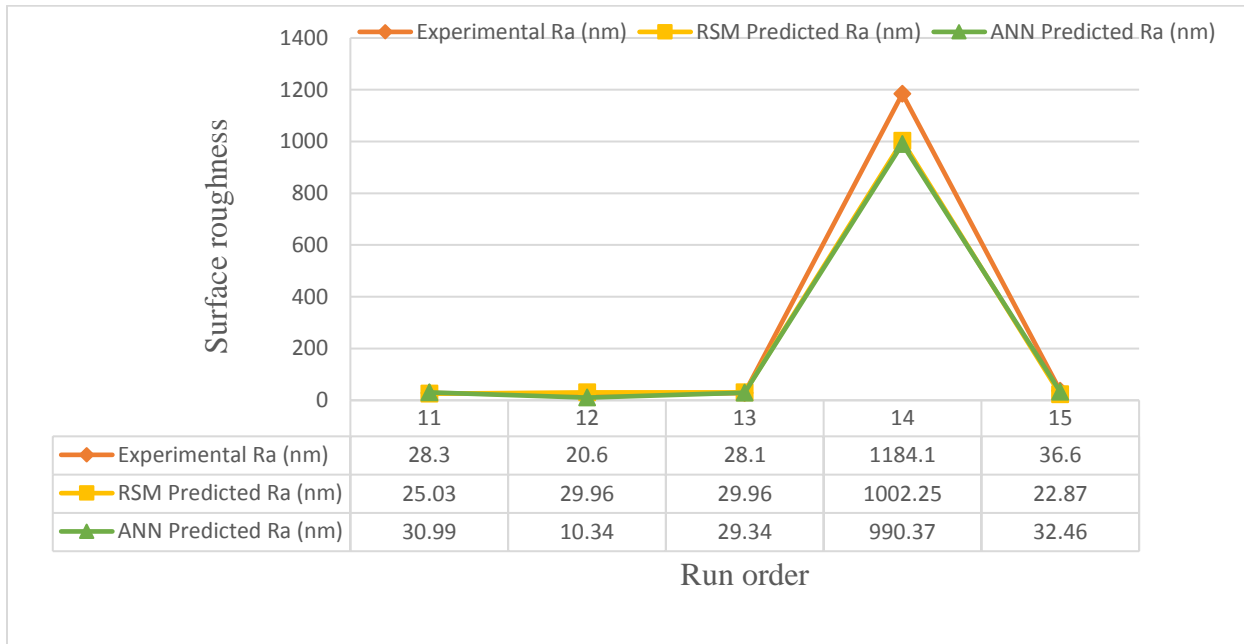
Figure 4.18**:** Comparison of experimental Ra, RSM and ANN Modeling

It is clearly seen (Figure 4.18) that the proposed models are capable of predicting the surface roughness. Nevertheless, the ANN model estimates the surface roughness with high accuracy compared to the RS model. So, the proposed models can be used effectively to predict the surface roughness in diamond turning of ONSI-56 contact lens polymers.

4.8 Experimental Investigation of Triboelectric Wear in ONSI-56 Contact Lens Polymer

4.8.1   Electrostatic Discharge (ESD) Experiment

According to Gubbels [11], tribo-electric wear can occur due to significant electrostatic discharge and the occurrence of electric fields on polymer surfaces. This results in so-called Lichtenberg figures. Lichtenberg figures originate when a dielectric is irradiated with electrons. These electrons get trapped inside the material and accumulate. Research in the ultra-high precision of glassy polymers, identifies Lichtenberg wear patterns on the tool as yields resulting from significant static charging and discharging [125]. A Lichtenberg figure that damaged a diamond cutting tool during polymer turning is shown in figure 4.19.

Nevertheless, during polymers machining, it has been established that the adhesion of the tool chip around the tool dictates the presence of an electrostatic force field [15]. This phenomenon known as tribo-electric charging is responsible for tool wear and poor surface finish.
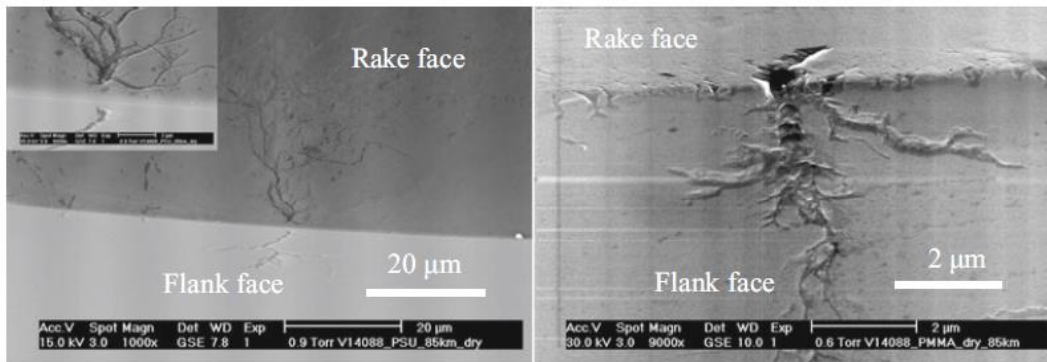
Figure 4.19: Lichtenberg figure on a diamond tool [11] originates from electric discharge

This section will present measurements for determining the electrostatic discharge in diamond turning of ONSI-56 contact lens polymer. It can be expected that turning parameters, such as cutting speed, feed rate and depth of cut, will directly influence the statics during turning. Besides these turning parameters, the environmental effect of relative humidity and workpiece properties may also influence the amount of charging [11]. In this study, only the influence of cutting parameters on ESDs are considered. This study will present measurements that were performed to describe the tribo-electric tool wear in diamond turning of ONSI-56 contact lens polymers. This experimental study is aimed at investigating the tribo-electric charging in the UHPM of ONSI-56

contact lens, and evaluating the effects of cutting parameters such as feed rate, cutting speed and depth of cut. The electrostatic sensor and monitor were implemented to provide online measurements of the ESDs. The experiments were conducted based on the setup discussed in chapter 3.

4.8.2 Response Surface Modeling

Box–Behnken Design (BBD), the effective response surface method (RSM) with the lowest number of experiment was used to plan the experiment using Design Expert 7 software. RSM can be used for many of purposes such as analyzing of experimental data or response prediction, RSM can be considered to be helpful in predicting the statics value. The experimental setup is depicted in figure 4.20. While table 4.17 shows the experimental results for the empirical relationship between the response parameter (ESDs) and the cutting parameters (speed, feed, and depth of cut) used in this study.
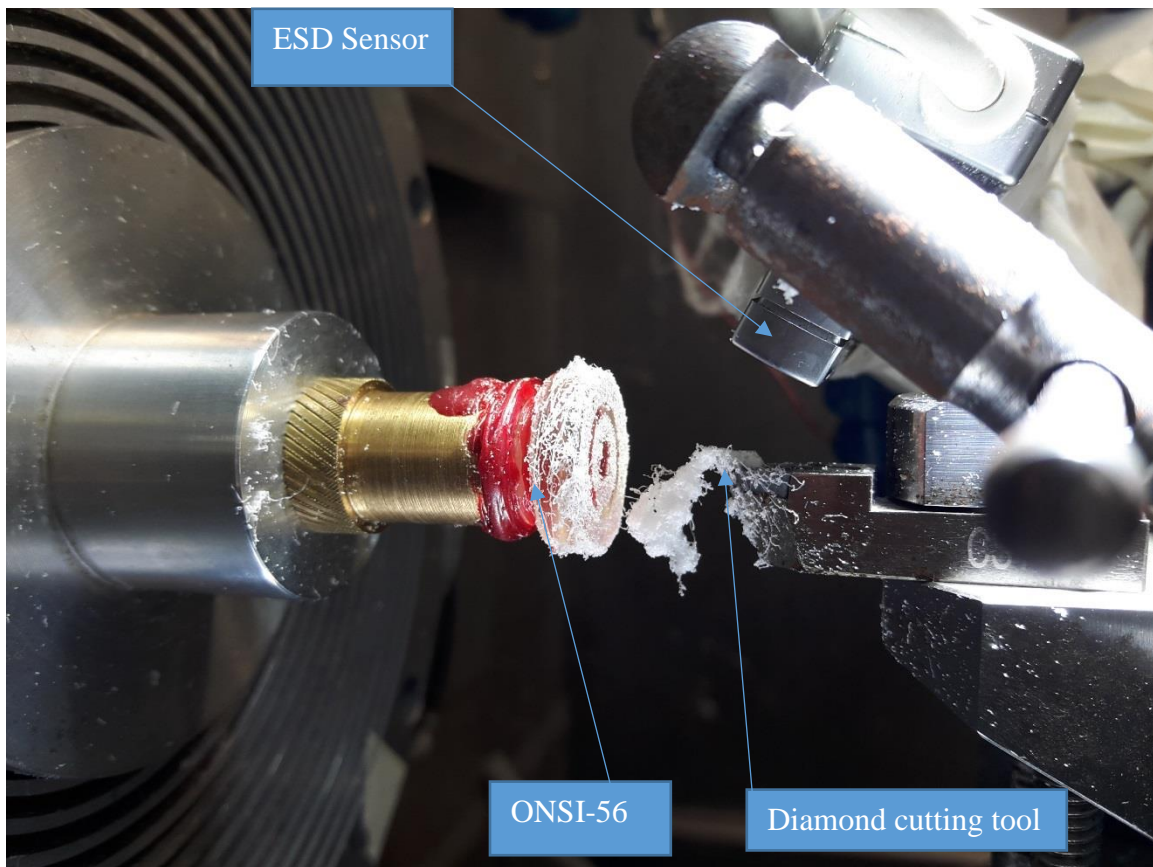
Figure 4.20: ONSI-56 Electrostatic discharge setup

Table 4.17: Experimental results

Run Order	Cutting Speed (rpm)	Feed Rate (mm/min)	Depth of Cut (μm)	Electrostatic Discharge (kV)
1	2100	2	10	0.4107
2	2100	7	25	0.571
3	200	2	25	1.859
4	4000	7	40	1.323
5	2100	2	40	1.553
6	2100	7	25	0.741
7	200	7	40	14.296
8	200	7	10	0.468
9	4000	2	25	0.339
10	2100	7	25	1.632
11	4000	7	10	0.929
12	2100	12	40	3.524
13	2100	12	10	1.433
14	200	12	25	4.619
15	4000	12	25	1.363

Also, figure 4.21 shows the series plots of the measured ESD. During the machining tests at speed of 200 rpm and 40 μm depth, tool–chip build-up was observed at the surface of the tool from experimental run 7 (ESD 14.296 kV). This was accounted to be as a result of continuous chip formation, which tangle around the workpiece and tool.

Figure 4.21: Series plots for ESD values

4.8.3 Determination of Appropriate Polynomial Equation to Represent RSM Model

The procedures for developing the electrostatics discharge models in this study have been well detailed by Alao [111]. According to Alao and Konneh [112], the development of RS models includes checking the response data for any transformation need, fitting of the input and output variables to know whether the relationship between them is linear, linear and two-factor interaction (2FI), second-order or higher-order function and investigating the p values. Design Expert software (7.1.6) version was used for analyzing the output data. To obtain an adequate model equation, response transformation check is necessary. This transformation is carried out using Box–Cox plotting technique available in Design Expert software.

4.8.4 Response Transformation Check

Based on the experimental results in table 4.17, the electrostatic discharge response ranges from 0.339 kV to 14.296 kV. The ratio of maximum to minimum is:

$$\frac{14.296}{0.339} = 42.171 \qquad (4.10)$$

95

However, a ratio greater than 10 usually indicates a transformation is required [113]. Therefore, a transformation is required for a ratio of 42.171. For this analysis, Box-Cox plotting technique is used for the selection of the transformed scale model.
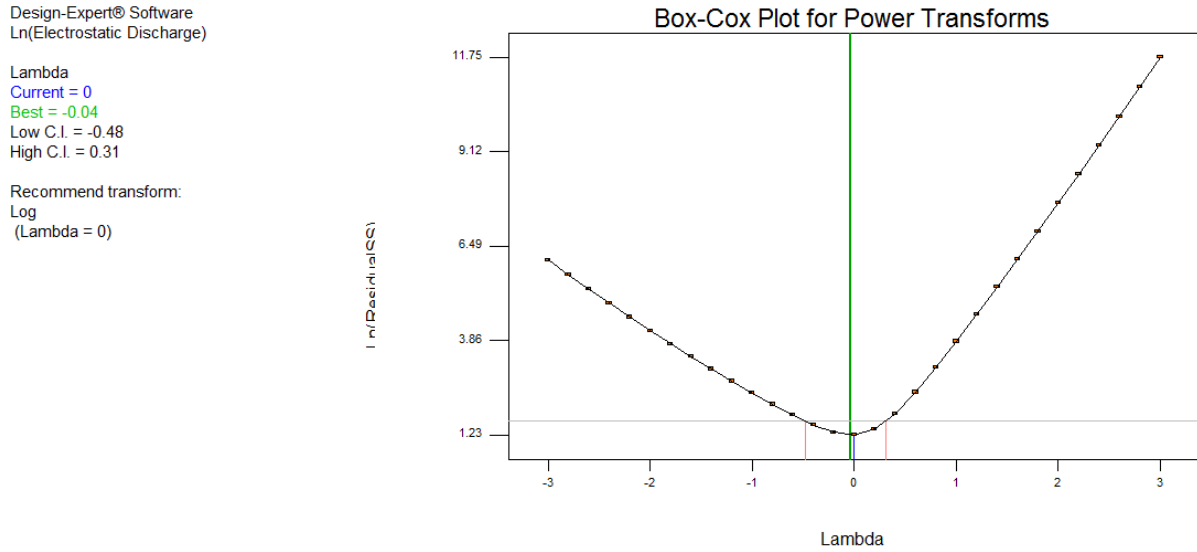
Figure 4.22: Box-Cox plot for transformed scale ESD

Based on the Box-Cox plot (Figure 4.22), natural log transformation was selected, which produced a model of the form

$$y' = Ln\ (y\ +\ k) \tag{4.11}$$

In this research, a natural log transformation was used to determine a suitable polynomial equation to represent the relationships between the input parameters (cutting peed, feed rate and depth of cut) and the electrostatic discharge (output response) by carrying out sum of squares sequential model and lack of fit test shown in tables 4.18 and 4.19 respectively. The result from the sequential model indicate linear vs mean and 2FI vs linear approach, however the lack of fit test suggests a linear and 2FI approach.

Table 4.18: Sequential Model Sum of Squares for ESD

Source	Sum of squares	df	Mean Square	F Value	p-Value Prob>F	Remark
Mean vs Total	1.23	1	1.23			
Linear vs Mean	9.56	3	3.19	8.17	0.0038	suggested
2FI vs Linear	2.45	3	0.82	3.56	0.0670	suggested
Quadratic vs 2FI	0.76	3	0.25	1.16	0.4106	
Cubic vs Quadratic	0.48	3	0.16	0.54	0.7010	Aliased
Residual	0.60	2	0.30			
Total	15.08	15	1.01			

Table 4.19: Lack of Fit Tests for ESD

Source	Sum of squares	df	Mean Square	F Value	p-Value prob>F	Remark
Linear	3.69	9	0.41	1.37	0.4913	Suggested
2FI	1.24	6	0.21	0.69	0.6933	Suggested
Quadratic	0.48	3	0.16	0.54	0.7010	
Cubic	0.000	0				Aliased
Pure Error	0.60	2	0.30			

4.8.5 Electrostatic Discharge Model Determination

Table 4.20 shows the statistical summary for each model that was output by Design Expert Software. A Linear and 2FI model were suggested, even though a linear model has lower R^2 and adjusted-R^2 (Adj-R^2) values than a quadratic and cubic models. This is because the cubic model is aliased, which means that the effects of each variable that caused different signals become indistinguishable. For a linear relationship, the R^2 and Adj-R^2 values are 0.6902 and 0.6058, respectively. It is clear that the quadratic model is not adequate for the experimental data. The 2FI model was therefore selected to fit the experimental data.

Table 4.20: Statistical summary for each model

Source	Std. Dev	R-Squared	Adjusted R-Squared	Predicted R-Squared	PRESS	Suggestion
Linear	0.62	0.6902	0.6058	0.4158	8.09	Suggested
2FI	0.48	0.8673	0.7679	6266	5.17	Suggested
Quadratic	0.47	0.9219	0.7812	3438	9.09	Not adequate
Cubic	0.55	0.9568	0.6976		+	Aliased

4.8.6 Analysis of Variance (ANOVA) for the Acquired ESD Model

ANOVA of experimental data is always done to analyze statistically the relative significance of the models and its terms on the response. The ANOVA have been performed to check whether the model is adequate as well as to check the significance of the individual model coefficients. The Model F-value of 8.72 in table 4.21 implies the model is significant. There is only a 0.37% chance that a "Model F-Value" this large could occur due to noise. A p-value lower than 0.05 indicates that the model is statistically significant, whereas a value higher than 0.1000 indicates that the model is not significant [116].

Table 4.21: ANOVA results for the acquired model

Response	**1**		**Electrostatic Discharge**			
Transform:	**Natural log**	**Constant:**	**0**			
ANOVA for Response Surface 2FI Model						
Analysis of variance table [Partial sum of squares - Type III]						
	Sum of		**Mean**	**F**	**p-value**	
Source	**Squares**	**df**	**Square**	**Value**	**Prob > F**	
Model	12.02	6	2.00	8.72	0.0037	significant
A-Speed	2.66	1	2.66	11.58	0.0093	
B-Feed	2.40	1	2.40	10.45	0.0120	
C-Depth	4.50	1	4.50	19.59	0.0022	
AB	0.057	1	0.057	0.25	0.6327	
AC	2.35	1	2.35	10.24	0.0126	
BC	0.045	1	0.045	0.20	0.6684	
Residual	1.84	8	0.23			
Lack of Fit	1.24	6	0.21	0.69	0.6933	not significant
Pure Error	0.60	2	0.30			
Cor Total	13.86	14				

In this case A, B, C and AC are significant model terms whereas AB and BC are insignificant model terms. However, the model can be improved by eliminating the terms that are not very significant even though table 4.22 shows high coefficient of determination R^2 value of 0.8673 and Adj-R^2 value of 0.7679.

Table 4.22: Regression coefficient analysis

Std. Dev.	0.48	R-Squared	0.8673
Mean	0.29	Adj R-Squared	0.7679
C.V. %	167.71	Pred R-Squared	0.6266
PRESS	5.17	Adeq Precision	10.683

4.8.7 Electrostatic Discharge Model Modification

After the significance of the parameters has been evaluated, the model was improved by eliminating the terms that are not very significant. The ANOVA results for the modified model describing the relationship between the statics and cutting parameters is shown in table 4.23

Table 4.23**:** ANOVA results for acquired ESD model (only the significant terms)

Source	Sum of squares	Degrees of Freedom	Mean Square	F- Value	p-Value Prob>F	Characteristics
Model	11.92	4	2.98	15.35	0.0003	*Significant*
A-Speed	2.66	1	2.66	13.72	0.0041	
B-Feed	2.40	1	2.40	12.38	0.0056	
C-Depth	4.50	1	4.50	23.20	0.0007	
AC	2.35	1	2.35	12.12	0.0059	
Residuals	1.94	10	0.19			
Lack of Fit	1.34	8	0.17	*0.56*	*0.7714*	*Not significant*
Pure Error	0.60	2	0.30			
Corr. Total	13.86	14				

ANOVA have been performed to check whether the modified model is adequate as well as to check the significance of the individual model coefficients. The Model F-value of 15.35 in table 4.23 implies the modified model is significant. There is only a 0.03% chance that a "Model F-Value" this large could occur due to noise. Values of "Prob>F" less than 0.05 indicate the model terms are significant. From the modified ANOVA table, it is clear that (based on p-value) the cutting speed (A), feed rate (B), depth of cut (C) and the interaction between speed and depth are the most sensitive factors that influence the electrostatics discharge. This implies that these factors have very large effects on ESD. The "Lack of Fit F-value" of 0.56 implies the Lack of Fit is not significant relative to the pure error. There is a 77.14% chance that a "Lack of Fit F-value" this large could occur due to noise. Non-significant lack of fit is good -- we want the model to fit. The lack of fit test of Fit value of 0.56 is not significant, indicating that all the data fit the model

adequately for this study. After determining the significant coefficients (at 95% confidence level), the final modified model was developed using only these coefficients and the final mathematical transformed scale 2FI model to estimate ESD is given by equation 4.12 and 4.13 below

$$\ln(ESD) = -2.50654 + 3.69073 \times 10^{-4}S + 0.10958F + 0.10651D - (2.69050 \times 10^{-5})SD \quad (4.12)$$

The equation can be rewritten as

$$(ESD) = e^{[-2.50654 + 3.69073 \times 10^{-4}S + 0.10958F + 0.10651D - (2.69050 \times 10^{-5})SD]} \quad (4.13)$$

Where: ESD = Electrostatic discharge, D = Depth of cut, F = Feed rate and S = Cutting speed

As can be seen from regression coefficient results (Table 4.24). The "Pred R-Squared" of 0.6706 is in reasonable agreement with the "Adj R-Squared" of 0.8040. For models to be adequate and accurate, it is suggested that Adj-R^2 should be greater or equal to 0.70 [117]. Adj-R^2 of 0.8040 indicate that the modified model is very significant.

Table 4.24**:** Summary of regression analysis results

Std.Dev.	0.44	R^2	0.8600
Mean	0.29	Adj-R^2	0.8040
C.V. %	154.12	Pred-R^2	0.6706
PRESS	4.56	Adeq-Precision	13.337

"Adeq Precision" measures the signal to noise ratio. A ratio greater than 4 is desirable. The ratio of 13.337 indicates an adequate signal. At the same time a relatively low value of the coefficient of variation (CV=154.12) indicates improved precision and reliability of the conducted experiments. Therefore, the modified model can be used to navigate the design space (ESD) for ONSI-56 contact lens polymers.

The coefficient of determination (R^2) is defined as the ratio of the explained variation to the total variation, and is a measure of the degree of fit [118]. Hence, Joglekar [119] suggested that a good

model fit should yield an R^2 of at least 0.80. This means that the modified response model evaluated in this study can explain the reaction very well, with an R^2 of 0.8600 and an Adj-R^2 of 0.8040 at a confidence level of 95% as shown in table 4.24. In addition, the model is very significant as is evident from its F-value (F_{Model} = 15.35) and very low probability value (p = 0.0003). A p-value lower than 0.05 indicates that the model is statistically significant, whereas a value higher than 0.1000 indicates that the model is not significant [116].

4.8.8   ESD Model Accuracy Check

To obtain an adequate model, an accuracy check is necessary. The RS model accuracy was checked by comparing the predicted and experimental electrostatic discharge (ESDs). Table 4.25 shows the prediction accuracy for RS model. The RSM results demonstrate that the proposed model in this study is suitable for predicting the ESDs with an R^2 of 0.8600.

Table 4.25: Comparison of measured and predicted ESD RS modelling

Run	Measured ESD (kV)	RSM Predicted ESD (kV)	Residuals (kV)	Error (%)
1	0.4107	0.364	0.0467	11.37
2	0.571	1.336	-0.765	133.98
3	1.859	1.363	0.496	26.68
4	1.323	0.733	0.59	44.59
5	1.553	1.632	-0.079	5.09
6	0.741	1.336	-0.595	80.29
7	14.296	10.805	3.491	24.42
8	0.468	0.522	-0.054	11.54
9	0.339	0.432	0.093	27.43
10	1.632	1.336	0.296	18.14
11	0.929	0.763	0.166	17.87
12	3.524	4.855	-1.331	37.77
13	1.433	1.088	0.345	24.08
14	4.619	4.096	0.523	11.32
15	1.363	1.297	0.066	4.84

Figure 4-23 shows the performance of RS model.
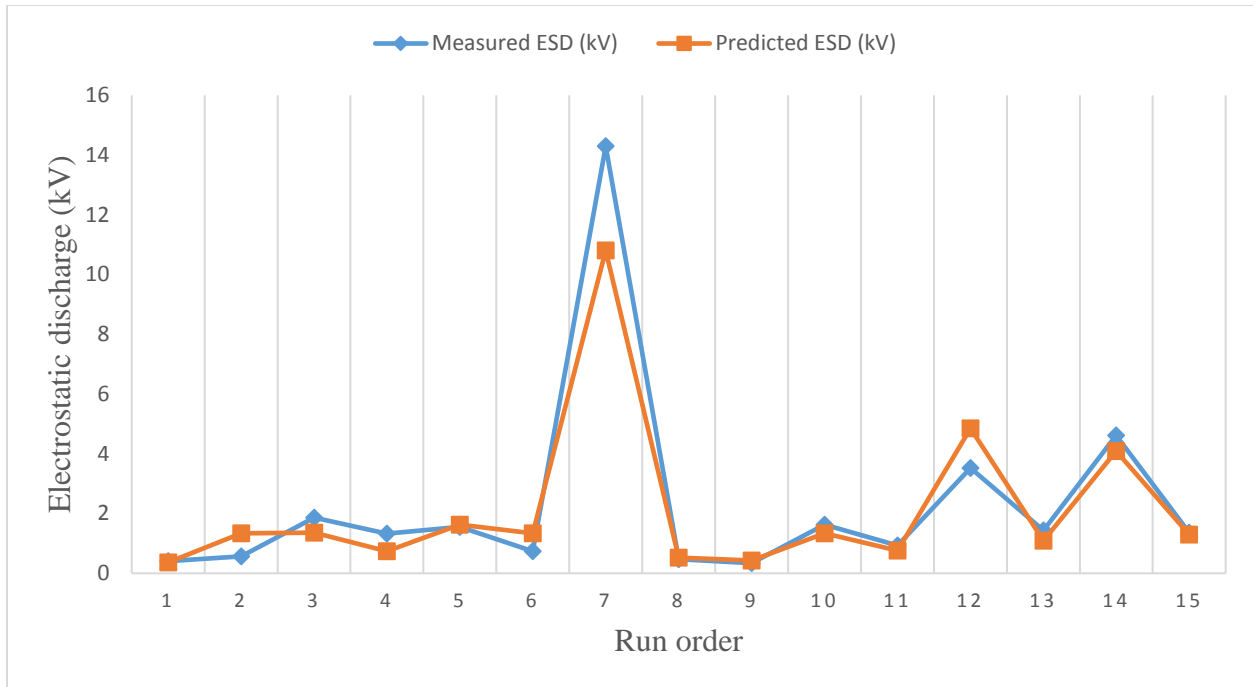
Figure 4.23: Comparison of measured and predicted ESD values for RS Model

In addition, a normal plot of residuals between the normal probability (%) and the internally studentized residuals and the plot of residuals versus the predicted response was also obtained. In this way, the residuals can be checked to determine how well the modified model satisfies the assumptions of ANOVA, and the internally studentized residuals can be used to measure the standard deviations separating the experimental and predicted values [120]. The normal probability plot of the residuals for ESD shown in figure 4.24 reveals that the residuals are falling on the straight line, which means the errors are distributed normally [121].
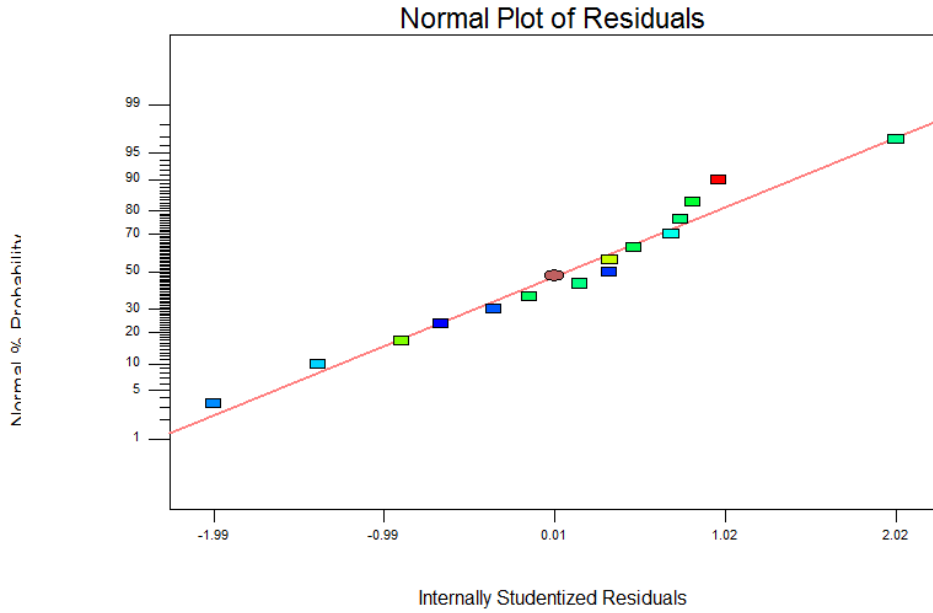
Figure 4.24: Normal Probability plot of residuals in ESD RS modelling

Figure 4-25 shows a plot of residuals versus predicted in ESD modelling. This indicates that the model possesses adequate normality of residuals and no constant error.
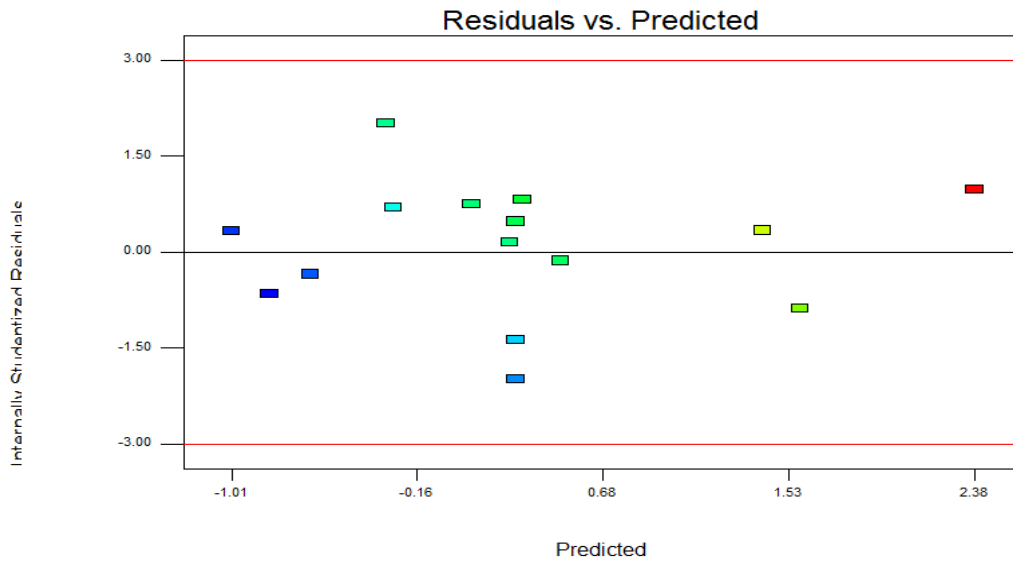
Figure 4.25: Probability plot of residuals vs Predicted in ESD RS modelling

4.9 Determination of Significant Factors Influencing the Electrostatics Discharge

In determining the cutting parameters influential to the ESD, the results from the modified ANOVA table 4.23 (Section 4.6.5) were studied. By checking the p values and F values in table 4.23, it is clearly seen that all the model terms are significant with depth of cut having the highest degree of significance followed by the cutting speed and the interaction between depth of cut and cutting speed. However, feed rate has the lowest degree of significance on the electrostatics discharge.

4.9.1   Effect of Depth of Cut

The influence of depth of cut in diamond turning of ONSI-56 contact lens is illustrated in figure 4.26. It can be clearly seen that the ESD values increases with an increase in depth of cut. This shows that ESD is directly proportional to depth of cut. It can be concluded that there is a simple linear relationship between ESD and depth of cut because an increase in depth of cut generates high ESD values.

At low cutting speed and low feed rate (Figure 4.26), the increase in depth of cut generates high ESD values range from $e^{-0.654} = 0.519$ kV to $e^{2.379} = 10.794$ kV
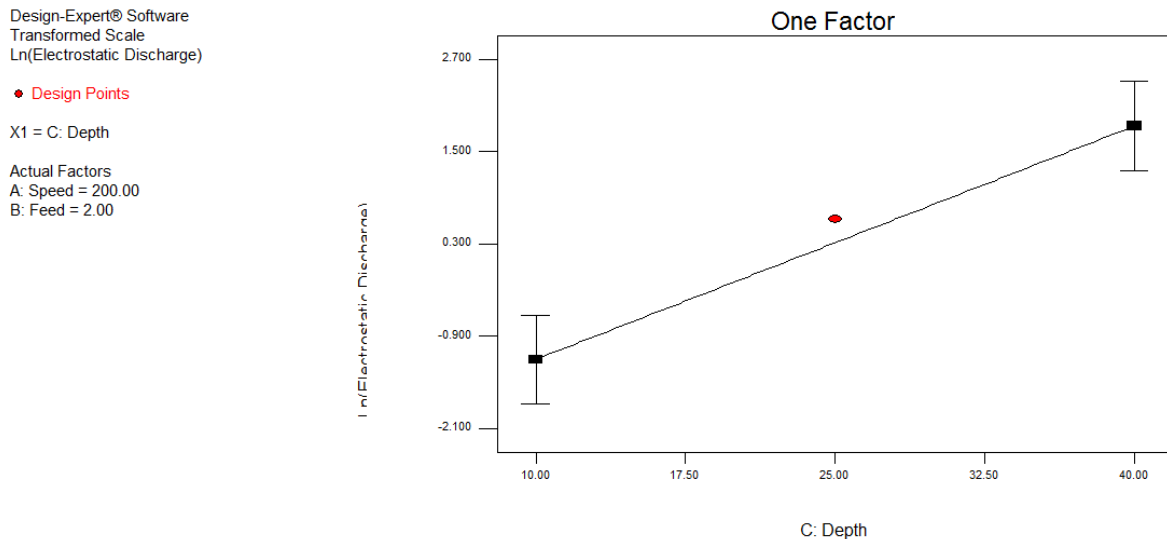
Figure 4.26**:** Variation of ESD with Depth of cut at low feed and low speed

Figure 4.27 Shows the variation of ESD and depth of cut at high cutting speed and high feed rate. In this case, an increase in depth of cut results in decrease of ESD values range from $e^{0.274} = 1.315$ kV to $e^{0.240} = 1.271$ kV

Design-Expert® Software
Transformed Scale
Ln(Electrostatic Discharge)

● Design Points

X1 = C: Depth

Actual Factors
A: Speed = 4000.00
B: Feed = 12.00

One Factor
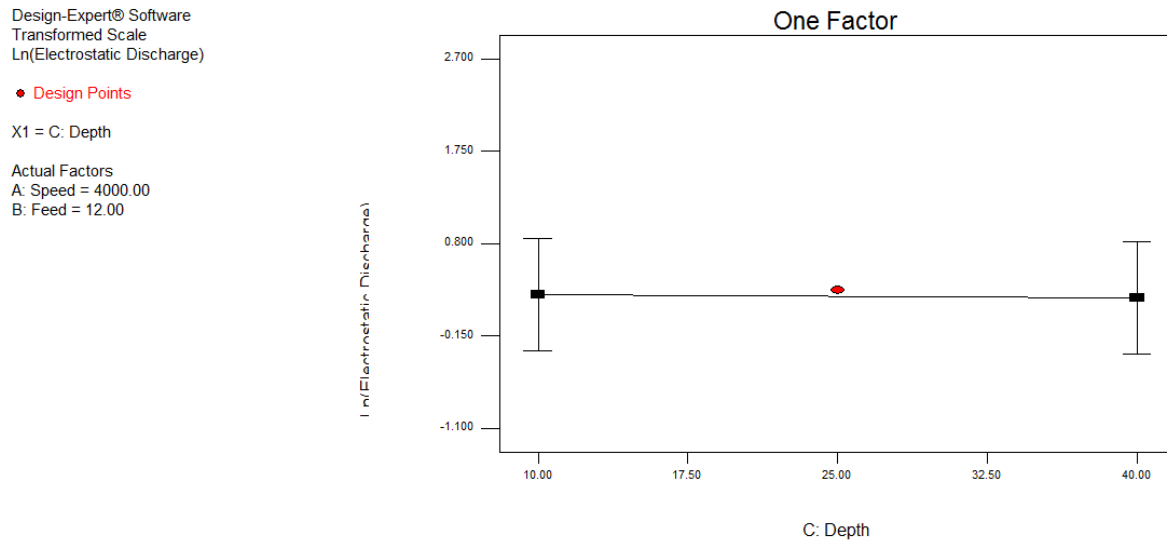
Figure 4.27: Variation of ESD with depth of cut high feed and high speed

During the experiment, an increase in the depth of cut, with constant cutting speed and feed rate, produces a thicker chip. The experiments that yielded the highest ESD values are shown below with a picture of the chips enclosed. During investigations, it was observed that some experiments resulted in accumulation of cut chips at the tool surface as shown in figure 4.28. These chips bundled up and formed a larger surface area of contact between the tool and polymer surface resulting in high ESD measurements.
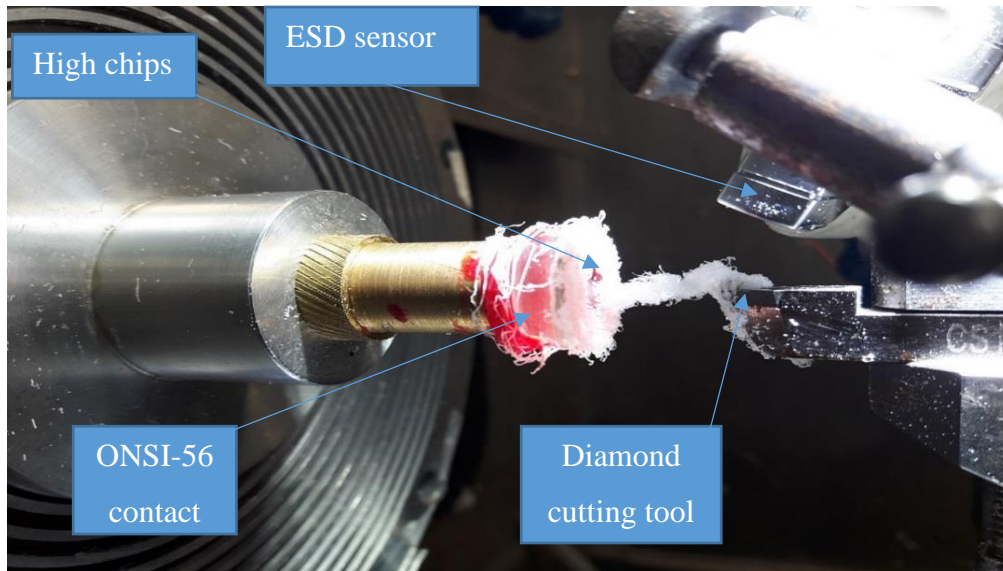
Figure 4.28: High chips build up from experimental run 7 (ESD of 14.296 kV)
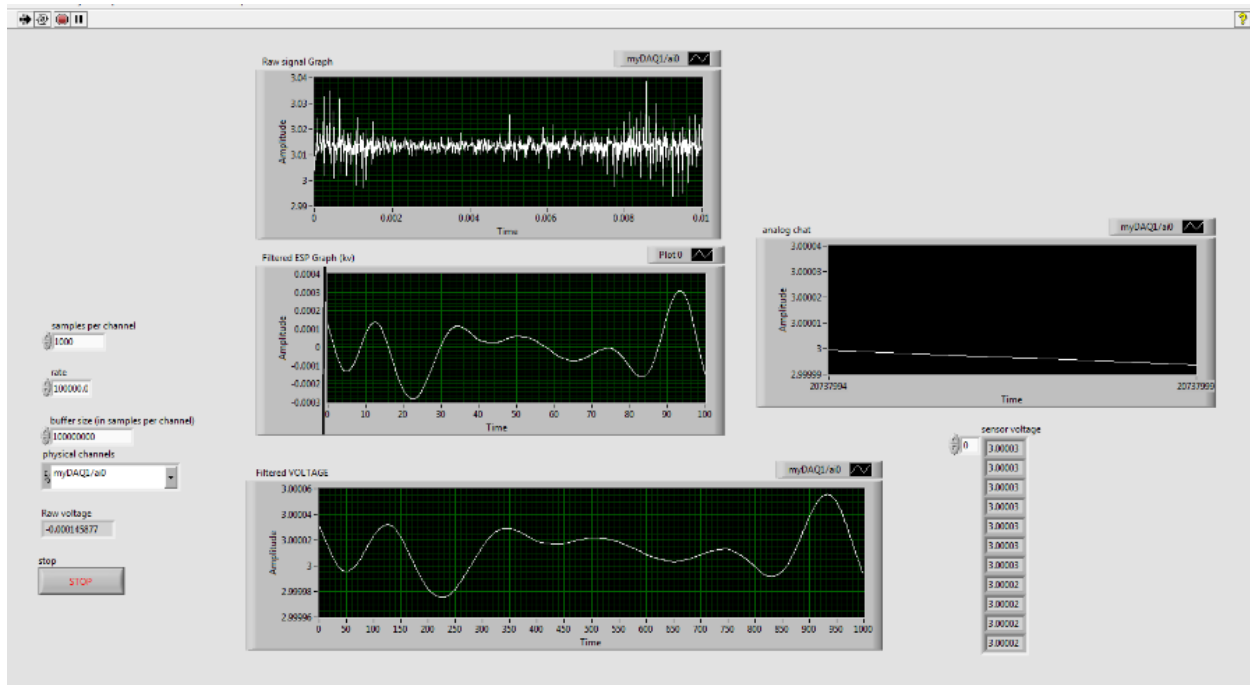
Figure 4.29: ESD signals for experimental run 7

During the machining tests at speed of 200 rpm and 40 µm depth, tool–chip build-up was observed at the surface of the tool (Experimental run 7). The results are, however, in agreement with the

results of Olufayo and Abou-El-Hossein [7]. This was accounted to be as a result of continuous chip formation, which tangle around the workpiece and tool. Figure 4.29 shows the progression of an acquired ESDs. It can be seen that this results agree with those found by Gubbels [68].

4.9.2 Effect of Cutting Speed

The effect of cutting speed is also analyzed during the experiments. According to modified ANOVA (Section 4.6.5), cutting speed is the second important parameter for ESD. One factor plot also shows that ESD values get bigger with decreasing cutting speed. Figure 4.30 illustrates that ESD values decrease from $e^{2.927} = 18.6715$ kV to $e^{0.240} = 1.2712$ kV with an increase in cutting speed.
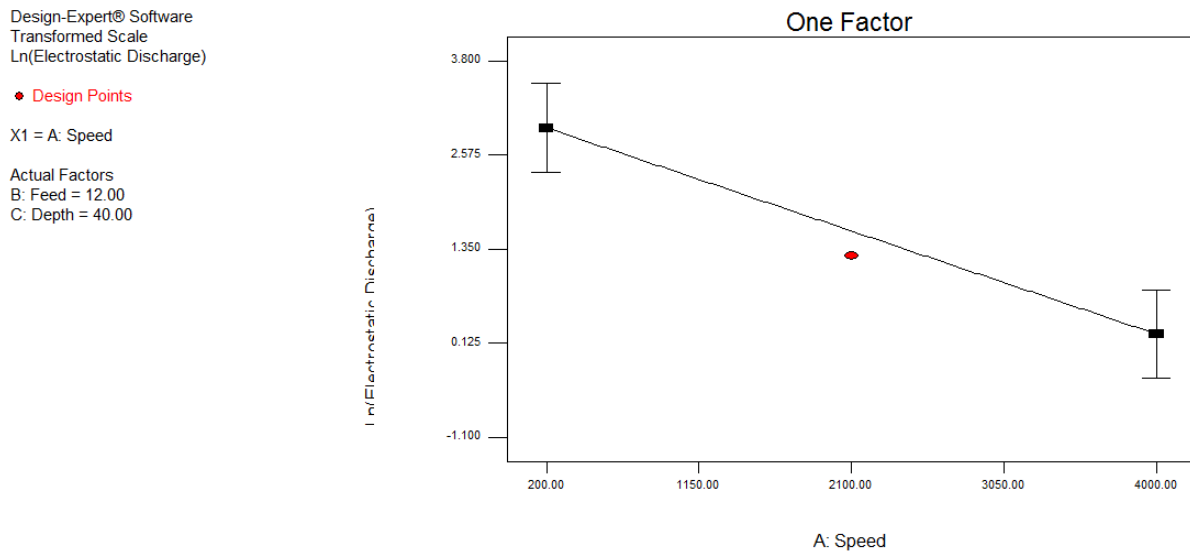
Figure 4.30: Variation of ESD with cutting speed at high feed and high depth

4.9.3 Effects of Feed Rate

Feed rate was another controlled parameter during this study. Depending on the effect test results, feed rate turned out to be the least important parameter when compared to depth of cut and cutting speed. Figure 4.31 shows the change of transformed scale ESD with feed rate for constant cutting speed and depth of cut. Increase in feed rate generates high ESD values range from $e^{-0.856} = 0.4249$ kV to $e^{0.240} = 1.2712$ kV

Design-Expert® Software
Transformed Scale
Ln(Electrostatic Discharge)

● Design Points

X1 = B: Feed

Actual Factors
A: Speed = 4000.00
C: Depth = 40.00

One Factor
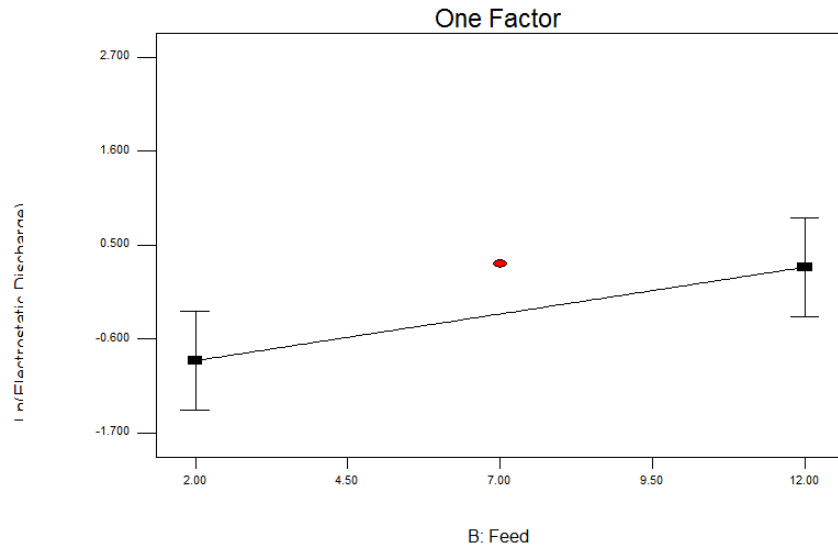
Figure 4.31: Variation of ESD with Feed rate at high speed and depth

4.9.4   Interaction Effect

There exists an interactive effect between cutting speed and depth of cut from modified ANOVA table (Section 4.6.5). The authentication of this interaction is shown in figure 4.32. As can be seen in figure. 4.32, at low depth of cut, increase in cutting speed, a negligible amount of static charges increased. However, at higher levels of depth of cut an opposite reaction was seen with a decrease in static generation. This shows there is an interaction between the cutting speed and depth of cut and these two parameters combine together to influence the generation of electrostatic charge. Figure 4.33 shows the 3D view of the interaction between cutting speed and depth of cut. Figure 4.34 shows the contour plot for the combined influence of cutting speed and depth at 7 mm/min feed rate on ESD.

110
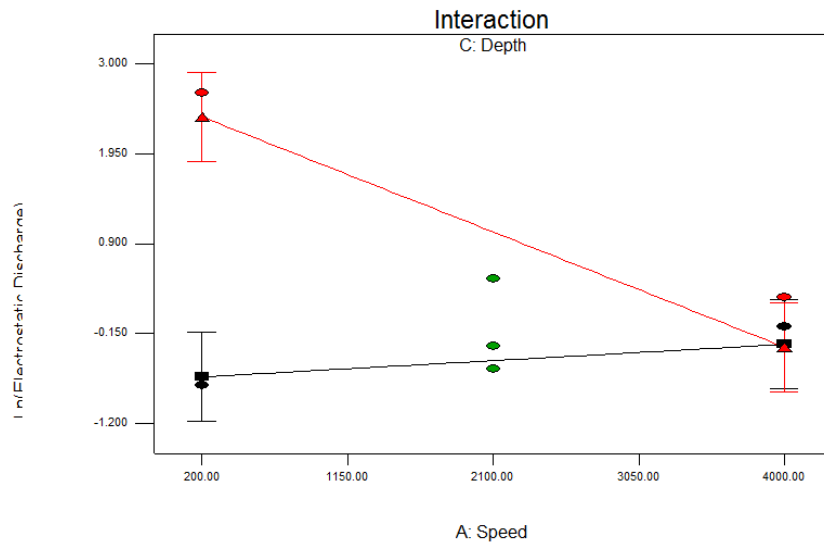
Figure 4.32: Behavior of ESD to interaction between depth and speed
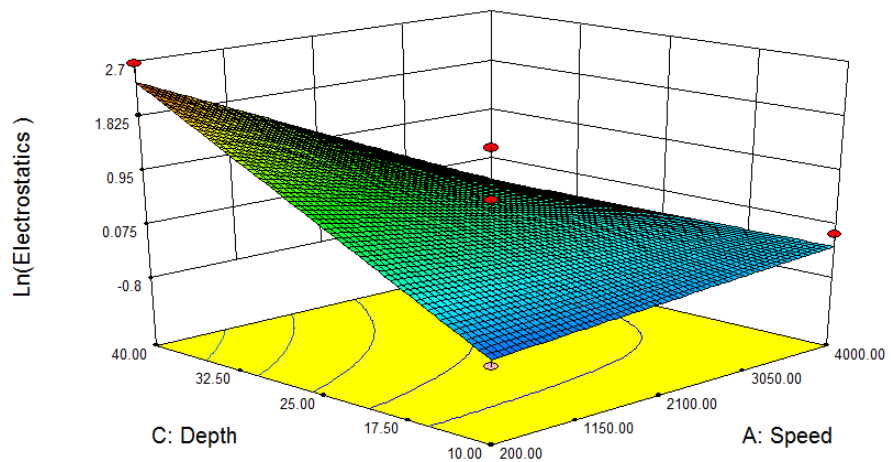
Figure 4.33: 3D view of the interaction between depth of cut and cutting speed
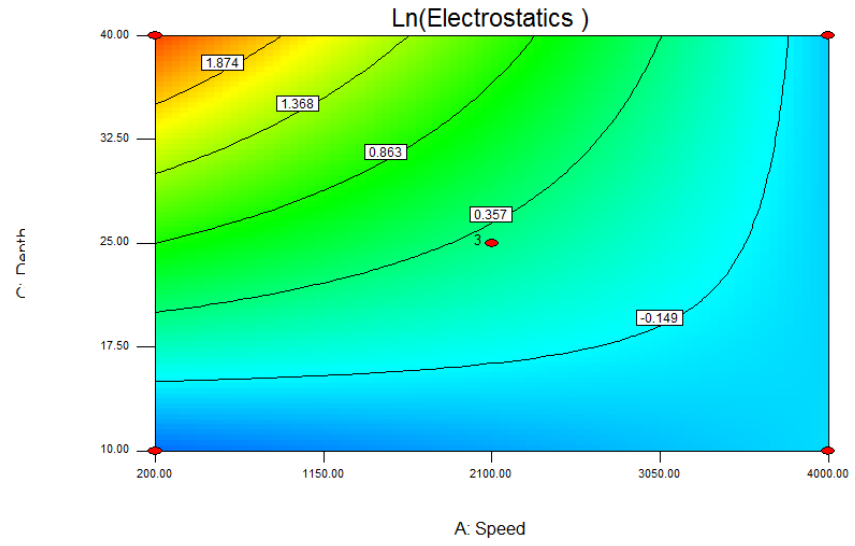
Figure 4.34: Contour plot for the combined influence of depth and cutting speed

4.10   Artificial Neural Network Model for Prediction of Electrostatic Discharge

The cutting parameters are the inputs and the electrostatic discharge is the output. The data are divided into two categories: training data and testing data. The training data are a random set of ten input samples from a total of 15 experimental findings. The testing data are the remaining five experimental findings, which does not intersect with the training data. The inputs and output were normalized before training the network since the parameters were in different ranges, these parameters were normalized within 0–1 ranges in order to prevent the simulated neurons from being driven too far into saturation. Table 4.26 shows the normalized ESD input and target data set for ANN modelling of ESD. The network is trained by using the Levenberg-Marquardt (LM) training function. Liu et al. [123] has proved that the sigmoidal function is easy to converge and provides fast learning speed using ANN model. Therefore, sigmoidal function is selected for the ANN model (equation 4.14).   Table 4.27 Shows the training parameters used in the Neural network.

$$f = \frac{1}{1 + e^{-x}} \qquad\qquad\qquad\qquad (4.14)$$

Table 4.26**:** Normalized Input and Target Data for ANN Model

Run order	Cutting speed (rpm)	Feed rate (mm/min)	Depth of cut (µm)	ESD (kV)
1	0.50	0.00	0.00	0.01
2	0.50	0.50	0.50	0.02
3	0.00	0.00	0.50	0.11
4	1.00	0.50	1.00	0.07
5	0.50	0.00	1.00	0.09
6	0.50	0.50	0.50	0.03
7	0.00	0.50	1.00	1.00
8	0.00	0.50	0.00	0.01
9	1.00	0.00	0.50	0.00
10	0.50	0.50	0.50	0.09
11	1.00	0.50	0.00	0.04
12	0.50	1.00	1.00	0.23
13	0.50	1.00	0.00	0.08
14	0.00	1.00	0.50	0.31
15	1.00	1.00	0.50	0.07

Table 4.27**:** Training parameters used

The number of layers	3
The number of neurons on the layers	Input: 3, Hidden:1,2,3 and 4, Output: 1
Learning rule	Levenburg-Marquatt
Activation function	Log-sigmoid
Mu	0.001
Error goal	2.779×10^{-5}
The normalization of data	0-1
The number of iteration	1000

The back-propagation algorithm is used to adjust the weights of the hidden layer neurons. In this study, the number of hidden layer neurons is varied from 1 to 4. Table 4.28 shows single hidden layer structure with 4 nodes produced the least MSE.

Table 4.28: Mean square error using different number of hidden neurons

Number of Hidden Neurons	Mean square error (MSE)
1	117×10^{-5}
2	7.686×10^{-5}
3	26.8×10^{-5}
4	2.779×10^{-5}

As shown in figure 4.35, the best test result is obtained from the network which has 4 hidden neurons in the hidden layer. Therefore, Single hidden layer with 4 neurons is used for prediction of electrostatic discharge.
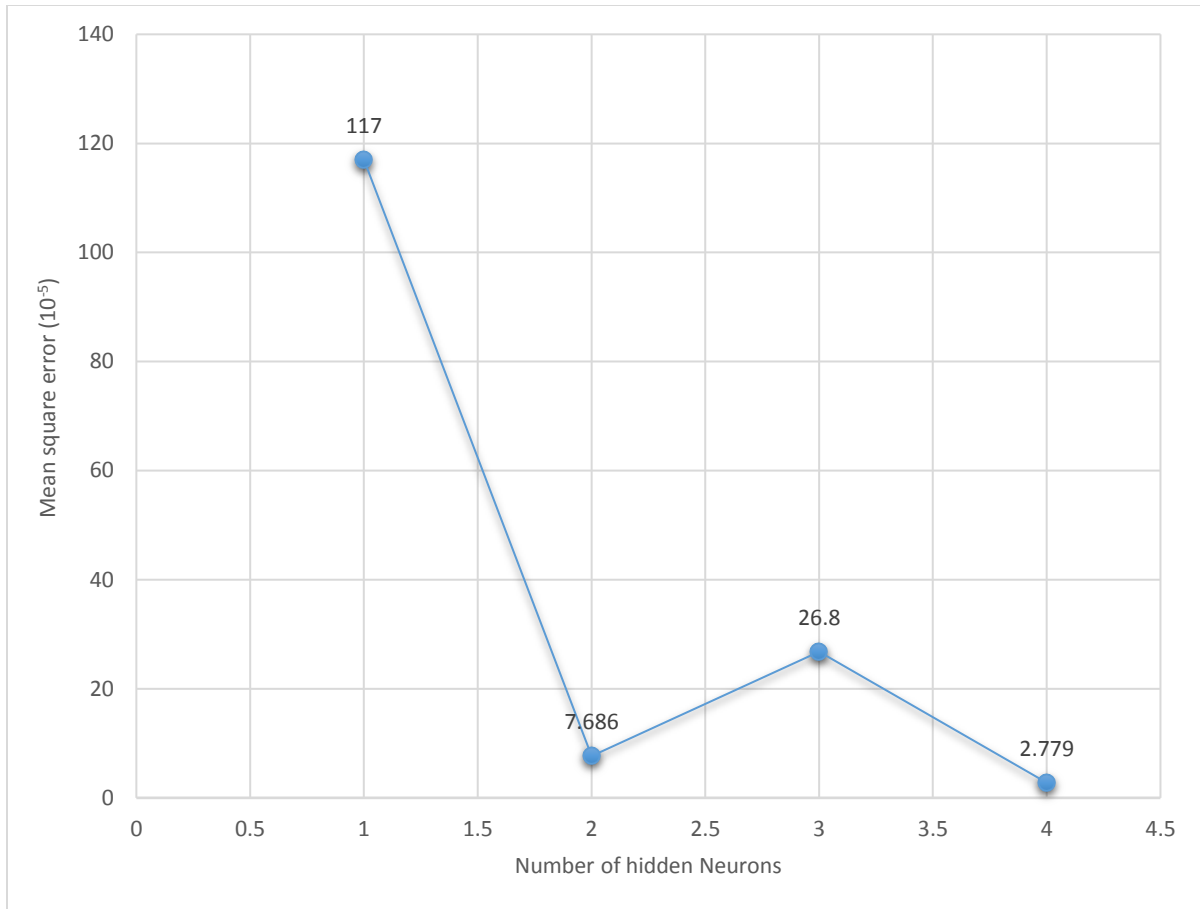
Figure 4.35 Performance of ANN with different hidden layer neurons

Training of the neural network model was performed using 10 experimental data out of 15 data as explained in Section 4.8. The trained network model was tested using five experimental data points (experiment 11-15), which were not used in the training process. The results predicted from the ANN model are compared with those obtained by experimental test in table 4.29 for 5 experimental test sets. It is seen from table 4.26 that ANN prediction is in good agreement with the experimental results.

Table 4.29**:** Comparison of ANN results with experimental findings (Experiment 11-15)

Run	Measured ESD (kV)	ANN Predicted ESD (kV)	Error (%)
11	0.929	1.1384	22.54
12	3.524	3.8059	7.99
13	1.433	1.5968	11.43
14	4.619	4.3726	5.33
15	1.363	1.3076	4.06

Then, figure 4.36 compares the neural network ESDs prediction with experimental test results for experiment 11-15 data sets. In this study, ANN structure shown in Figure 4.37 is used for modeling and predicting electrostatic discharge in turning operations. This fully connected hierarchical network structure has an input layer, a hidden layer, and an output layer.
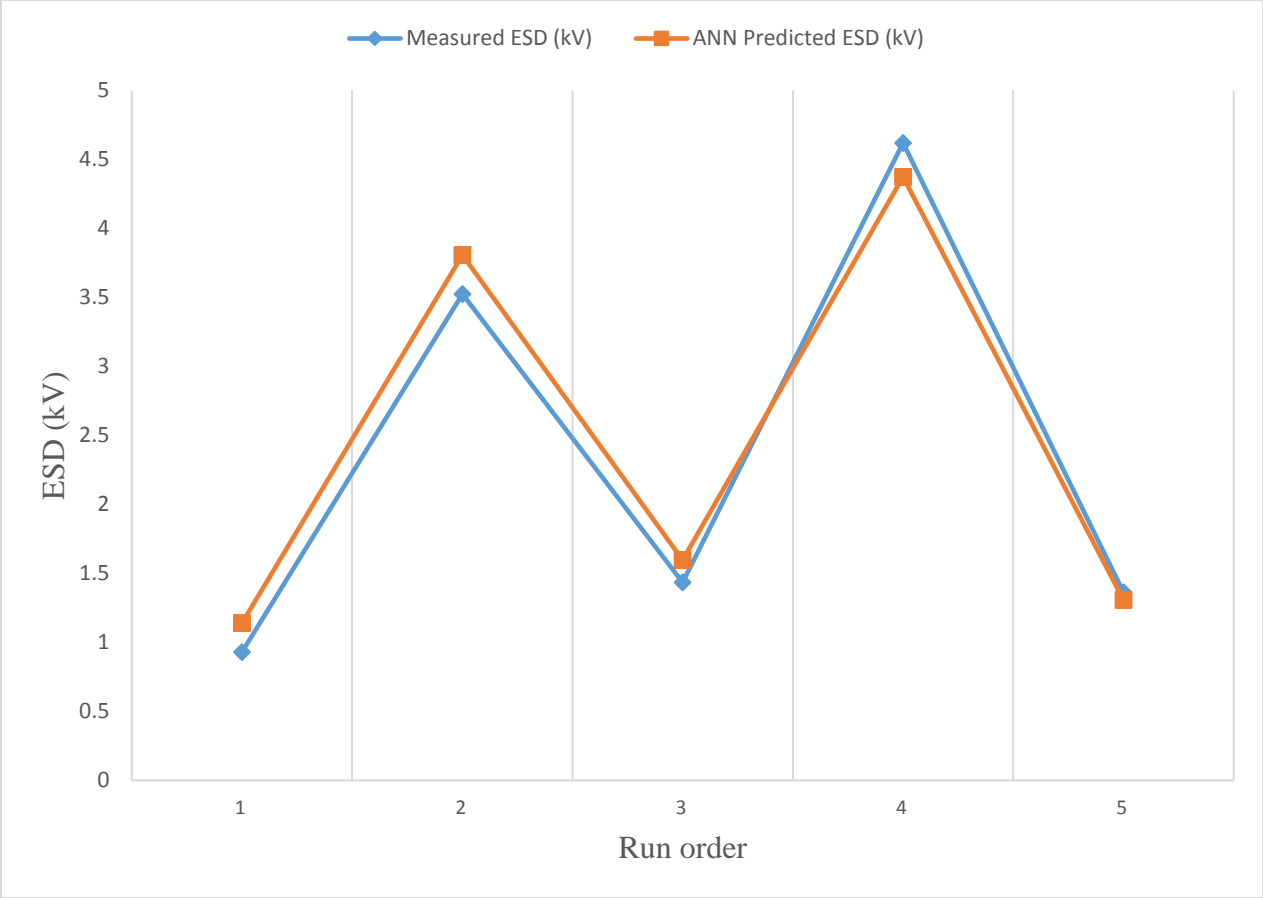
Figure 4.36: Comparison of measured and predicted data of the electrostatic discharge
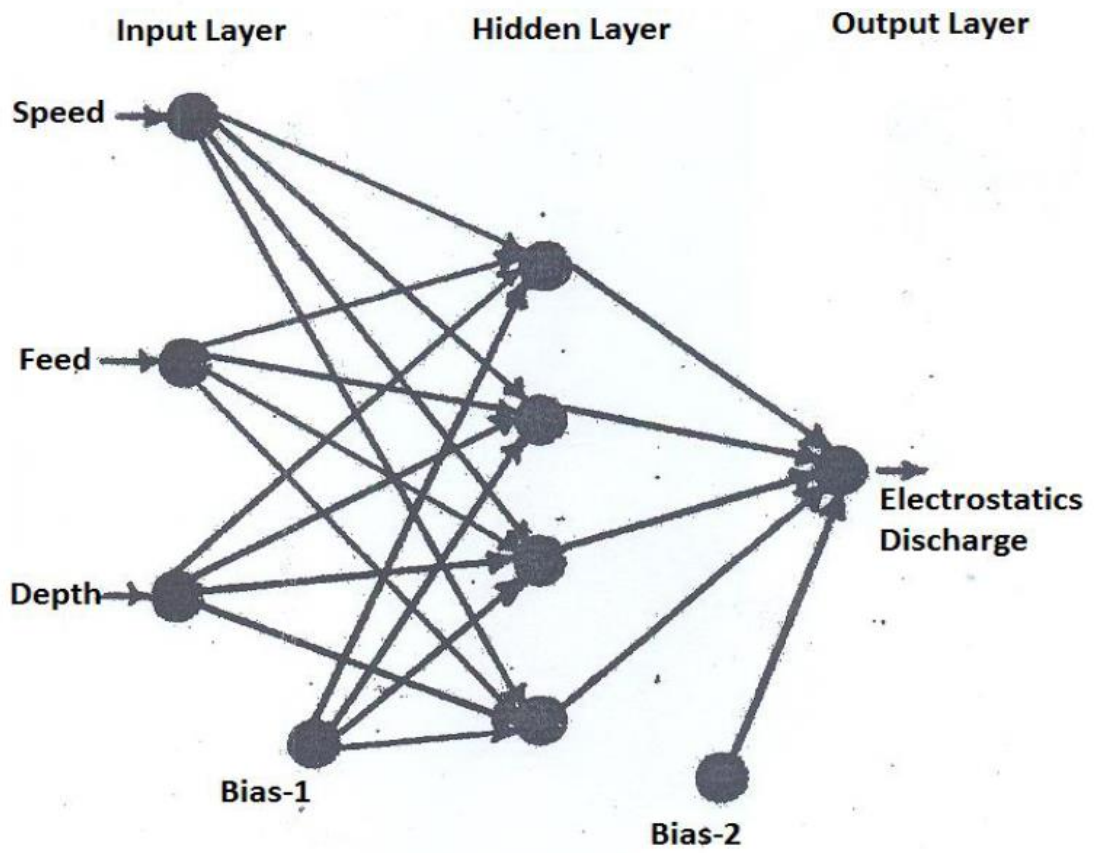
Figure 4.37: ANN Structure

4.10.1 Comparison of ANN and RSM Models for ESD

In this section, the comparison between RSM and ANN modeling will be carried out. Both methods have been performed for the diamond turning of ONSI-56 polymer and prediction models have been obtained. To compare the modeling results of RSM and ANN with the experimental results, five random factors (experiment 11-15) are used. The performance criteria considered is the mean absolute percentage error (MAPE). Equation 4.15 is used to calculate the MAPE for the models.

$$MAPE = \left(\frac{1}{n} \sum_{i=1}^{n} \left| \frac{R_{a,i} - R^P_{a,i}}{R_{a,i}} \right| \times 100 \right) \tag{4.15}$$

Where: MAPE = mean absolute percentage error, n = the total number of measurements, i = the estimated measurement for a specific run, $R_{a,i}$ = the measured electrostatic discharge for a specific run, $R^p_{a,i}$ = the predicted electrostatic discharge for a specific run

Table 4.30 shows the ESDs comparison according to the accuracy values of RS model and neural network model.

Table 4.30: Comparison of ESD experimental values with predicted RSM and ANN

Run order	Experimental ESD (kV)	RSM Predicted ESD (kV)	ANN Predicted ESD (kV)
11	0.929	0.763	1.1384
12	3.524	4.855	3.8059
13	1.433	1.088	1.5968
14	4.619	4.096	4.3726
15	1.363	1.297	1.3076
MAPE		*19.18*	*10.27*

From table 4.30, the prediction error of the RSM model for the ESD is 19.18%. The error rate has been calculated as 10.27% by ANN prediction model. The results of the ANN model indicate it is

much more robust and accurate in estimating the values of ESD when compared with the response surface model.

	1	2	3	4	5
Experimental ESD (kV)	0.929	3.524	1.433	4.619	1.363
RSM-BBD Predicted ESD (kV)	0.763	4.855	1.088	4.096	1.297
ANN Predicted ESD (kV)	1.1384	3.8059	1.5968	4.3726	1.3076
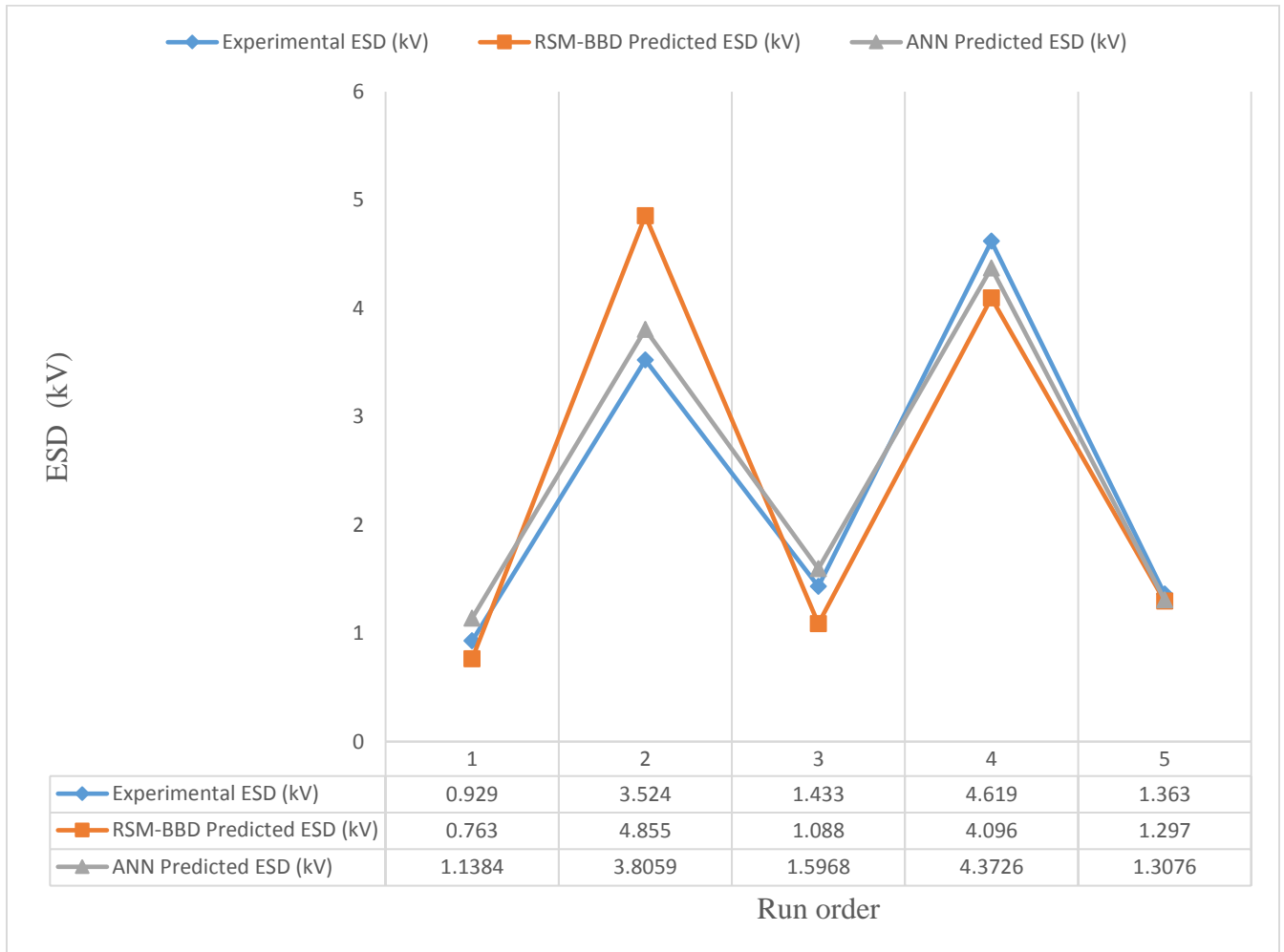
Figure 4.38: Comparison of experimental ESD, with RSM and ANN Models

It is clearly seen (Figure 4.38) that the ANN model estimates the ESD with high accuracy compared to the RSM model. So, the proposed models can be used effectively to predict the electrostatic discharge in diamond turning of ONSI-56 contact lens polymers.

4.11   Summary of Results

The objectives of this research work were aimed at machining ONSI-56 contact lens polymers to optical quality and analyze the surface roughness and electrostatic discharge for saving cost and time for high production rates. The effect of feed rate, depth of cut, and the spindle speed on surface roughness of machined ONSI-56 specimens were experimentally investigated. Cutting speed is found to be the most dominant factor during finish turning of ONSI-56. RSM and ANN models have been used to observe the influence of process parameters and predict the surface roughness.

However, during electrostatics evaluation, a similar RSM and ANN models were also used to generate predictive models for ESDs with respect to the cutting speed, feed rate and depth of cut. Depth of cut is found as the most dominant factor. Results of the ESD shows that increase in depth of cut generates high ESD values.

CHAPTER FIVE

5   CONCLUSION AND RECOMMENDATIONS

5.1 Introduction

In this research, the overall aim is to machine ONSI-56 contact lens polymers to optical quality and analyze the surface roughness and electrostatic discharge for saving cost and time for high production rates. This chapter concludes the findings in the research and highlights suggested recommendations for further improvements on the research.

5.2 Conclusions

In this dissertation, finish cutting conditions of ONSI-56 with a monocrystalline diamond tool were investigated. The effect of feed rate, depth of cut, and the spindle speed on surface roughness of machined ONSI-56 specimens were experimentally investigated. Cutting speed is found to be the most dominant factor during finish turning of ONSI-56; and the square of spindle speed, feed rate, and the interaction between feed and speed have followed, respectively. Box-Behnken RSM and ANN models have been used to observe the influence of process parameters and predict the surface roughness. The best average surface finish is achieved as 6 nm. The optimal conditions for the best R_a = 6 nm were found to be at the feed rate of 7 µm/rev, cutting speed of 2100 rpm and depth of cut of 25 µm. Whereas the poor R_a = 1184.1 nm was achieved at low speed of 200 rpm, high feed rate of 12 µm/rev and moderate depth of cut 25 µm. Analysis of variance (ANOVA) showed that the transformed scale model effectively interpreted the experimental data with coefficients of determination of R^2 = 0.89 and adjusted R^2 = 0.84. the prediction error of the RSM model for the surface roughness is 23.29%. The error rate has been calculated as 18.28% by ANN prediction model.

Whereas during electrostatics evaluation, a similar RSM and ANN models were also used to generate predictive models for ESDs with respect to the cutting speed, feed rate and depth of cut. Depth of cut is found as the most dominant factor followed by cutting speed, feed rate and the interaction between depth and speed. Results of the ESD shows that increase in depth of cut generates high ESD values. Analysis of variance (ANOVA) showed that the transformed scale model effectively interpreted the experimental data with coefficients of determination of R^2 = 0.86

and adjusted $R^2 = 0.80$. the prediction error of the RSM model for the surface roughness is 19.18%. The error rate has been calculated as 10.27% by ANN prediction model.

It is highly recommended that a feed rate less than 7 µm/rev, depth of cut less than 25 µm and a spindle speed less than 2100 rpm are to be chosen as cutting parameters in order to obtain high quality ONSI-56 surfaces having average surface roughness below 10 nm.

5.3 Recommendations

In this study, monocrystalline diamond cutting tool was used. Alternative diamond tools (e.g. polycrystalline) can also be tried for finish cutting of ONSI-56 so that the cost of production can be minimized without sacrificing surface quality. Dry cutting conditions is used during all the experiments. Pressurized cutting fluid like kerosene can also be examined for finish turning of ONSI-56. Turning parameters such as cutting speed, feed rate and depth of cut directly influence statics values, besides these turning parameters, the environmental effect of relative humidity and workpiece properties may also influence the amount of charging. Relative humidity variation can also be used to see the effects on the statics values. During the experiments, tool parameters like rake angle and clearance angle were not varied, effects of these parameters can also be analyzed to obtain optimum surface quality.

REFERENCES

[1]   Douglas Harper H. "Thesaurus.com," in *Dictionary.reference.com*, ed, 2016.

[2]   Olufayo O, Abou-El-Hossein K. "Preliminary investigation of surface finish of a contact lens polymer in ultra-high precision diamond turning," in *Robotics and Mechatronics Conference (RobMech), 2013 6th*, 2013, pp. 117-122.

[3]   Mamalis A, Lavrynenko S. "On the precision single-point diamond machining of polymeric materials," *Journal of materials processing technology,* vol. 181, pp. 203-205, 2007.

[4]   Baker L. "Optical Production Technology," *Journal of Modern Optics,* vol. 30, pp. 1042-1042, 1983.

[5]   Evans C J. "Precision engineering: an evolutionary perspective," *Philosophical Transactions of the Royal Society of London A: Mathematical, Physical and Engineering Sciences,* vol. 370, pp. 3835-3851, 2012.

[6]   Benjamin R. "Diamond turning at a large optical manufacturer," in *22nd Annual Technical Symposium*, 1978, pp. 81-87.

[7]   Venkatesh V, Izman S. "Mechanics of Materials Cutting," *Precision engineering,* vol. 1, pp. 80-107, 2007.

[8]   Bolat M. "Machining of polycarbonate for optical applications," Msc thesis, Middle east technical university, 2013.

[9]   Heinrich M, Wildsmith C. "Need for precision engineering in astigmatic contact lenses," in *Proceedings of the ASPE Topical Meeting on Freeform Optics*, 2004, pp. 18-22.

[10]   Smith E F. *Single-point diamond turning of amorphous thermoplastic polymers*, 1989.

[11]   Gubbels G P H. "Diamond turning of glassy polymers," Phd thesis, Eindhoven university of technology, 2006.

[12]   Saini V, Sharma D, Kalla S, Chouhan T. "Optimisation of process parameter in ultra-precision diamond turning of polycarbonate material," in *Proceedings of the International Conference on Manufacturing Excellence MANFEX*, 2012.

[13]   Carr J W, Feger C. "Ultraprecision machining of polymers," *Precision Engineering,* vol. 15, pp. 221-237, 1993.

[14]   Research T M. "Contact Lens Market - Global Industry Analysis, Size, Share, Growth, Trends and Forecast 2016 - 2024," 29 August, 2016.

[15] Olufayo O, Abou-El-Hossein K, Kadernani M. "Tribo-electric Charging in the Ultra-high Precision Machining of Contact Lens Polymers," *Procedia Materials Science,* vol. 6, pp. 194-201, 2014.

[16] Fried J R. *Polymer science and technology*: Pearson Education, 2014.

[17] Read M L. "The Impact of Material Surface Characteristics on the Wetting Properties of Silicone Hydrogel Contact Lenses," PhD Thesis, The University of Manchester, 2010.

[18] De Gennes P-G. *Scaling concepts in polymer physics*: Cornell university press, 1979.

[19] Rubenstein M, Colby R. "Polymer Physics: Oxford University Press," ed: Oxford, UK, 2003.

[20] Maldonado-Codina C, Efron N. "Hydrogel lenses-material and manufacture: a review," *Optometry in Practice,* vol. 4, pp. 101-115, 2003.

[21] Wichterle O, Lim D. "Hydrophilic gels for biological use," 1960.

[22] Sciences A C. "*Polymers in everyday things - contact lenses.*" Available from: http://www.rsc.org/Education/Teachers/Resources/Inspirational/resources/3.1.1.pdf

[23] Olufayo O. "Ultra-high Precision Manufacturing of Contact Lens Polymers," PhD Thesis, Nelson Mandela Metropolitan University, 2014.

[24] Efron N. *Contact lens practice*, Second edition ed.: Elsevier Health Sciences, 2010.

[25] Tighe B. "Soft lens materials," *Contact lens practice. Oxford: Butterworth-Heinemann,* pp. 71-84, 2002.

[26] Li L. "Investigation of the optical effects of single point diamond machined surfaces and the applications of micro machining," The Ohio State University, 2009.

[27] Ikawa N, Donaldson R, Komanduri R, König W, McKeown P, Moriwaki T, *et al.* "Ultraprecision metal cutting—the past, the present and the future," *CIRP Annals-Manufacturing Technology,* vol. 40, pp. 587-594, 1991.

[28] Davies M A, Evans C J, Vohra R R, Bergner B C, Patterson S R. "Application of precision diamond machining to the manufacture of microphotonics components," in *Optical Science and Technology, SPIE's 48th Annual Meeting*, 2003, pp. 94-108.

[29] Luo X, Goel S, Reuben R L. "A quantitative assessment of nanometric machinability of major polytypes of single crystal silicon carbide," *Journal of the European Ceramic Society,* vol. 32, pp. 3423-3434, 2012.

[30]   Corbett J, McKeown P, Peggs G, Whatmore R. "Nanotechnology: international developments and emerging products," *CIRP Annals-Manufacturing Technology,* vol. 49, pp. 523-545, 2000.

[31]   Taniguchi N. "Current status in, and future trends of, ultraprecision machining and ultrafine materials processing," *CIRP Annals-Manufacturing Technology,* vol. 32, pp. 573-582, 1983.

[32]   McKeown P. "The role of precision engineering in manufacturing of the future," *CIRP Annals-Manufacturing Technology,* vol. 36, pp. 495-501, 1987.

[33]   Taniguchi N. "On the basic concept of nanotechnology," in *Proc. Intl. Conf. Prod. Eng. Tokyo, Part II, Japan Society of Precision Engineering*, 1974, pp. 18-23.

[34]   Saito T T. "Machining of optics: an introduction," *Applied optics,* vol. 14, pp. 1773-1776, 1975.

[35]   Chiu W, Lee W. "Development of ultra-precision machining technology," in *Factory 2000-The Technology Exploitation Process, Fifth International Conference on (Conf. Publ. No. 435)*, 1997, pp. 486-490.

[36]   Thompson D, Chrislock J, Newton L. "Development of an inexpensive, high accuracy diamond turning machine," in *25th Annual Technical Symposium*, 1982, pp. 144-153.

[37]   Thompson D. "Theoretical tool movement required to diamond turn an off-axis paraboloid on axis," in *20th Annual Technical Symposium*, 1976, pp. 23-31.

[38]   Douglass S S. "Machining system for turning nonaxisymmetric surfaces," *Dissertation Abstracts International Part B: Science and Engineering[DISS. ABST. INT. PT. B- SCI. & ENG.],* vol. 44, 1984.

[39]   Patterson S, Magrab E. "Design and testing of a fast tool servo for diamond turning," *Precision Engineering,* vol. 7, pp. 123-128, 1985.

[40]   Moriwaki T, Shamoto E. "Ultraprecision diamond turning of stainless steel by applying ultrasonic vibration," *CIRP Annals-Manufacturing Technology,* vol. 40, pp. 559-562, 1991.

[41]   Masuzawa T. "State of the art of micromachining," *CIRP Annals-Manufacturing Technology,* vol. 49, pp. 473-488, 2000.

[42]   Hocheng H, Hsieh M. "Signal analysis of surface roughness in diamond turning of lens molds," *International Journal of Machine Tools and Manufacture,* vol. 44, pp. 1607-1618, 2004.

[43]   Khan G S. "Characterization of Surface Roughness and Shape Deviations of Aspheric Surfaces," 2008.

[44]   Yip A. "Factors Affecting Surface Topography in Diamond Turning," MSc Thesis, McMaster University, Canada, 2014.

[45]   Cheung C-f B. "Modelling and simulation of nano-surface generation in ultra-precision machining," The Hong Kong Polytechnic University, 2000.

[46]   Jasinevicius R G, Duduch J G, Porto A J V, Purquério B M. "Critical aspects on the behavior of material from the mechanical tool-workpiece interaction in single point diamond turning," *Journal of the Brazilian Society of Mechanical Sciences,* vol. 21, pp. 509-518, 1999.

[47]   Lee W, To S, Cheung C. "Effect of crystallographic orientation in diamond turning of copper single crystals," *Scripta Materialia,* vol. 42, pp. 937-945, 2000.

[48]   Xiao K, Zhang L. "The role of viscous deformation in the machining of polymers," *International journal of mechanical sciences,* vol. 44, pp. 2317-2336, 2002.

[49]   Dhar N, Kamruzzaman M. "Cutting temperature, tool wear, surface roughness and dimensional deviation in turning AISI-4037 steel under cryogenic condition," *International Journal of Machine Tools and Manufacture,* vol. 47, pp. 754-759, 2007.

[50]   Trent E M, Wright P K. *Metal cutting*: Butterworth-Heinemann, 2000.

[51]   Zeng S, Wan, Xiaojin, Li, Wenlong, Yin, Zhouping, Xiong Y. "A novel approach to fixture design on suppressing machining vibration of flexible workpiece," *International journal of machine tools and manufacture,* vol. 58, pp. 29-43, 2012.

[52]   Zhang S J, To, S., Zhang, G.Q., Zhu Z W. "A review of machine-tool vibration and its influence upon surface generation in ultra-precision machining," *International Journal of Machine Tools and Manufacture,* vol. 91, pp. 34-42, 2015.

[53]   Chen C-C, Liu N-M, Chiang K-T, Chen H-L. "Experimental investigation of tool vibration and surface roughness in the precision end-milling process using the singular spectrum analysis," *The International Journal of Advanced Manufacturing Technology,* vol. 63, pp. 797-815, 2012.

[54]   Thomas M, Beauchamp Y, Youssef A, Masounave J. "Effect of tool vibrations on surface roughness during lathe dry turning process," *Computers & industrial engineering,* vol. 31, pp. 637-644, 1996.

[55]   Asilturk I. "On-line surface roughness recognition system by vibration monitoring in CNC turning using adaptive neuro-fuzzy inference system (ANFIS)," *International Journal of Physical Sciences,* vol. 6, pp. 5353-5360, 2011.

[56] Sohn A, Lamonds L, Garrard K. "Modeling of vibration in single-point diamond turning," in *Proceedings of the ASPE, American Society for Precision Engineering, 21st Annual Meeting, Monterey, CA*, 2006, pp. 15-20.

[57] Abuthakeer S S, Mohanram P, Kumar G M. "The effect of spindle vibration on surface roughness of workpiece in dry turning using anova," *Vol 3/Issue 4/Apr 2011,* p. 13, 2011.

[58] Lee W, Cheung C, To S. "Materials induced vibration in ultra-precision machining," *Journal of Materials Processing Technology,* vol. 89, pp. 318-325, 1999.

[59] Özel T, Karpat Y. "Predictive modeling of surface roughness and tool wear in hard turning using regression and neural networks," *International Journal of Machine Tools and Manufacture,* vol. 45, pp. 467-479, 2005.

[60] Aslan E, Camuşcu N, Birgören B. "Design optimization of cutting parameters when turning hardened AISI 4140 steel (63 HRC) with Al 2 O 3+ TiCN mixed ceramic tool," *Materials & design,* vol. 28, pp. 1618-1622, 2007.

[61] Al-Ahmari A. "Predictive machinability models for a selected hard material in turning operations," *Journal of Materials Processing Technology,* vol. 190, pp. 305-311, 2007.

[62] Kopač J, Bahor M, Soković M. "Optimal machining parameters for achieving the desired surface roughness in fine turning of cold pre-formed steel workpieces," *International Journal of Machine Tools and Manufacture,* vol. 42, pp. 707-716, 2002.

[63] Huang L, Chen J C. "A multiple regression model to predict in-process surface roughness in turning operation via accelerometer," *Journal of Industrial Technology,* vol. 17, pp. 1-8, 2001.

[64] Xu H, Zhang X, Xu M, Li X. "Study on the control of surface roughness in single point diamond turning," in *6th International Symposium on Advanced Optical Manufacturing and Testing Technologies (AOMATT 2012)*, 2012, pp. 84161D-84161D-7.

[65] Khatri N, Mishra V, Sarepaka R G V. "Optimization of process parameters to achieve nano level surface quality on polycarbonate," *International Journal of Computer Applications,* vol. 48, pp. 39-44, 2012.

[66] Goel B, Singh S, Sarepaka R V. "Optimizing single point diamond turning for mono-crystalline germanium using grey relational analysis," *Materials and Manufacturing Processes,* vol. 30, pp. 1018-1025, 2015.

[67] Zhang S, To S, Zhang G. "Diamond tool wear in ultra-precision machining," *The International Journal of Advanced Manufacturing Technology,* pp. 1-29, 2016.

[68]   Gubbels G, Van Der Beek G, Hoep A, Delbressine F, Van Halewijn H. "Diamond tool wear when cutting amorphous polymers," *CIRP Annals-Manufacturing Technology,* vol. 53, pp. 447-450, 2004.

[69]   Pauling L. "A resonating-valence-bond theory of metals and intermetallic compounds," in *Proceedings of the Royal Society of London A: Mathematical, Physical and Engineering Sciences*, 1949, pp. 343-362.

[70]   Paul E, Evans C J, Mangamelli A, McGlauflin M L, Polvani R S. "Chemical aspects of tool wear in single point diamond turning," *Precision Engineering,* vol. 18, pp. 4-19, 1996.

[71]   Yan J, Zhang Z, Kuriyagawa T. "Mechanism for material removal in diamond turning of reaction-bonded silicon carbide," *International Journal of Machine Tools and Manufacture,* vol. 49, pp. 366-374, 2009.

[72]   Lane B, Dow T A, Scattergood R. "Thermo-chemical wear model and worn tool shapes for single-crystal diamond tools cutting steel," *Wear,* vol. 300, pp. 216-224, 2013.

[73]   Narulkar R. *Investigation on the mechanism of wear of single crystal diamond tool in nanometric cutting of iron using molecular dynamics (MD) and the development of generalized potential energy surfaces (GPES) based on ab initio calculations*, 2009.

[74]   Rhorer R L, Evans C J. "Fabrication of optics by diamond turning," *Handbook of optics,* vol. 1, pp. 41.1-41.3, 1995.

[75]   Kwetkus B, Sattler K. "Analysis of repeated-contact electrification curves," *Journal of Physics D: Applied Physics,* vol. 25, p. 1400, 1992.

[76]   Beardsmore-Rust S, Watson P, Prance R, Harland C, Prance H. "Quantitative measurement of tribo-electric charging phenomena of dielectric materials," in *Proc. ESA Annual Meeting on Electrostatics*, 2009.

[77]   Brezoczky B, Seki H. "Triboattraction: friction under negative load," *Langmuir,* vol. 6, pp. 1141-1145, 1990.

[78]   McCarty L S, Whitesides G M. "Electrostatic charging due to separation of ions at interfaces: contact electrification of ionic electrets," *Angewandte Chemie International Edition,* vol. 47, pp. 2188-2207, 2008.

[79]   Liu C, Bard A J. "Electrostatic electrochemistry at insulators," *Nature materials,* vol. 7, pp. 505-509, 2008.

[80]   Hogue M, Buhler C, Calle C, Matsuyama T, Luo W, Groop E. "Insulator–insulator contact charging and its relationship to atmospheric pressure," *Journal of electrostatics,* vol. 61, pp. 259-268, 2004.

[81]   Németh E, Albrecht V, Schubert G, Simon F. "Polymer tribo-electric charging: dependence on thermodynamic surface properties and relative humidity," *Journal of Electrostatics,* vol. 58, pp. 3-16, 2003.

[82]   Goupy J, Creighton L. *Introduction to design of experiments with JMP examples*: SAS Publishing, 2007.

[83]   Ting H, Abou-El-Hossein K, Chua H. "Application of design of experiment for modelling of etching of ceramics," presented at the 2nd Engineering Conference on Sustainable Engineering Infrastructural Development and Management, Kuching, Sarawak, Malaysia: Faculty of Engineering, UMS, 2008.

[84]   Mohruni A S. "Performance evaluation of uncoated and coated carbide tools when end milling of titanium alloy using response surface methodology," Universiti Teknologi Malaysia, 2008.

[85]   Telford J K. "A Brief Introduction to Design of Experiments," *Johns Hopkins APL Technical Digest,* vol. 27, pp. 224-232, 2007.

[86]   Proust M. in *Design of Experiments Guide* vol. 11, ed. United States of America: SAS Institute Inc., Cary, NC, USA, 2014, pp. 29-31.

[87]   Mettas H G A. "Design of Experiments and Data Analysis," presented at the Annual RELIABILITY and MAINTAINABILITY Symposium, San Jose, CA, USA, January 25-28, 2010., 2010.

[88]   Lakshminarayanan A, Balasubramanian V. "Comparison of RSM with ANN in predicting tensile strength of friction stir welded AA7039 aluminium alloy joints," *Transactions of Nonferrous Metals Society of China,* vol. 19, pp. 9-18, 2009.

[89]   Reddy B S, Padmanabhan G, Reddy K V K. "Surface roughness prediction techniques for CNC turning," *Asian Journal of Scientific Research,* vol. 1, pp. 256-264, 2008.

[90]   Dean A, Voss D. (1999, 11/11/2015). *Design and Analysis of Experiments* [Online resources].

[91]   Manohar M, Joseph J, Selvaraj T, Sivakumar D. "Application of Box Behnken design to optimize the parameters for turning Inconel 718 using coated carbide tools," *International Journal of Scientific & Engineering Research,* vol. 4, pp. 620-644, 2013.

[92]   Krenker A, Kos A, Bešter J. *Introduction to the artificial neural networks*: INTECH Open Access Publisher, 2011.

[93]   Asiltürk I, Çunkaş M. "Modeling and prediction of surface roughness in turning operations using artificial neural network and multiple regression method," *Expert Systems with Applications,* vol. 38, pp. 5826-5832, 2011.

[94]   Amin M K M. "Multiple self-organised spiking neural networks," University of Aberdeen, 2009.

[95]   Lai H-M, Padua G W, Wei L S. "Properties and microstructure of zein sheets plasticized with palmitic and stearic acids," *Cereal chemistry,* vol. 74, pp. 83-90, 1997.

[96]   "Lagado Premium Gp Materials," ed, 2016.

[97]   "Installation and Maintenance Manual Electrostatic Sensor Series IZD10-*10," ed, 2016.

[98]   Assender H, Bliznyuk V, Porfyrakis K. "How surface topography relates to materials' properties," *Science,* vol. 297, pp. 973-976, 2002.

[99]   Sferrazza M, Xiao C, Jones R A L, Bucknall D G, Webster J, Penfold J. "Evidence for capillary waves at immiscible polymer/polymer interfaces," *Physical review letters,* vol. 78, p. 3693, 1997.

[100] Goldbeck-Wood G, Bliznyuk V, Burlakov V, Assender H, Briggs G, Tsukahara Y, *et al.* "Surface structure of amorphous polystyrene: comparison of sfm imaging and lattice chain simulations," *Macromolecules,* vol. 35, pp. 5283-5289, 2002.

[101] Tadmor Z, Gogos C. "Principles of Polymer Processing, A John Wiley & Sons," *Inc., Publication,* 2006.

[102] Meeten G. "Optical properties of polymers," *Elsevier Applied Science Publishers Ltd, Crown House, Linton Road, Barking, Essex IG 11 8 JU, UK, 1986.,* 1986.

[103] Curtis A, Wilkinson C. "Topographical control of cells," *Biomaterials,* vol. 18, pp. 1573-1583, 1997.

[104] Bennett J M. "Recent developments in surface roughness characterization," *Measurement Science and Technology,* vol. 3, p. 1119, 1992.

[105] Vermeltfoort P B, van der Mei H C, Busscher H J, Hooymans J M, Bruinsma G M. "Physicochemical factors influencing bacterial transfer from contact lenses to surfaces with different roughness and wettability," *Journal of Biomedical Materials Research Part B: Applied Biomaterials,* vol. 71, pp. 336-342, 2004.

[106] Baguet J, Sommer F, Claudon-Eyl V, Duc T M. "Characterization of lacrymal component accumulation on worn soft contact lens surfaces by atomic force microscopy," *Biomaterials,* vol. 16, pp. 3-9, 1995.

[107] Vorburger T, Raja J. *Surface finish metrology tutorial*: National Inst. of Standards and Technology, 1990.

[108] Srivatsan T. "A review of:"Fundamentals Of Machining And Machine Tools" by Goeffrey Boothroyd and Winston A. Knight Marcel Dekker, Inc., New York Second edition, 542 pages, hardcover, 1989," *Material And Manufacturing Process,* vol. 5, pp. 485-487, 1990.

[109] "Taylor Hopson Pgi Dimension Profilometer," ed: AMETEK® Precitech, Inc., 2016.

[110] Benardos P, Vosniakos G-C. "Predicting surface roughness in machining: a review," *International Journal of Machine Tools and Manufacture,* vol. 43, pp. 833-844, 2003.

[111] Alao A. "Precision micro-scaled partial ductile mode machining of silicon," MSc Thesis, International Islamic University, Malaysia, 2007.

[112] Alao A, Konneh M. "A response surface methodology based approach to machining processes: modelling and quality of the models," *International Journal of Experimental Design and Process Optimisation,* vol. 1, pp. 240-261, 2009.

[113] Stat-Ease I M, USA. "Design-Expert ® Version 7.1.6 software," ed, 2008.

[114] Myers R H, Montgomery D C, Anderson-Cook C M. *Response surface methodology: process and product optimization using designed experiments*: John Wiley & Sons, 2016.

[115] Segurola J, Allen N S, Edge M, Mc Mahon A. "Design of eutectic photoinitiator blends for UV/visible curable acrylated printing inks and coatings," *Progress in organic coatings,* vol. 37, pp. 23-37, 1999.

[116] Zhang Z, Zheng H. "Optimization for decolorization of azo dye acid green 20 by ultrasound and H_2O_2 using response surface methodology," *Journal of hazardous materials,* vol. 172, pp. 1388-1393, 2009.

[117] Alao A-R, Konneh M. "Surface finish prediction models for precision grinding of silicon," *The International Journal of Advanced Manufacturing Technology,* vol. 58, pp. 949-967, 2012.

[118] Burton M, Kurien K. "Effects of solute concentration in radiolysis of water," *The Journal of Physical Chemistry,* vol. 63, pp. 899-904, 1959.

[119] Joglekar A, May A. "Product excellence through design of experiments," *Cereal Foods World,* vol. 32, pp. 857-&, 1987.

[120] Liu H-L, Chiou Y-R. "Optimal decolorization efficiency of Reactive Red 239 by UV/TiO2 photocatalytic process coupled with response surface methodology," *Chemical Engineering Journal,* vol. 112, pp. 173-179, 2005.

[121] Kumar S, Kumar P, Shan H. "Effect of evaporative pattern casting process parameters on the surface roughness of Al–7% Si alloy castings," *Journal of materials processing technology,* vol. 182, pp. 615-623, 2007.

[122] Asiltürk İ, Ünüvar A. "Intelligent adaptive control and monitoring of band sawing using a neural-fuzzy system," *Journal of materials processing technology,* vol. 209, pp. 2302-2313, 2009.

[123] Liu X, Gu H. "Hyperbolic tangent function based two layers structure neural network," in *Electronics and Optoelectronics (ICEOE), 2011 International Conference on*, 2011, pp. V4-376-V4-379.

[124] Sharma V S, Dhiman S, Sehgal R, Sharma S. "Estimation of cutting forces and surface roughness for hard turning using neural networks," *Journal of Intelligent Manufacturing,* vol. 19, pp. 473-483, 2008.

[125] Gubbels G, Van Der Beek G, Delbressine F, Schellekens P. "Electrostatic tool wear in diamond turning of amorphous polymers," in *4th euspen International Conference, Glasgow, Scotland, UK*, 2004.

[126] "Precitech Nanoform® 250 Ultragrind ", ed: AMETEK® Precitech, Inc., 2016.

APPENDIX A: TECHNICAL SPECIFICATIONS OF SINGLE POINT DIAMOND TURNING MACHINE

Table A-1 Technical Specifications of Precitech Nanoform 250 Ultragrind [126]

Technical Product Specification **Nanoform® 250 ultra**

Machine Base and Control	Description	
Machine Base	Sealed natural granite base provides exceptional long term machine tool stability	
Machine Type	Ultra precision, two, three or four axes CNC contouring machine	
Vibration Isolation	FEA optimized dual sub-frames for the ultimate in environmental isolation	
Control System	UPx™ Control System with optional Adaptive Control Technology	
Operating System	QNX real time operating system	
Programming Resolution	0.01 nanometer linear / 0.0000001° Rotary	
File Transfer / Storage	USB, CD-RW, Ethernet, On-board data storage backup	
Performance	Surface Roughness (RA) < 1.0 nm, Form Accuracy (P-V) < 0 .1 micron	

Linear Hydrostatic Slideways	Description	
Type	Hydrostatic oil bearing slideways with liquid cooling capability	
Travel	X and Z: 220 mm (8.6 inch)	
Maximum Feedrate	4,000 mm/minute (157 inch/minute)	
Drive System	AC linear motor	
Position Feedback Resolution	16 picometers (0.016 nanometers)	
X-axis Straightness	**Horizontal:** 0.2 micron (8 micro inch) full travel 0.05 micron/25 mm (2 micro inch)	
Z-axis Straightness	**Horizontal:** 0.2 micron (8 micro inch) full travel 0.05 micron/25 mm (2 micro inch)	
Vertical Straightness	0.375 micron (15 micro inch) full travel	

Workholding/Positioning Spindle	High Speed HS 75 Spindle	High Performance SP 150 Spindle
Type	Slot-type thrust bearing	Slot-type thrust bearing
Material	Steel shaft/Bronze journal	Steel shaft/Bronze journal
Standard Swing Capacity	250 mm (9.8 inch) diameter	250mm (9.8 inch) diameter
Motor	Integral brushless motor	Integral brushless motor
Load Capacity	27 Kg (60 pounds) @ 100 PSI	85 Kg (187 pounds)
Axial Stiffness	105 N/micron (600,000 pounds)	230 N/micron (1,314,000 pounds/inch)
Radial Stiffness	35 N/micron (200,000 pounds/inch)	130 N/micron (743,600 pounds/inch)
Motion Accuracy	Axial/Radial ≤ 20 nm (0.8 micro inch)	Axial/Radial ≤ 15 nm (0.6 micro inch)
Thermal Control Optional	Liquid cooled chiller +/- 0.1C Accuracy	Liquid cooled chiller +/- 0.1C Accuracy
C-axis Feedback Resolution		0.026 arc-sec
C-axis Position Accuracy		+/- 1 arc-sec
C-axis Max Speed		3,000 RPM
Work Holding Spindle Max speed	18,000 RPM	7,000 RPM

Rotary B-axis	HydroRound Rotary B-axis	
Type	Bi-conic, self compensated, oil hydrostatic bearing, DC Brushless direct drive motor	
Tabletop Size	330 mm (13 inch)	
Swing Capacity	222 mm (8.75 inch) diameter	
Load Capacity	225 Kg (500 pounds)	
Maximum Speed	10 RPM continuous / 50 RPM intermittent	
Motor Torque	4.1 N-m (3 Ft-pounds)	
Position Feedback Resolution	0.004 arc-sec	
Positioning Accuracy	+/- 1 arc-sec	
Radial Error Motion	0.10 micron (4 micro inch) @ 1 inch above table	
Coning Error	1.0 nm/mm (1.0 micro inch/inch)	
Radial Stiffness	225 N/micron (1,280,000 pounds/inch)	
Axial Stiffness	600 N/micron (3,428,000 pounds/inch)	
Moment Stiffness	3.4 N-m/micro radian (30 inch-pounds/micro radian) (144 inch-pounds/arc-sec)	

Facility Requirements	Nanoform® 250 ultra
Power	208 +/-10% or 230 +/-10% VAC - 3.0 KVA 1 phase - 50/60 Hz
Air Supply	Typical: 12 SCFM @100 PSIG
Machine Footprint	914 mm x 2120 mm x 1700 mm (36 inch x 83.5 inch x 67 inch)
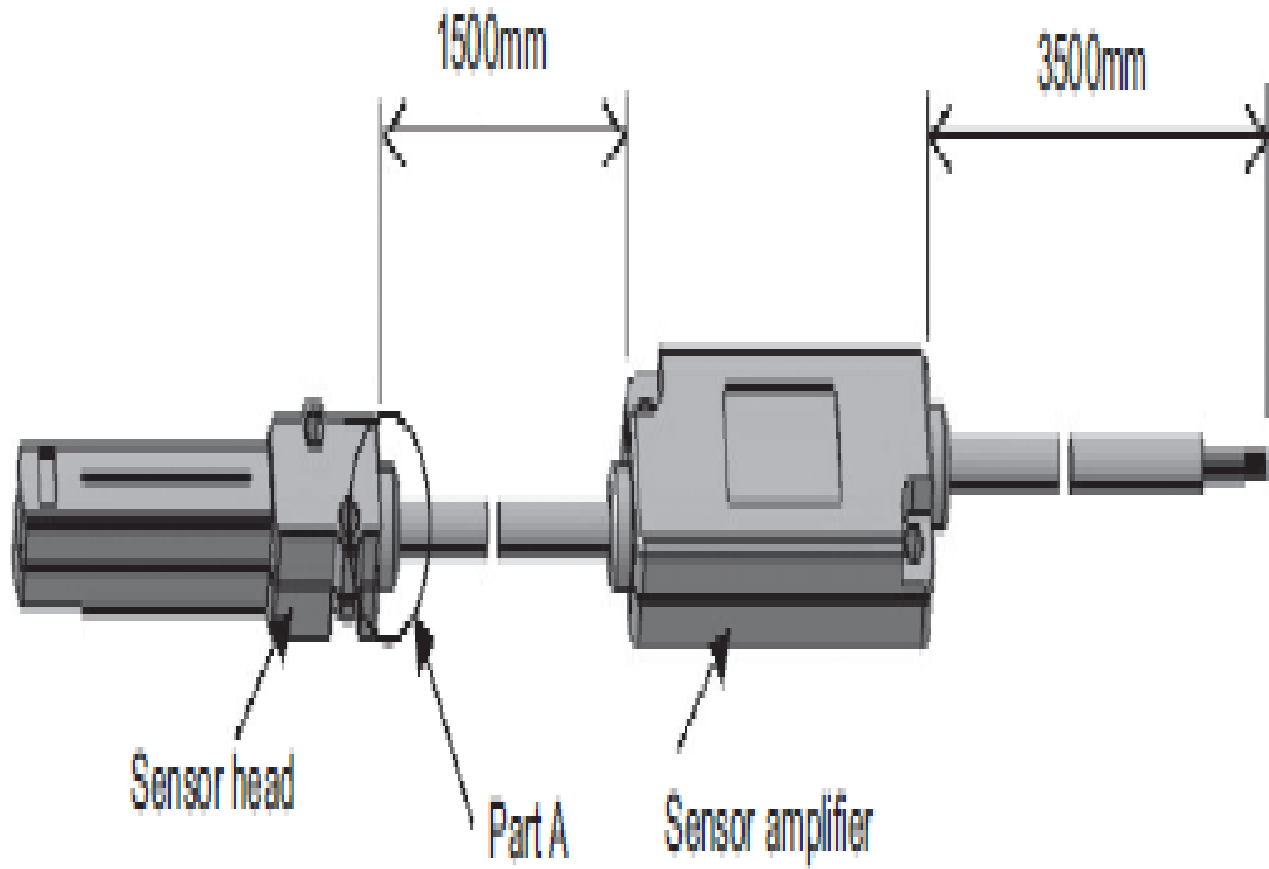
Figure B.1 Electrostatic sensor

∘Names of individual parts

LCD display

Output (OUT1) display (Green)

Output (OUT2) display (Red)

△ button

SET button

▽ button
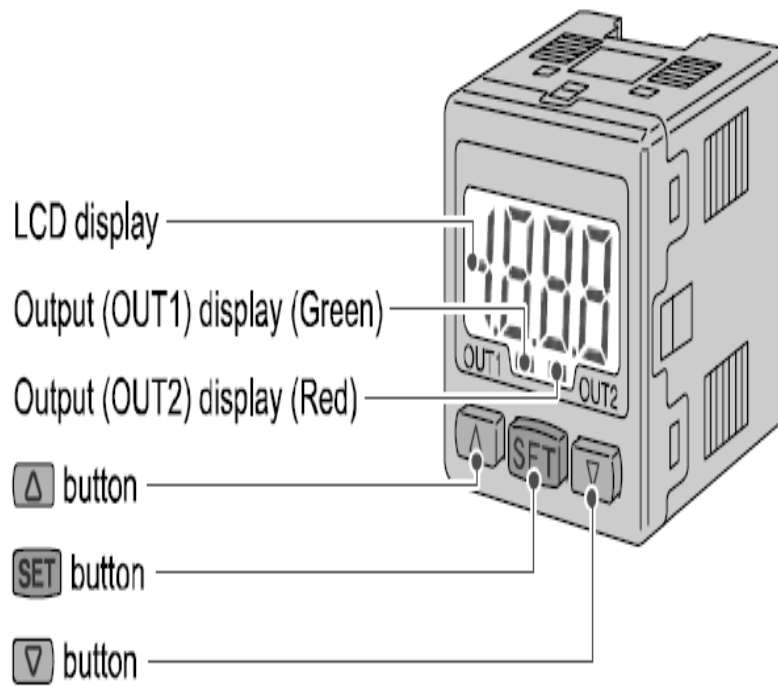
Figure B.2 Electrostatic discharge monitor

Table B.1

Specification

■Specifications

Model No.	IZE11□	
Connected sensor	Sensor for ±0.4 kV	Sensor for ±20kV
Rated measured range	-0.4 to +0.4 kV [1]	-20 to +20 kV [2]
Set min. unit	0.001 kV	0.1 kV
Set measurement distance	10 to 50 mm	25 to 75 mm
Power supply voltage	24 VDC ±10% (Protected against inverse connection)	
Current consumption	50 mA or less (Except current consumption at sensor)	
Sensor input	1 to 5 VDC (Input impedance: 1MΩ)	
Input number	1 input	
Input protection	Protection against excess voltage (up to 26.4V)	
Hysteresis	Hysteresis mode: Variable Window comparator mode: Variable	
Switch output	NPN or PNP open collector output 2 outputs	
Max. load current	80 mA	
Max. applied voltage	30 VDC (at NPN output)	
Residual voltage	1 V or less (at 80 mA load current)	
Response time (including sensor response time)	100 ms. or less, Chattering-proof function working, Response time is 500 ms, 1 s, 2 s or less	
Analog output — Short circuit protection	Short protection equipped	
Analog output — Voltage output	Output voltage: 1 to 5 V (within rated measurement range) Output impedance: Approx. 1 kΩ	
Analog output — Accuracy (to display value 25 °C)	±1%F.S.	
Analog output — Current output	Output current: 4 to 20 mA (Rated measurement range) Max. load impedance: 600 Ω (at 24 VDC) Min. load impedance: 50Ω	
Analog output — Accuracy (to display value 25 °C)	±1%F.S.	
Analog output — Response time (including sensor response time)	200 ms (No filter) 1.5 s (with filter) or less	
Indicator accuracy	±0.5%F.S. ±1 digit	
Display method	3 1/2 digits 7 segment display, two color (red/green) indication, sampling cycle: 5 times /1 s	
Indicator lamp	OUT1: Turns on when ON (green), OUT2: Turns on when ON (red)	
Environment — Enclosure	IP40	
Environment — Operating temp. range	Operation: 0 to 50 °C, Storage: -10 to 60 °C (No condensation or freezing)	
Environment — Operating humidity range	Operation storage: 35 to 85%R.H. (No condensation)	
Environment — Withstand voltage	1000 VAC, 1 min. Between live parts and enclosure at monitor alone	
Environment — Insulation resistance	50 MΩ or more at 500 VDC, Between live parts and enclosure at monitor alone	
Temp. characteristic	±0.5%F.S. (25 °C reference)	
Connection	Power and output lead wire: 5P connector, Connector for sensor lead wire: 4P connector	
Material	Front case: PBT, Back case: PBT	
Weight	30 g (Power and output lead wire not included)	
Standard	CE, UL/CSA	

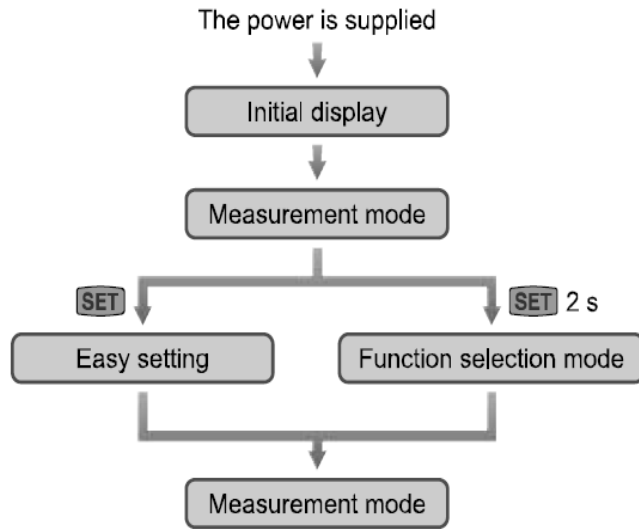[1]: Rated value when the distance between charged object and the sensor is 25 mm.

[2]: Rated value when the distance between charged object and the sensor is 50 mm.

SMC

Electrostatic sensor model no.	IZD10-110	IZD10-510
Measuring range	+/- 0.4kV (when detection distance 25 mm) NOTE 1	+/- 20kV (when detection distance 50 mm) NOTE 1
Output voltage	1 to 5V (Output impedance Approx. 100ohms)	
Effective detection distance	10 to 50mm	25 to 75mm
Linearity	+/- 5% F.S. (when 0 to 50°C, detection distance 25 mm)	+/- 5% F.S. (when 0 to 50°C, detection distance 50 mm)
Output delay time	Within 100ms	
Source voltage	DC24V +/-10%	
Power consumption	40mA or less	
Operating ambient temp.	0 to 50°C	
Operating ambient humidity	35 to 85%Rh (Non-condensing)	
Material	Case material : ABS Amplifier material : ABS	
Vibration resistance	Withstand 50Hz Fluctuation 1mm XYZ 2 hours for each	
Impact resistance	100m/s2	
Weight	185g (Including cable)	

NOTE 1: Relationship between measuring range and output voltage depends on detection distance.
See the chart in "3.3 Output signal" for the details of this relationship.

Setting

○Setting procedures

The power is supplied
↓
Initial display
↓
Measurement mode

SET ↓   SET 2 s ↓
Easy setting   Function selection mode

↓
Measurement mode

○Initial display

The power is supplied
↓
Product type
↓ Approx. 1 s
Switch output type
↓ Approx. 1 s
Analog output type
↓ Approx. 1 s
Measurement mode
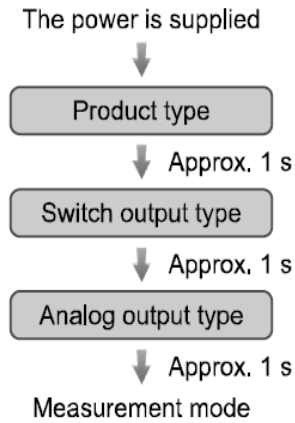
Item	Display	Content
Product type	Esd	IZE11☐ series
Switch output type	nPn	NPN open collector output
	PnP	PNP open collector output
Analog output type	1_5	Voltage output (1 to 5 V)
	420	Current output (4 to 20 mA)
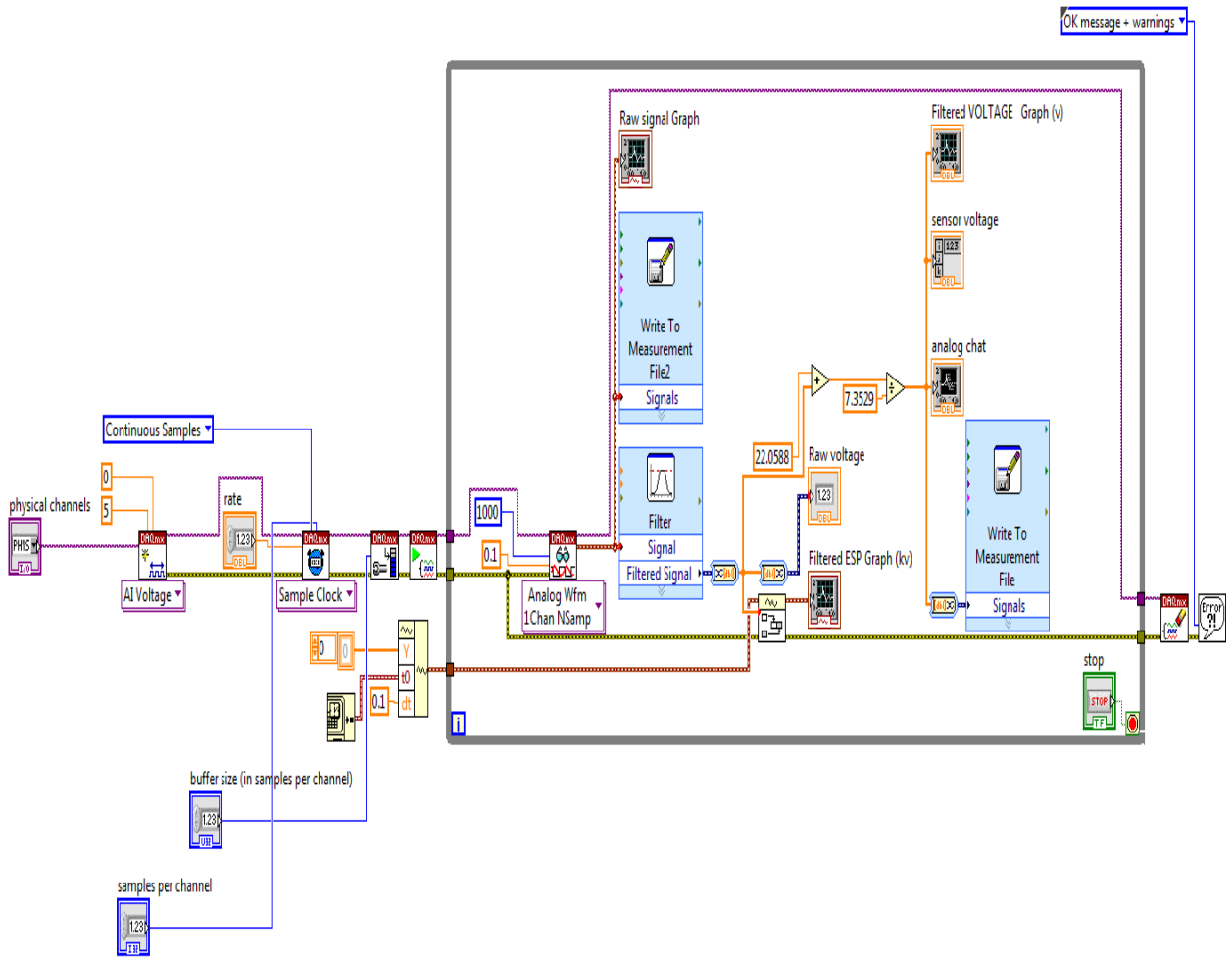
APPENDIX D: SOME MATLAB CODES

```matlab
function createfigure(X1, YMatrix1, X2, Y1, X3, Y2, X4, Y3)

%CREATEFIGURE(X1, YMATRIX1, X2, Y1, X3, Y2, X4, Y3)

%  X1:  vector of x data

%  YMATRIX1:  matrix of y data

%  X2:  vector of x data

%  Y1:  vector of y data

%  X3:  vector of x data

%  Y2:  vector of y data

%  X4:  vector of x data

%  Y3:  vector of y data

 %  Auto-generated by MATLAB on 15-Nov-2016 17:08:02

 % Create figure

figure1 = figure('Tag','TRAINING_PLOTPERFORM','NumberTitle','off',...

    'Name','Neural Network Training Performance (plotperform), Epoch 8, Minimum
gradient reached.');

% Create axes

axes1 = axes('Parent',figure1,'YScale','log','YMinorTick','on');

%% Uncomment the following line to preserve the X-limits of the axes

% xlim(axes1,[0 8]);

%% Uncomment the following line to preserve the Y-limits of the axes

% ylim(axes1,[9e-06 0.11]);
```

143

```matlab
hold(axes1,'all');

% Create multiple lines using matrix input to semilogy

semilogy1 = semilogy(X1,YMatrix1,'Parent',axes1,'LineWidth',2);

set(semilogy1(1),'Color',[0 0 1],'DisplayName','Train');

set(semilogy1(2),'Color',[0 0.8 0],'DisplayName','Validation');

set(semilogy1(3),'Color',[1 0 0],'DisplayName','Test')

% Create semilogy

semilogy(X2,Y1,'Parent',axes1,'LineStyle',':','Color',[0 0.48 0],...

    'DisplayName','Best');

% Create semilogy

semilogy(X3,Y2,'Parent',axes1,'MarkerSize',16,'Marker','o','LineWidth',1.5,...

    'LineStyle','none',...

    'Color',[0 0.48 0]);

% Create semilogy

semilogy(X4,Y3,'Parent',axes1,'LineStyle',':','Color',[0 0 0]);

% Create title

title('Best Validation Performance is 1.4933e-05 at epoch 5',...

    'FontWeight','bold',...

    'FontSize',12);

% Create ylabel
```

```matlab
ylabel('Mean Squared Error  (mse)','FontWeight','bold','FontSize',12);

 % Create xlabel

xlabel('8 Epochs','FontWeight','bold','FontSize',12);

 % uicontrol currently does not support code generation, enter 'doc uicontrol'
for correct input syntax

% In order to generate code for uicontrol, you may use GUIDE. Enter 'doc guide'
for more information

% uicontrol(...);

% Create legend

legend(axes1,'show');

 function createfigure(X1, Y1, Y2, Y3)

%CREATEFIGURE(X1, Y1, Y2, Y3)

%  X1:  vector of x data

%  Y1:  vector of y data

%  Y2:  vector of y data

%  Y3:  vector of y data

 %  Auto-generated by MATLAB on 15-Nov-2016 17:09:49

 % Create figure

figure1 = figure('Tag','TRAINING_PLOTTRAINSTATE','NumberTitle','off',...

    'Name','Neural Network Training Training State (plottrainstate), Epoch 8,
Minimum gradient reached.');

 % uicontrol currently does not support code generation, enter 'doc uicontrol'
for correct input syntax
```

```matlab
% In order to generate code for uicontrol, you may use GUIDE. Enter 'doc guide'
for more information

 % uicontrol(...);

 % Create subplot

subplot1 = subplot(3,1,1,'Parent',figure1,'YScale','log','YMinorTick','on',...

    'XTickLabel','');

%% Uncomment the following line to preserve the X-limits of the axes

% xlim(subplot1,[0 8]);

box(subplot1,'on');

hold(subplot1,'all');

 % Create semilogy

semilogy(X1,Y1,'Parent',subplot1,'MarkerFaceColor',[1 0 0],'LineWidth',2);

% Create ylabel

ylabel('gradient');

% Create title

title('Gradient = 2.0054e-11, at epoch 8');



% Create subplot

subplot2 = subplot(3,1,2,'Parent',figure1,'YScale','log','YMinorTick','on',...

    'XTickLabel','');

%% Uncomment the following line to preserve the X-limits of the axes
```

```matlab
% xlim(subplot2,[0 8]);

box(subplot2,'on');

hold(subplot2,'all');

 % Create semilogy

semilogy(X1,Y2,'Parent',subplot2,'MarkerFaceColor',[1 0 0],'LineWidth',2);

% Create ylabel

ylabel('mu');

% Create title

title('Mu = 1e-10, at epoch 8');

% Create subplot

subplot3 = subplot(3,1,3,'Parent',figure1);

%% Uncomment the following line to preserve the X-limits of the axes

% xlim(subplot3,[0 8]);

box(subplot3,'on');

hold(subplot3,'all');

% Create plot

plot(X1,Y3,'Parent',subplot3,'MarkerFaceColor',[1 0 0],'Marker','diamond',...
    'LineWidth',1,...
    'LineStyle','none');

% Create ylabel

ylabel('val fail');
```

```matlab
% Create xlabel

xlabel('8 Epochs');

% Create title

title('Validation Checks = 3, at epoch 8');




function createfigure(X1, YMatrix1, X2, Y1, X3, YMatrix2, X4, X5, YMatrix3, X6, X7, YMatrix4, X8)

%CREATEFIGURE(X1, YMATRIX1, X2, Y1, X3, YMATRIX2, X4, X5, YMATRIX3, X6, X7, YMATRIX4, X8)

%  X1:  vector of x data

%  YMATRIX1:  matrix of y data

%  X2:  vector of x data

%  Y1:  vector of y data

%  X3:  vector of x data

%  YMATRIX2:  matrix of y data

%  X4:  vector of x data

%  X5:  vector of x data

%  YMATRIX3:  matrix of y data

%  X6:  vector of x data

%  X7:  vector of x data

%  YMATRIX4:  matrix of y data
```

148

```matlab
%  X8:  vector of x data

 %  Auto-generated by MATLAB on 15-Nov-2016 17:10:47

 % Create figure

figure1 = figure('Tag','TRAINING_PLOTREGRESSION','NumberTitle','off',...

    'Name','Neural Network Training Regression (plotregression), Epoch 8,
Minimum gradient reached.');

 % uicontrol currently does not support code generation, enter 'doc uicontrol'
for correct input syntax

% In order to generate code for uicontrol, you may use GUIDE. Enter 'doc guide'
for more information

% uicontrol(...);

% Create subplot

subplot1 = subplot(2,2,1,'Parent',figure1,'PlotBoxAspectRatio',[1 1 1]);

%% Uncomment the following line to preserve the X-limits of the axes

% xlim(subplot1,[0 0.31]);

%% Uncomment the following line to preserve the Y-limits of the axes

% ylim(subplot1,[0 0.31]);

box(subplot1,'on');

hold(subplot1,'all');

% Create xlabel

xlabel('Target','FontWeight','bold','FontSize',12);

 % Create ylabel
```

```matlab
ylabel('Output ~= 0.96*Target + 0.0027','FontWeight','bold','FontSize',12);

% Create title

title('Training: R=0.99858','FontWeight','bold','FontSize',12);

 % Create multiple lines using matrix input to plot

plot1 = plot(X1,YMatrix1,'Parent',subplot1);

set(plot1(1),'LineStyle',':','DisplayName','Y = T','Color',[0 0 0]);

set(plot1(2),'LineWidth',2,'DisplayName','Fit')

% Create plot

plot(X2,Y1,'Parent',subplot1,'Marker','o','LineStyle','none',...

    'DisplayName','Data',...

    'Color',[0 0 0]);

% Create legend

legend1 = legend(subplot1,'show');

set(legend1,'Location','NorthWest');

% Create subplot

subplot2 = subplot(2,2,2,'Parent',figure1,'PlotBoxAspectRatio',[1 1 1]);

%% Uncomment the following line to preserve the X-limits of the axes

% xlim(subplot2,[0.00457411940378739 0.301184165438277]);

%% Uncomment the following line to preserve the Y-limits of the axes

% ylim(subplot2,[0.00457411940378739 0.301184165438277]);

box(subplot2,'on');
```

```matlab
hold(subplot2,'all');

% Create xlabel

xlabel('Target','FontWeight','bold','FontSize',12);

% Create ylabel

ylabel('Output ~= Inf*Target + -Inf','FontWeight','bold','FontSize',12);

% Create title

title('Validation: R=0','FontWeight','bold','FontSize',12);

% Create multiple lines using matrix input to plot

plot2 = plot(X3,YMatrix2,'Parent',subplot2);

set(plot2(1),'LineStyle',':','DisplayName','Y = T','Color',[0 0 0]);

set(plot2(2),'LineWidth',2,'Color',[0 1 0],'DisplayName','Fit');

% Create plot

plot(X4,Y1,'Parent',subplot2,'Marker','o','LineStyle','none',...

    'DisplayName','Data',...

    'Color',[0 0 0]);

% Create legend

legend2 = legend(subplot2,'show');

set(legend2,'Location','NorthWest');

% Create subplot

subplot3 = subplot(2,2,3,'Parent',figure1,'PlotBoxAspectRatio',[1 1 1]);

%% Uncomment the following line to preserve the X-limits of the axes
```

```matlab
% xlim(subplot3,[0.0045741194037839 0.37]);

%% Uncomment the following line to preserve the Y-limits of the axes

% ylim(subplot3,[0.0045741194037839 0.37]);

box(subplot3,'on');

hold(subplot3,'all');

% Create xlabel

xlabel('Target','FontWeight','bold','FontSize',12);

% Create ylabel

ylabel('Output ~= 0.013*Target + 0.0061','FontWeight','bold','FontSize',12);

% Create title

title('Test: R=1','FontWeight','bold','FontSize',12);

% Create multiple lines using matrix input to plot

plot3 = plot(X5,YMatrix3,'Parent',subplot3);

set(plot3(1),'LineStyle',':','DisplayName','Y = T','Color',[0 0 0]);

set(plot3(2),'LineWidth',2,'Color',[1 0 0],'DisplayName','Fit');

% Create plot

plot(X6,Y1,'Parent',subplot3,'Marker','o','LineStyle','none',...

    'DisplayName','Data',...

    'Color',[0 0 0]);

% Create legend

legend3 = legend(subplot3,'show');
```

```matlab
set(legend3,'Location','NorthWest')

% Create subplot

subplot4 = subplot(2,2,4,'Parent',figure1,'PlotBoxAspectRatio',[1 1 1]);

%% Uncomment the following line to preserve the X-limits of the axes

% xlim(subplot4,[0 0.37]);

%% Uncomment the following line to preserve the Y-limits of the axes

% ylim(subplot4,[0 0.37]);

box(subplot4,'on');

hold(subplot4,'all')

% Create xlabel

xlabel('Target','FontWeight','bold','FontSize',12);

% Create ylabel

ylabel('Output ~= 0.38*Target + 0.011','FontWeight','bold','FontSize',12);

% Create title

title('All: R=0.58343','FontWeight','bold','FontSize',12);

% Create multiple lines using matrix input to plot

plot4 = plot(X7,YMatrix4,'Parent',subplot4);

set(plot4(1),'LineStyle',':','DisplayName','Y = T','Color',[0 0 0]);

set(plot4(2),'LineWidth',2,'Color',[0.4 0.4 0.4],'DisplayName','Fit');

% Create plot

plot(X8,Y1,'Parent',subplot4,'Marker','o','LineStyle','none',...
```

```matlab
    'DisplayName','Data',...

    'Color', [0 0 0])

% Create legend

legend4 = legend(subplot4,'show');

set(legend4,'Location','NorthWest');
```